NATIONAL AERONAUTICS AND SPACE ADMINISTRATION

Technical Memorandum 33-747

Volume I

A Collection of Articles on S/X-Band Experiment Zero Delay Ranging Tests

Edited by
T. Y. Otoshi

JET PROPULSION LABORATORY
CALIFORNIA INSTITUTE OF TECHNOLOGY
PASADENA, CALIFORNIA

November 1, 1975

NATIONAL AERONAUTICS AND SPACE ADMINISTRATION

Technical Memorandum 33-747

Volume I

A Collection of Articles on S/X-Band Experiment Zero Delay Ranging Tests

Edited by
T. Y. Otoshi

JET PROPULSION LABORATORY
CALIFORNIA INSTITUTE OF TECHNOLOGY
PASADENA, CALIFORNIA

November 1, 1975

Prepared Under Contract No NAS 7-100
National Aeronautics and Space Administration

TECHNICAL REPORT STANDARD TITLE PAGE

1. Report No. 33-747, Vol. I	2. Government Accession No.	3. Recipient's Catalog No.
4. Title and Subtitle A COLLECTION OF ARTICLES ON S/X-BAND EXPERIMENT ZERO DELAY RANGING TESTS		5. Report Date November 1, 1975 6. Performing Organization Code
7. Author(s) JPL Staff (Edited by T. Y. Otoshi)		8. Performing Organization Report No.
9. Performing Organization Name and Address JET PROPULSION LABORATORY California Institute of Technology 4800 Oak Grove Drive Pasadena, California 91103		10. Work Unit No. 11. Contract or Grant No. NAS 7-100 13. Type of Report and Period Covered Technical Memorandum
12. Sponsoring Agency Name and Address NATIONAL AERONAUTICS AND SPACE ADMINISTRATION Washington, D.C. 20546		14. Sponsoring Agency Code

15. Supplementary Notes

16. Abstract

Within this collection, a set of articles is concerned with the development of special test equipment and a new dual-frequency Zero Delay Device (ZDD) that were required for range tests and the measurement of ground station delays for the Mariner-Venus-Mercury 1973 S/X-Band Experiment.

Another set of articles is concerned with test data obtained at DSS 14 (Goldstone, California) after installation of the ZDD on the 64-m antenna. It is shown that large variations of range were observed as a function of antenna elevation angle and were sensitive to antenna location. A new ranging calibration configuration that was subsequently developed and a technique for determining the appropriate Z-correction are described. Zero delay test data at DSS 14 during the Mariner 10 Venus-Mercury-Encounter periods (1974 Days 12-150) are presented.

The final set of articles is concerned with the theoretical analysis and experimental verifications of the (1) effects of multipath and (2) effects of discontinuities on range delay measurements. The last article shows how a movable subreflector technique and the multipath theory can be used to isolate principal multipath errors on the 64-m antenna and, therefore, enable a more accurate determination of the actual ground station range delay.

17. Key Words (Selected by Author(s))	18. Distribution Statement
Electronics and Electrical Engineering Mariner Venus/Mercury 1973 Project	Unclassified -- Unlimited

19. Security Classif. (of this report)	20. Security Classif. (of this page)	21. No. of Pages	22. Price
Unclassified	Unclassified	126	

HOW TO FILL OUT THE TECHNICAL REPORT STANDARD TITLE PAGE

Make items 1, 4, 5, 9, 12, and 13 agree with the corresponding information on the report cover. Use all capital letters for title (item 4). Leave items 2, 6, and 14 blank. Complete the remaining items as follows:

3. Recipient's Catalog No. Reserved for use by report recipients.

7. Author(s). Include corresponding information from the report cover. In addition, list the affiliation of an author if it differs from that of the performing organization.

8. Performing Organization Report No. Insert if performing organization wishes to assign this number.

10. Work Unit No. Use the agency-wide code (for example, 923-50-10-06-72), which uniquely identifies the work unit under which the work was authorized. Non-NASA performing organizations will leave this blank.

11. Insert the number of the contract or grant under which the report was prepared.

15. Supplementary Notes. Enter information not included elsewhere but useful, such as: Prepared in cooperation with... Translation of (or by)... Presented at conference of... To be published in...

16. Abstract. Include a brief (not to exceed 200 words) factual summary of the most significant information contained in the report. If possible, the abstract of a classified report should be unclassified. If the report contains a significant bibliography or literature survey, mention it here.

17. Key Words. Insert terms or short phrases selected by the author that identify the principal subjects covered in the report, and that are sufficiently specific and precise to be used for cataloging.

18. Distribution Statement. Enter one of the authorized statements used to denote releasability to the public or a limitation on dissemination for reasons other than security of defense information. Authorized statements are "Unclassified—Unlimited," "U. S. Government and Contractors only," "U. S. Government Agencies only," and "NASA and NASA Contractors only."

19. Security Classification (of report). NOTE: Reports carrying a security classification will require additional markings giving security and downgrading information as specified by the Security Requirements Checklist and the DoD Industrial Security Manual (DoD 5220.22-M).

20. Security Classification (of this page). NOTE: Because this page may be used in preparing announcements, bibliographies, and data banks, it should be unclassified if possible. If a classification is required, indicate separately the classification of the title and the abstract by following these items with either "(U)" for unclassified, or "(C)" or "(S)" as applicable for classified items.

21. No. of Pages. Insert the number of pages.

22. Price. Insert the price set by the Clearinghouse for Federal Scientific and Technical Information or the Government Printing Office, if known.

Preface

The work described in this report was performed by the Telecommunications Division of the Jet Propulsion Laboratory.

Volume I includes all of the articles that relate to zero delay ranging tests published by the Communications Elements Research Section in the Jet Propulsion Laboratory's *The Deep Space Network Progress Report* These articles were published during the period January 1973 through October 1975.

It is hoped that this document will serve as a useful and convenient reference for members of the Ranging Accuracy Team, Network Operations, and Navigation Team, and others who use ranging calibration data.

Contents

Abstract

Within this collection, a set of articles is concerned with the development of special test equipment and a new dual-frequency Zero Delay Device (ZDD) that were required for range tests and the measurement of ground station delays for the Mariner-Venus-Mercury 1973 S/X-Band Experiment.

Another set of articles is concerned with test data obtained at DSS 14 (Goldstone, California) after installation of the ZDD on the 64-m antenna. It is shown that large variations of range were observed as a function of antenna elevation angle and were sensitive to antenna location. A new ranging calibration configuration that was subsequently developed and a technique for determining the appropriate Z-correction are described. Zero delay test data at DSS 14 during the Mariner 10 Venus-Mercury-Encounter periods (1974 Days 12–150) are presented.

The final set of articles is concerned with the theoretical analysis and experimental verifications of the (1) effects of multipath and (2) effects of discontinuities on range delay measurements. The last article shows how a movable subreflector technique and the multipath theory can be used to isolate principal multipath errors on the 64-m antenna and, therefore, enable a more accurate determination of the actual ground station range delay.

Reprinted from *The Deep Space Network Progress Report*, Technical Report 32-1526, Vol. XIII, Feb 15, 1973, pp 72–81

S/X-Band Experiment: Development of Special Telecommunications Development Laboratory Support Test Equipment

T. Y Otoshi and O B. Parham
Communications Elements Research Section

This article documents the design of an X-band down converter and a doppler extractor receiver that were specially developed and supplied to the Telecommunications Development Laboratory in July 1971 The special equipment enabled preliminary tests to be made on the performance of a combined S/X-band radio system similar to that which will be used for the Mariner Venus/Mercury 1973 mission

I. Introduction

The S/X-band experiment to be performed with the Mariner Venus/Mercury 1973 (MVM 73) spacecraft is a dual-frequency experiment to measure the electron content of the interplanetary media between Earth and the planets Venus and Mercury (Ref. 1). An uplink signal of approximately 2113 MHz will be transmitted to the spacecraft from the 64-m-diameter antenna at DSS 14. This uplink signal as received by the spacecraft radio system will be coherently multiplied by ratios of 240/221 and 880/221 to produce S- and X-band carrier frequencies of approximately 2295 MHz and 8415 MHz The coherent S- and X-band signals will then be transmitted back to the DSS 14 ground system. A measurement of the dispersiveness of the S- and X-band phase and range data as received back at the ground station provides scientific information required for determining total interplanetary electron content

A Block IV ground radio system currently being developed by the Division will be installed at DSS 14 for the S/X experiment The Block IV system will be a phase-stabilized system enabling simultaneous reception of S- and X-band frequencies and will yield dispersive S/X doppler and S/X range data

At the time the preliminary tests were conducted (September through October 1971), the Block IV system having S/X capability was not yet available Therefore, it was necessary to utilize a Block III system that had only S-band capability. The Block III system was converted into an X-band phase-locked loop receiver by means of

an X-band to 50-MHz down converter, which will be described in this article As was shown in a report by Brunn (Ref 2), the preliminary ranging and carrier phase test data were successfully obtained.

II. X-Band Down Converter

A block diagram of the X-band down converter is shown in Fig. 1. An input X-band signal (in the frequency range of 8400 to 8450 MHz) is down converted to produce a 50-MHz intermediate frequency (IF) output signal This output signal is then fed into the 50-MHz IF input stage of a Block III receiver The Block III phase-locked loop VCO output (nominally 23 4 MHz) is fed back into the down converter assembly, doubled, and then added to a coherent bias signal of approximately 51 7 MHz, which is produced by a frequency synthesizer and a 5-MHz frequency standard. An output signal of approximately 98 6 MHz is then filtered and multiplied by 85 to provide a phase-locked local oscillator frequency that is 50 MHz lower than the input X-band signal Many of the mixers, amplifiers, and multipliers are of the same design as those implemented in the Block IV system The Telecommunications Development Laboratory (TDL) X-band receiver system was purposely designed to be similar to the Block IV system so that preliminary test data would give a valid indication of MVM 73 S/X radio system performance

Figure 2 shows the front, top, and rear views of the fabricated assembly Table 1 shows typical noise figure and image rejection data of this assembly as measured in the laboratory After installation at the TDL, a noise figure measurement was again made on the X-band down converter The single sideband noise figure of the converter for the Channel 19 X-band input frequency (8421 79 MHz) was determined to be $(10\,2 \pm 0.5)$ dB as defined at the Type N input port of the converter assembly The increase in noise figure was attributed to minor adjustments made after data of Table 1 had been obtained

III. X-Band Doppler Extractor Receiver

X-band doppler data were obtained by use of an S/X translator and an X-band doppler extractor receiver similar to that which will be used in the Block IV system

A block diagram of the TDL X-band doppler extractor system is shown in Fig 3 The doppler extraction method is similar to that of the Block IV system except that the first IF is 50 MHz instead of 325 MHz.

Figure 4 shows the fabricated receiver portion of the TDL X-band doppler extractor system A special purpose S/X translator (zero delay device) is currently being fabricated and will be supplied to TDL for S/X test purposes

IV. Acknowledgment

The equipment described in this article was developed with the cooperation and assistance of R MacClellan, C Johns, and H Donnelly of the RF Systems Development Section. R. Clauss of the Communications Elements Research Section developed the low-loss waveguide X-band filter

References

1 Levy, G , Dickinson, R , and Stelzried, C., "RF Techniques Research S/X Band Experiment," in *Supporting Research and Advanced Development,* Space Programs Summary 37-61, Vol III, pp 93–95, Jet Propulsion Laboratory, Pasadena, Calif , Feb 20, 1970.

2 Brunn, D L , "S/X Band Ranging and Phase Tests," Interoffice Memo No 3396-72-060, Jet Propulsion Laboratory, Pasadena, Calif , Feb 23, 1972 (JPL internal document)

Table 1 Noise figures and image rejections of X-band down converter

Frequency, MHz	Single-sideband noise figure, dB	Image rejection, dB
8400	12 2	41
8405	11 2	39
8410	11 0	37
8415	10 6	37
8420	9 6	36
8425	8 6	35
8430	8 5	34
8435	9 2	31
8440	10.0	30
8445	11 2	28
8450	12.4	25

SPECIAL PARTS	MODEL
FREQUENCY SYNTHESIZER	DANA 7010 DIGIPHASE SYNTHESIZER
51.7-MHz BAND-PASS FILTER	TELONIC TSF-51.71-1.4-4TS1
98.6-MHz BAND-PASS FILTER	TELONIC TSF-98.56-2.8-6TS1
×5 MULTIPLIER	DESIGNED BY R. MacCLELLAN, JPL
×17 MULTIPLIER	ZETA LAB 5048-01
8375-MHz BAND-PASS FILTER	TELONIC TCH-8375-64-4TS
SINGLE BALANCED X-BAND MIXER AND 50-MHz PREAMPLIFIER	LEL XAH7-50-20
WR 112 BAND-PASS FILTER	DESIGNED BY R. CLAUSS, JPL

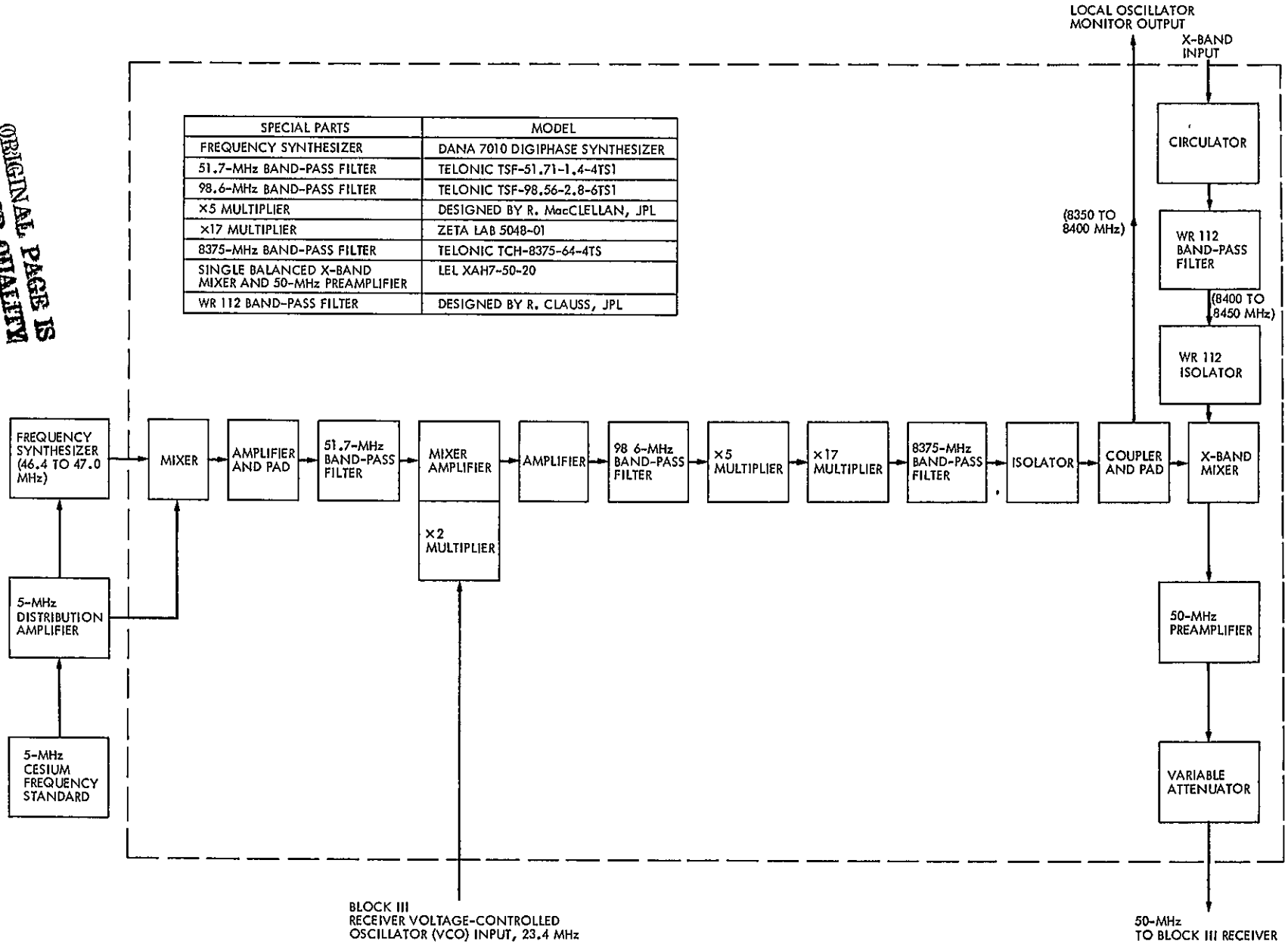

Fig. 1. Block diagram of TDL X-band to 50-MHz down converter

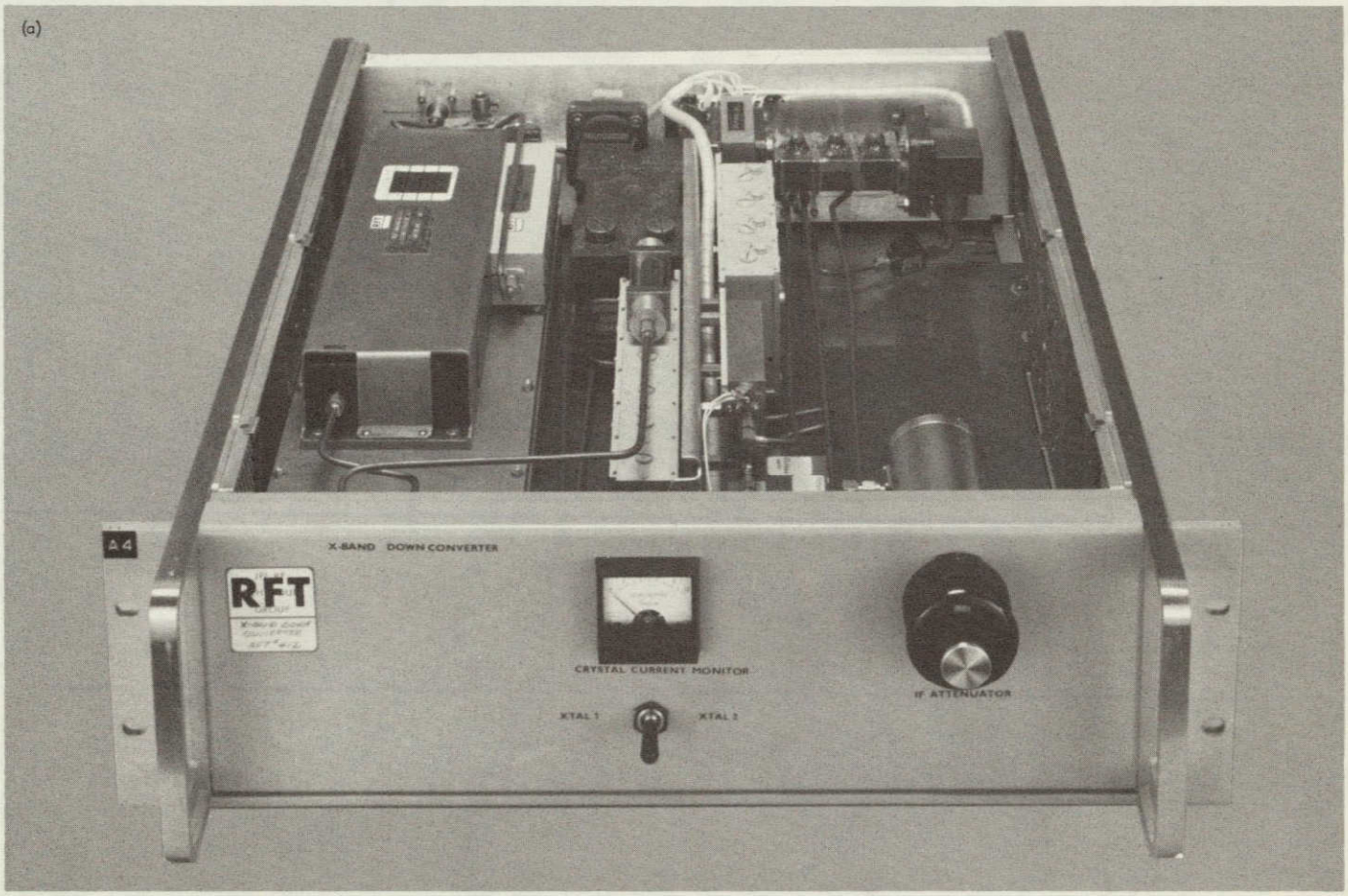

Fig. 2. TDL X-Band to 50-MHz down converter: (a) front view; (b) top view; (c) rear view

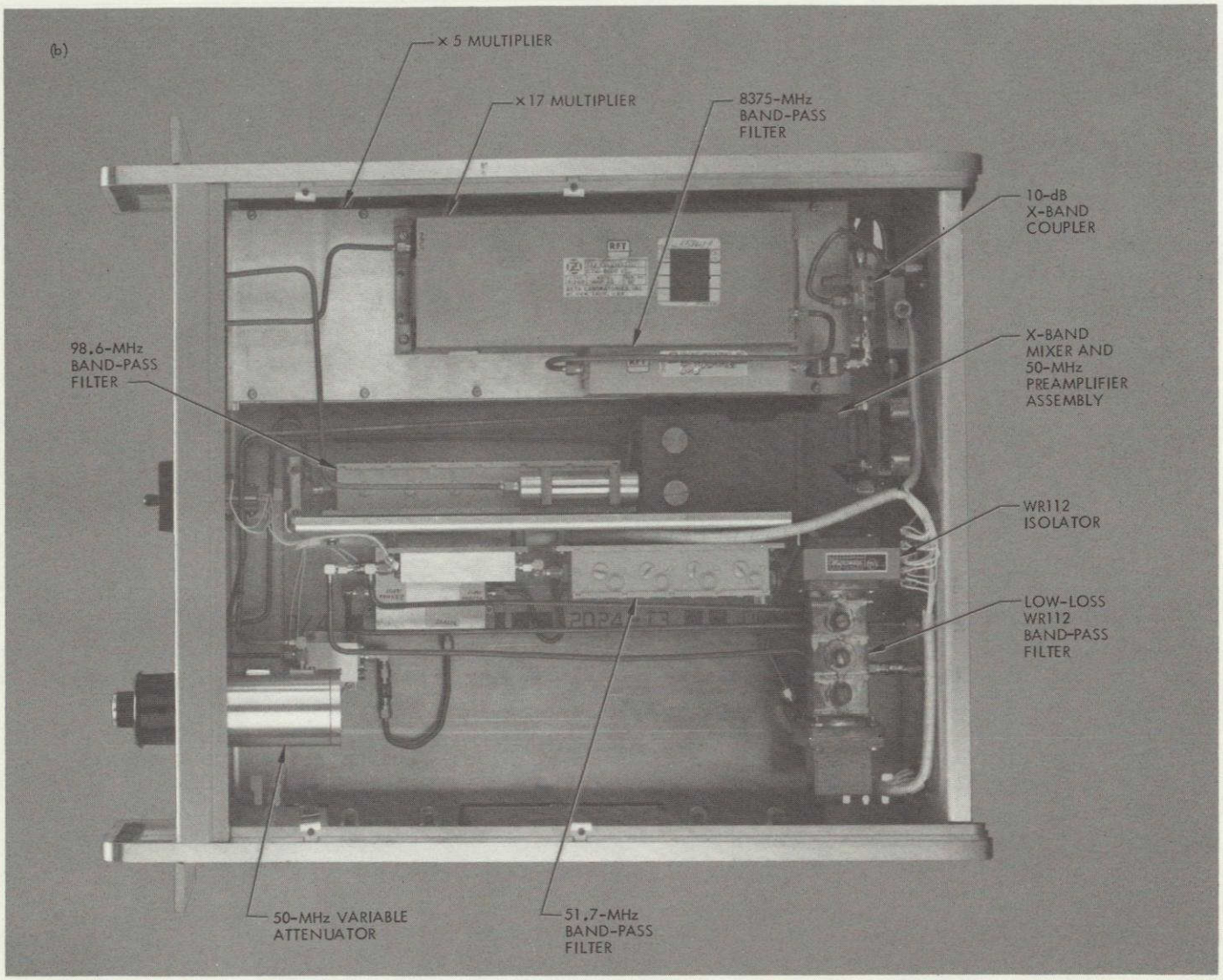

Fig. 2 (contd)

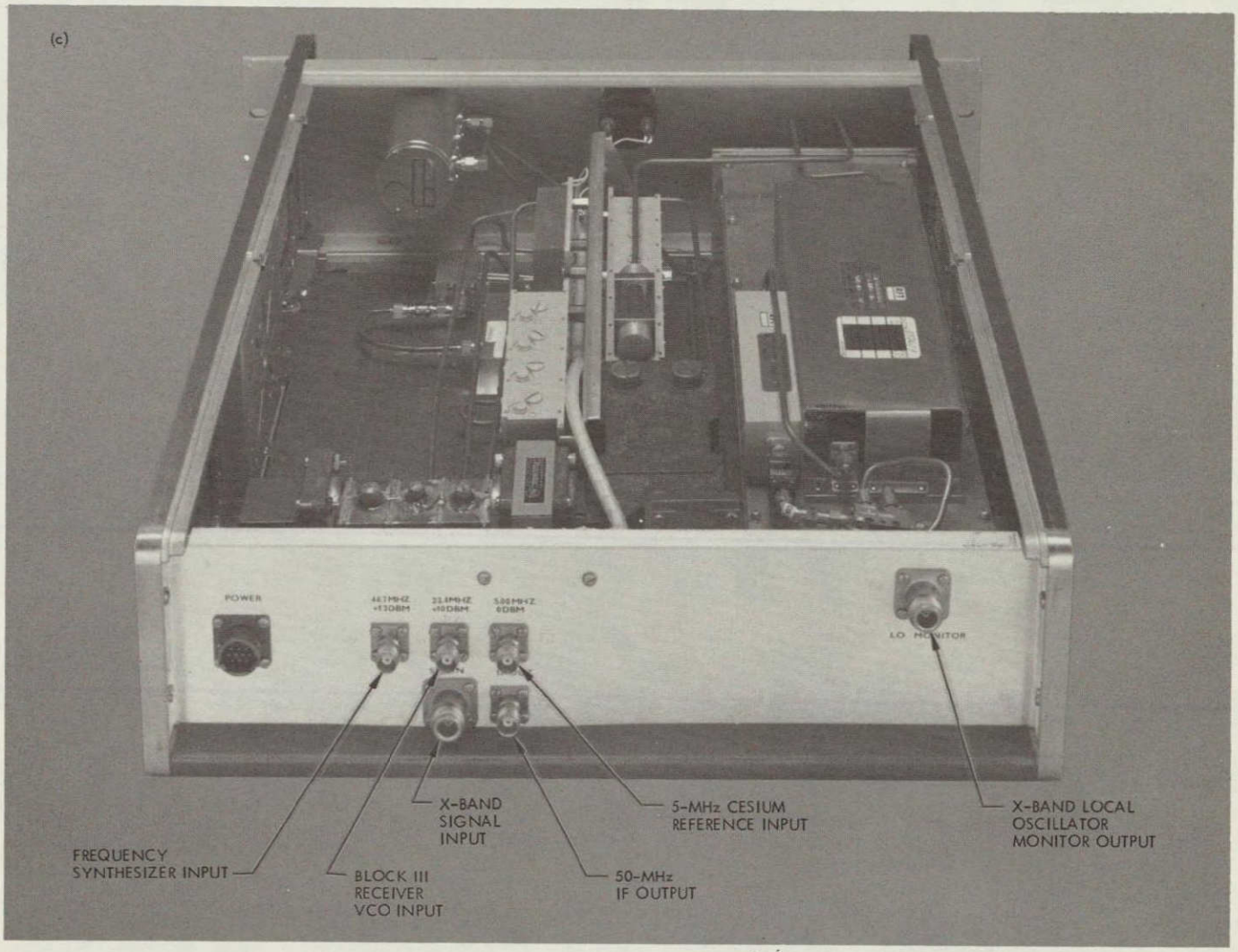

Fig. 2 (contd)

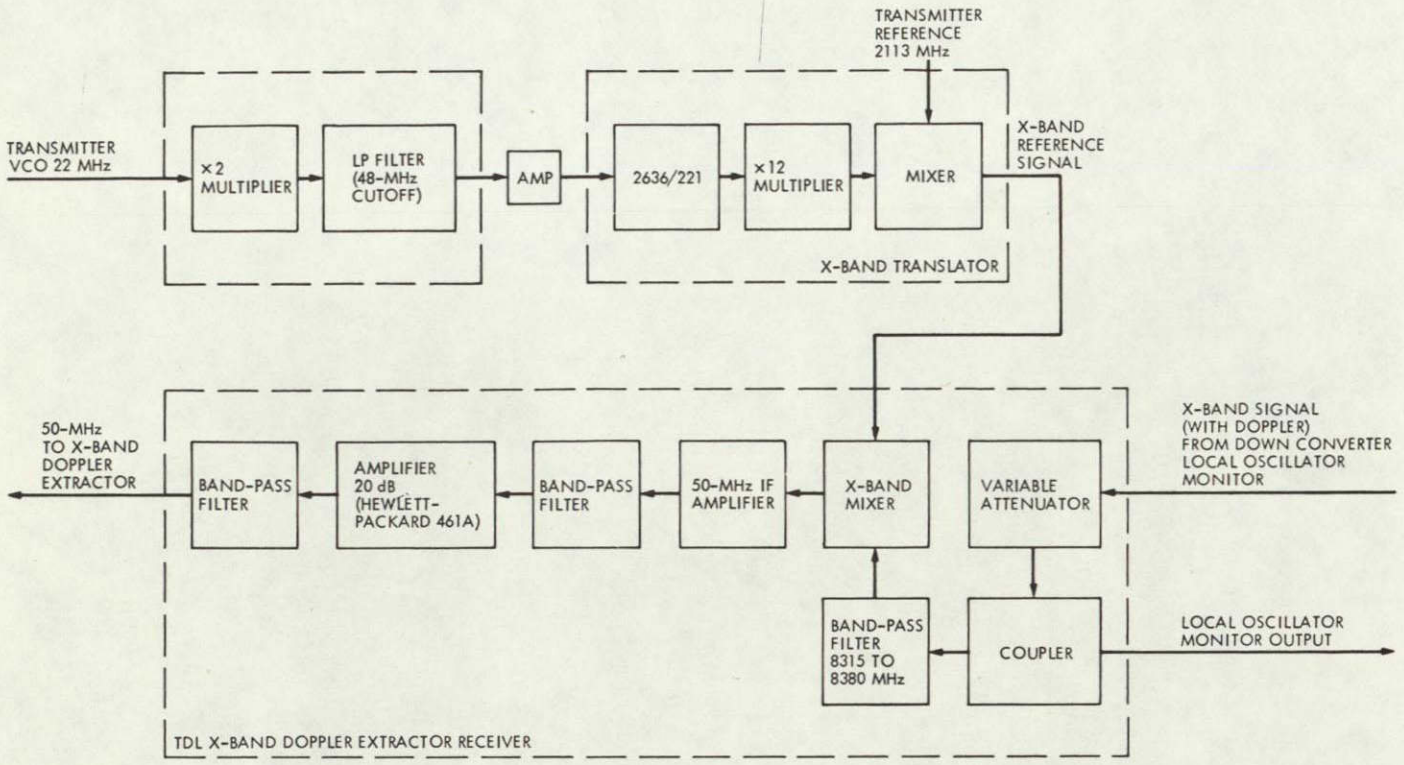

Fig. 3. Block diagram of TDL X-band doppler extractor system

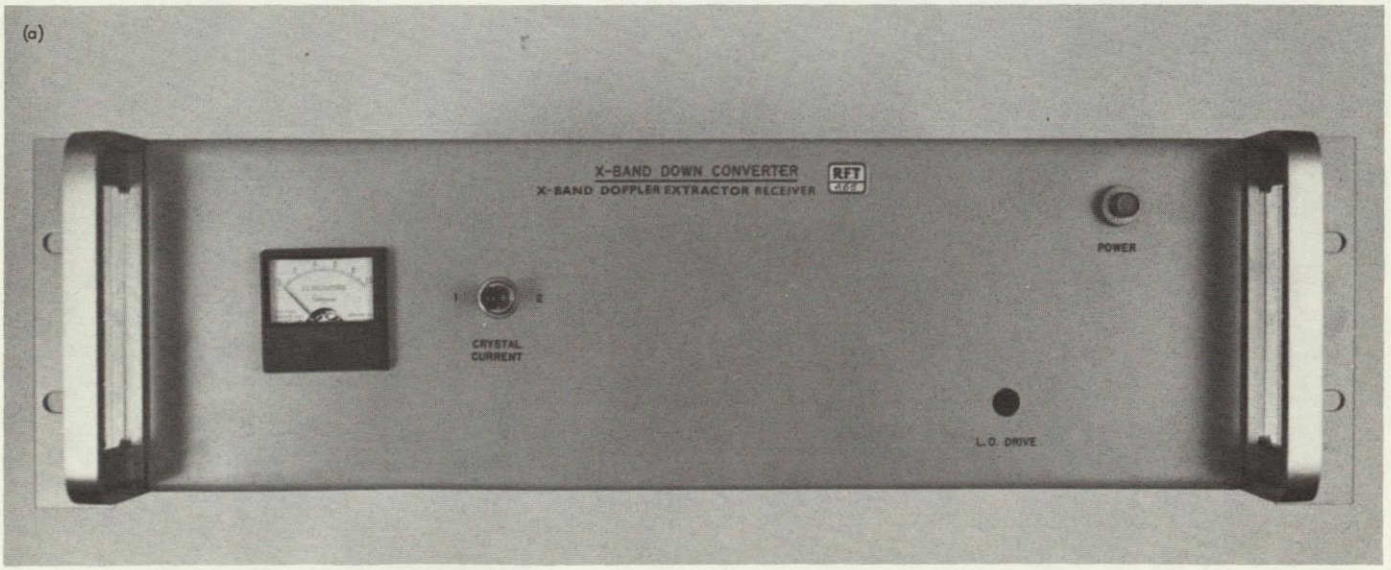

Fig. 4. TDL X-band doppler extractor receiver: (a) front view; (b) top view; (c) rear view

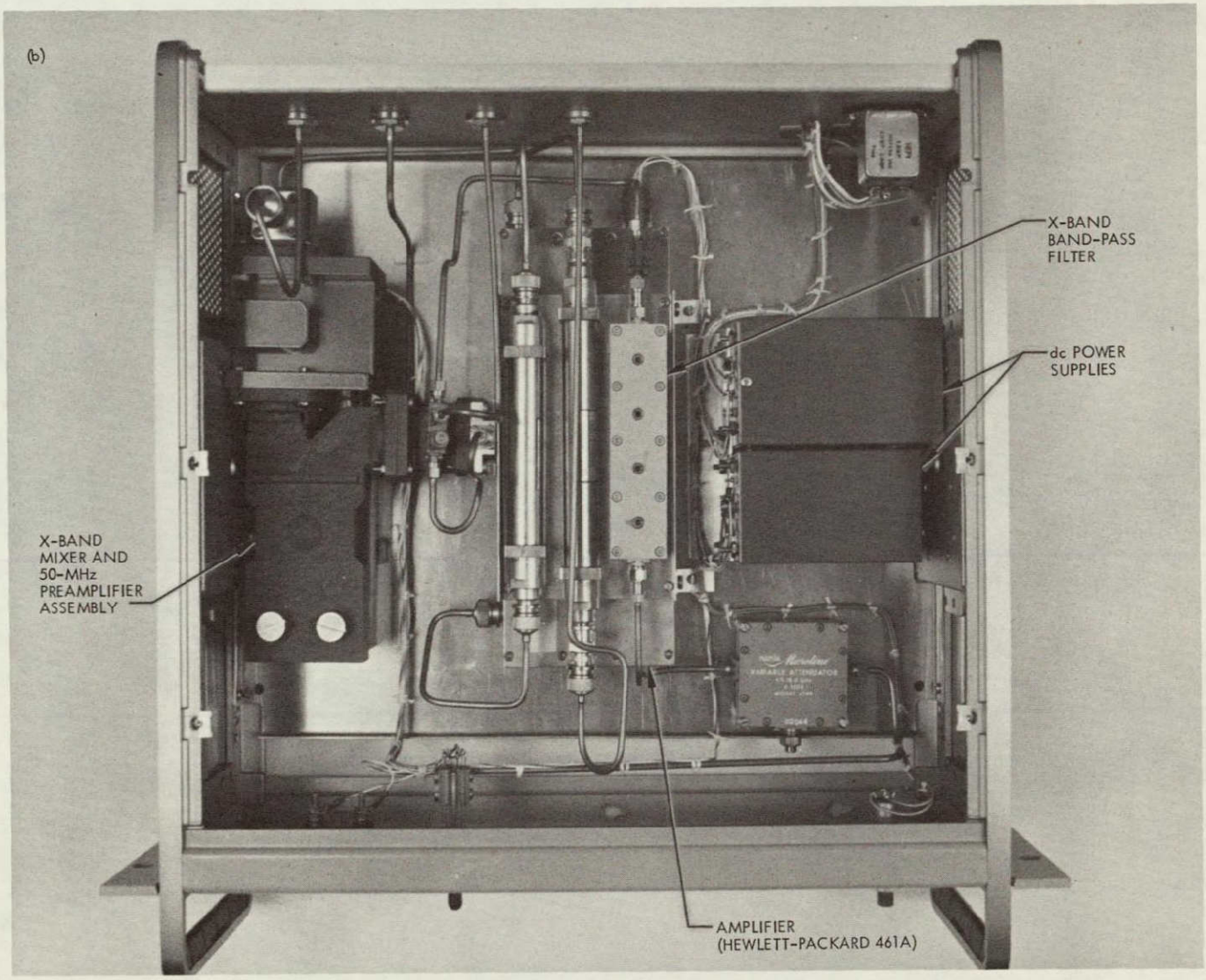
(b)
X-BAND
BAND-PASS
FILTER
dc POWER
SUPPLIES
X-BAND
MIXER AND
50-MHz
PREAMPLIFIER
ASSEMBLY
AMPLIFIER
(HEWLETT-PACKARD 461A)

Fig. 4 (contd)

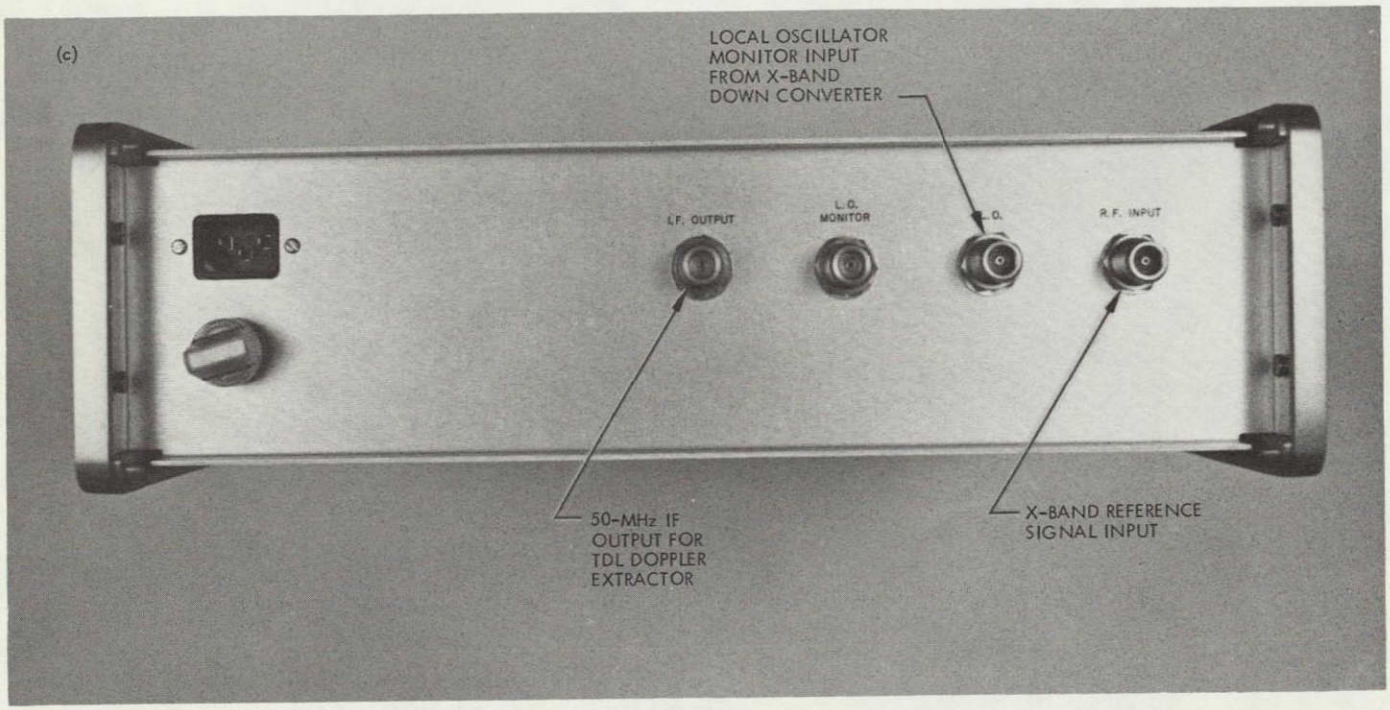
(c)
LOCAL OSCILLATOR
MONITOR INPUT
FROM X-BAND
DOWN CONVERTER
I.F. OUTPUT
L.O.
MONITOR
L.O.
R.F. INPUT
50-MHz IF
OUTPUT FOR
TDL DOPPLER
EXTRACTOR
X-BAND REFERENCE
SIGNAL INPUT

Fig. 4 (contd)

Reprinted from *The Deep Space Network Progress Report*, Technical Report 32-1526, Vol. XIV, Apr. 15, 1973, pp. 73–80.

S/X-Band Experiment: Zero Delay Device

T. Y. Otoshi and P. D. Batelaan
Communications Elements Research Section

A zero delay device currently being developed for the S/X band experiment is described. Preliminary group delay and transmission coefficient phase data are presented for some of the components in the zero delay device.

I. Introduction

The S/X band experiment to be performed with the Mariner Venus-Mercury 1973 spacecraft is a dual-frequency experiment to measure the electron content of the interplanetary media between Earth and the planets Venus and Mercury (Ref. 1). An uplink signal of approximately 2113 MHz will be transmitted to the spacecraft from the 64-m diam antenna at DSS 14. This uplink signal as received by the spacecraft radio system will be coherently multiplied by ratios of 240/221 and 880/221 to produce S- and X-band carrier frequencies of approximately 2295 and 8415 MHz. The coherent S- and X-band signals will then be transmitted back to the DSS 14 ground system. A measurement of the dispersiveness of the S- and X-band phase and range (or group delay) data as received back at the ground station provides scientific information required for determining total interplanetary electron content.

To calibrate group delay which is due only to the ground antenna system, a zero delay device (ZDD) is used. This device is physically installed on the ground antenna and permits group delay of the ground system to be calibrated as a function of antenna pointing direction and ambient temperatures. This article describes the ZDD which is currently being developed for the S/X experiment. Preliminary group delay and phase data on some ZDD components are also presented.

II. Description of the S/X ZDD

Figure 1 shows a simplified block diagram of the ZDD calibration system. The ZDD assembly will be installed in a low profile position on the side of the Mod-III section of the 64-m diam antenna at DSS 14. A reference 2113-MHz carrier with range-code modulation from the Mu-2 ranging machine and Block IV exciter assembly is fed into a 400-kW klystron amplifier. The amplified 2113-MHz signal is transmitted through the S-band megawatt transmit (SMT) cone microwave system and then radiated out of the SMT cone horn. A small fraction of the signal reflected from the subreflector is received by the ZDD

S-band horn. This received 2113-MHz signal is mixed with coherent 182 and 6302 MHz local oscillator frequencies provided by the Block IV exciter. As a result of mixing, down-link test signals of approximately 2295 and 8415 MHz are generated and radiated out of the ZDD S- and X-band horns back toward the subreflector. These down-link signals are received by the X-band (multiple-frequency X- and K-band (MXK) cone) and S-band (SMT cone) microwave systems. The microwave systems are followed by Block IV receivers and a Mu-2 ranging system which extract the desired S/X range information.

In essence, the function of the ZDD is to simulate a stationary spacecraft which is located on the ground antenna itself. For the S/X experiment, the ZDD will purposely be installed on the side of the Mod-III section. This location permits transmission line lengths between the ZDD and Block IV exciter to be kept physically short, and therefore, help minimize possible temperature effects on differential S/X phase and group delays.

Figure 2 is a preliminary detailed block diagram of the ZDD assembly. The ZDD assembly includes such components as S- and X-band horns, remotely controllable switches and step attenuators, mixers, and a band-pass filter. In order to have a reliable ZDD system, it is necessary that the individual components be electrically stable with regard to carrier phase and group delay. Some of the ZDD components were tested for group delay and phase stability as functions of ambient temperatures. The results are summarized in the following.

III. Test Results

A Hewlett-Packard Model 8542A automatic network analyzer was used to measure group delays and transmission coefficient phase. As described in Ref. 2, group delay can be determined from the slope of the transmission coefficient phase versus frequency characteristic curve. The advantages of using this network analyzer system are: (1) rapid and inexpensive data taking and (2) good accuracies achieved because calibration corrections are automatically applied by a computer. The tests were performed by the Western Automatic Test Service (WATS) of Palo Alto, California.

Figure 3 shows a remotely controllable step attenuator manufactured by Weinschel Engineering of Gaithersburg, Maryland. The attenuation of this device can be changed in 1-dB increments over a total dynamic range of 69 dB. Test data at pertinent S/X frequencies are summarized in Table 1. The group delay results shown are typical of data obtained over an S-band frequency range of 2000 to 2500 MHz and an X-band frequency range of 8000 to 9000 MHz. Significant test results of this device can be summarized as follows:

(1) The group delay is essentially the same at S- and X-band frequencies. In addition, the group delay is independent of attenuation setting.

(2) The transmission coefficient phase is somewhat dependent upon attenuation setting.

(3) Based on three sets of measurements in the attenuation range of 0 to 40 dB, the measured group delay values repeated to within 0.01 ns. Measured phase values repeated to within 0.1 and 0.3 deg at S- and X-band frequencies, respectively.

Figure 4 shows a remotely controllable broadband coaxial switch manufactured by Hewlett-Packard Company at Palo Alto. Test data at pertinent S/X frequencies are presented in Table 2. The group delay test results shown are typical of those obtained over the S-band frequency range of 2000 to 2500 MHz and those obtained over the X-band frequency range of 8000 to 9000 MHz. Based on the test results, it was found that for this device: (1) the group delay was essentially the same at both S- and X-band frequencies, (2) the group delay and phase values vary only slightly over the ambient temperature range of 4.4°C (40°F) to 37.8°C (100°F), and (3) based on three sets of measurements, the group delay nominal values of Table 2 repeated to within 0.01 ns and phase values typically to within 0.2 deg.

Figure 5 shows a 2113-MHz coaxial bandpass filter manufactured by Telonic Industries of Laguna Beach, California. This filter has a 3-dB bandwidth of 400 MHz. Its purpose is to filter out possible harmonic products that could be generated by the X-band mixer and re-radiated out the ZDD S-band horn. Table 3 shows the test results over the filter passband. Properties of this filter can be summarized as follows: (1) the group delay varies about 1 ns in the 400-MHz passband and (2) group delay and phase data variations with temperature are small over the ambient temperature range of 4.4°C (40°F) to 37.8°C (100°F). It is also of interest to note that the group delay of 2 ns for the filter in the passband is about 7.5 times greater than the group delay of an air-dielectric coaxial line having the same physical length (8 cm) as the filter.

IV. Conclusions

Preliminary group and phase delay data have been presented for some components being installed in the ZDD assembly. It was found that for broadband coaxial devices such as the step attenuator and coaxial switches, the group delays were essentially the same at both S- and X-band frequencies. Variations of group delay and phase with ambient temperatures were negligibly small over the temperature ranges of 4.4°C (40°F) to 37.8°C (100°F).

References

1. Levy, G., Dickinson, R., and Stelzried, C., "RF Techniques Research: S/X Band Experiment," in *Supporting Research and Advanced Development*, Space Programs Summary 37-61, Vol. III, pp. 93–95, Jet Propulsion Laboratory, Pasadena, Calif., Feb. 20, 1970.
2. Adams, S. F., *Microwave Theory and Applications*, pp. 428–429, Prentice-Hall, Inc., Englewood Cliffs, N.J., 1969.

Table 1. Test data for Weinschel Model AE 97-69-3 step attenuator

Attenuator setting, dB	Group delay, ns			Estimated error limits, ns	Transmission coefficient phase, deg			Estimated error limits,[a] deg
	2110 MHz	2300 MHz	8420 MHz		2110 MHz	2300 MHz	8420 MHz	
0	0.93	0.95	0.93	±0.12	4.9	−59.7	30.0	±0.4
1	0.95	0.97	0.95		−2.6	−68.0	−0.4	
2	0.94	0.96	0.95		−0.7	−65.6	7.3	
3	0.94	0.96	0.96		−1.0	−66.1	5.7	
4	0.94	0.96	0.94		−0.7	−65.6	7.0	
5	0.93	0.96	0.96		−0.6	−65.6	7.6	
6	0.94	0.98	0.96		−0.2	−65.0	9.2	
7	0.94	0.96	0.95		0.4	−64.2	10.0	
8	0.93	0.97	0.96		1.5	−63.2	14.3	
9	0.94	0.97	0.95		0.2	−64.5	11.2	
10	0.96	0.98	0.96	±0.13	−14.3	−80.6	−46.4	±0.5
20	0.96	0.99	0.96	±0.14	−10.9	−77.1	−34.1	±0.5
30	0.98	1.00	0.99	±0.16	−18.6	−85.4	−68.5	±0.6
40	1.00	0.99	0.97	±0.22	−16.8	−83.7	−54.6	±0.8
50	1.06	1.03	1.07	±0.33	−35.5	−102.8	−129.9	±1.2
60	1.3	1.1	1.1	±0.67	−29.5	−98.6	−114.6	±2.4

[a]Manufacturer's specs on the HP 8542A automatic network analyzer.

Table 2. Test data for HP 8761A coaxial switch

Frequency, MHz	Group delay, ns			Transmission coefficient phase, deg		
	4.4°C (40°F)	21.1°C (70°F)	37.8°C (100°F)	4.4°C (40°F)	21.1°C (70°F)	37.8°C (100°F)
Port 1 to C						
2110	0.24	0.23	0.24	−164.4	−164.6	−164.5
2300	0.21	0.21	0.21	−178.9	−179.2	−179.1
8420	0.22	0.22	0.22	66.3	65.3	65.7
Port 2 to C						
2110	0.24	0.24	0.23	−164.4	−164.4	−164.5
2300	0.21	0.21	0.21	−178.9	−179.0	−179.1
8420	0.22	0.22	0.22	66.3	65.8	65.8

Table 3. Test results for Telonic TBP 2114-400-4EF1 bandpass filter

Frequency, MHz	21.1°C (70°F) Insertion loss, dB	Group delay, ns			Transmission coefficient phase, deg		
		4.4°C (40°F)	21.1°C (70°F)	37.8°C (100°F)	4.4°C (40°F)	21.1°C (70°F)	37.8°C (100°F)
1750	10.5	–	1.46	–	–	142.2	–
1800	5.5	–	2.19	–	–	110.6	–
1850	1.6	–	2.71	–	–	63.2	–
1910	0.42	2.32	2.37	2.39	2.2	4.1	5.0
2000	0.47	2.00	2.03	2.00	−65.7	−64.8	−64.2
2100	0.53	2.02	2.03	2.03	−137.8	−137.2	−136.9
2200	0.47	2.22	2.21	2.21	146.2	146.4	146.6
2290	0.80	3.22	3.24	3.23	62.9	62.7	62.9
2350	4.7	–	3.13	–	–	−15.5	–
2400	11.7	–	2.04	–	–	−62.4	–

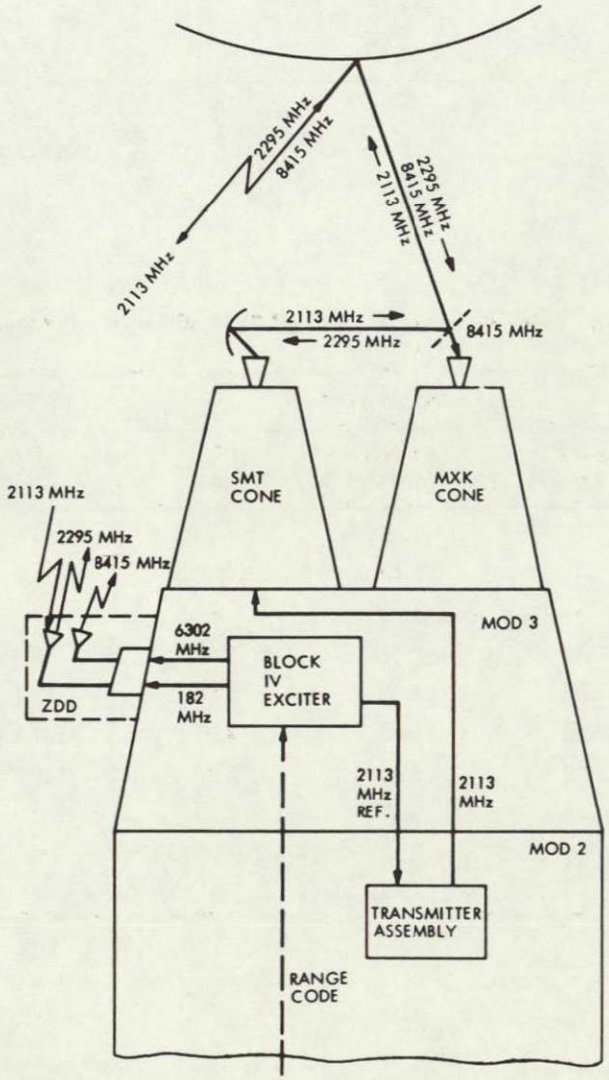

Fig. 1. Simplified block diagram of ZDD calibration system for S/X experiment

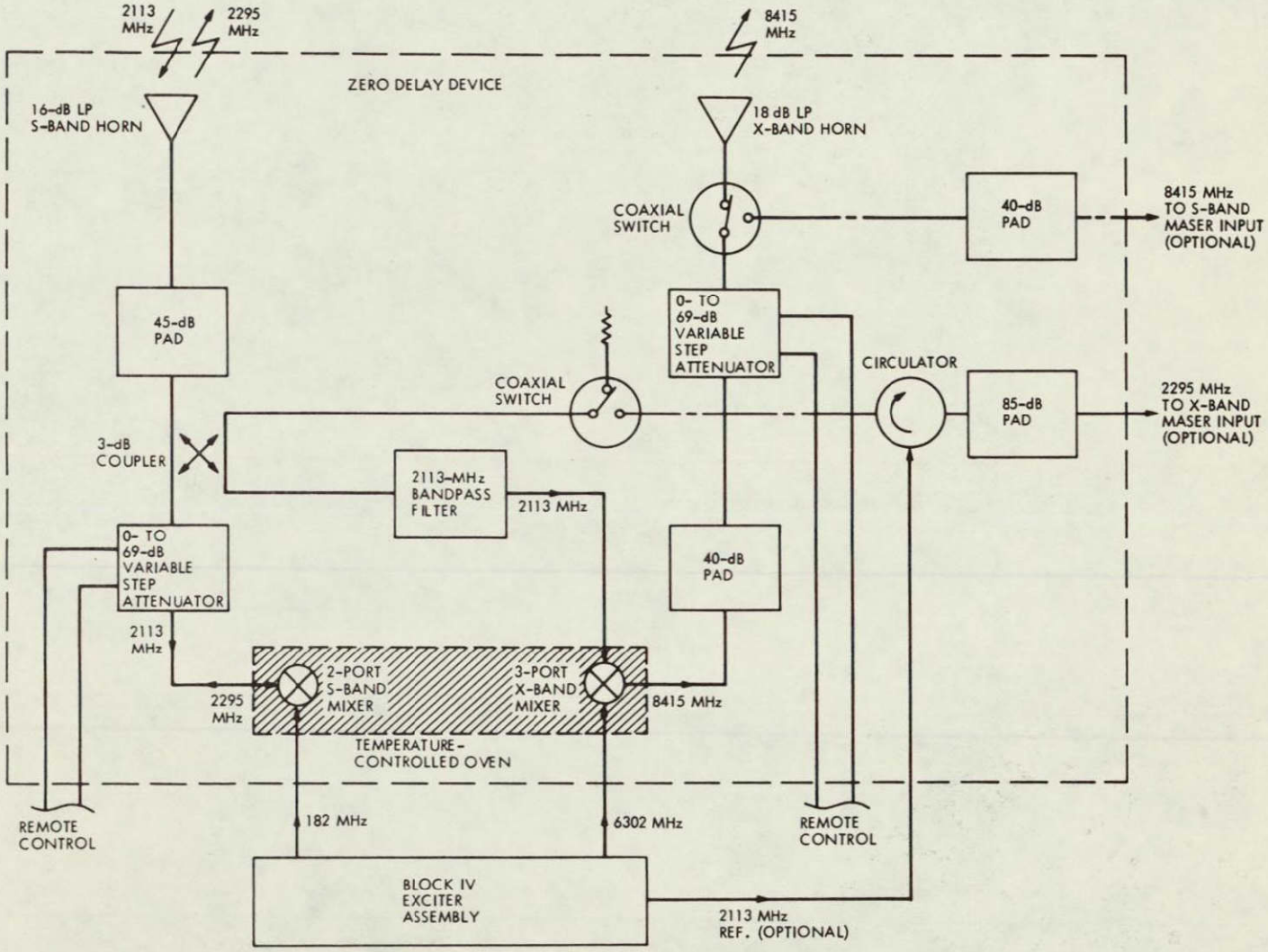

Fig. 2. Preliminary block diagram of ZDD assembly

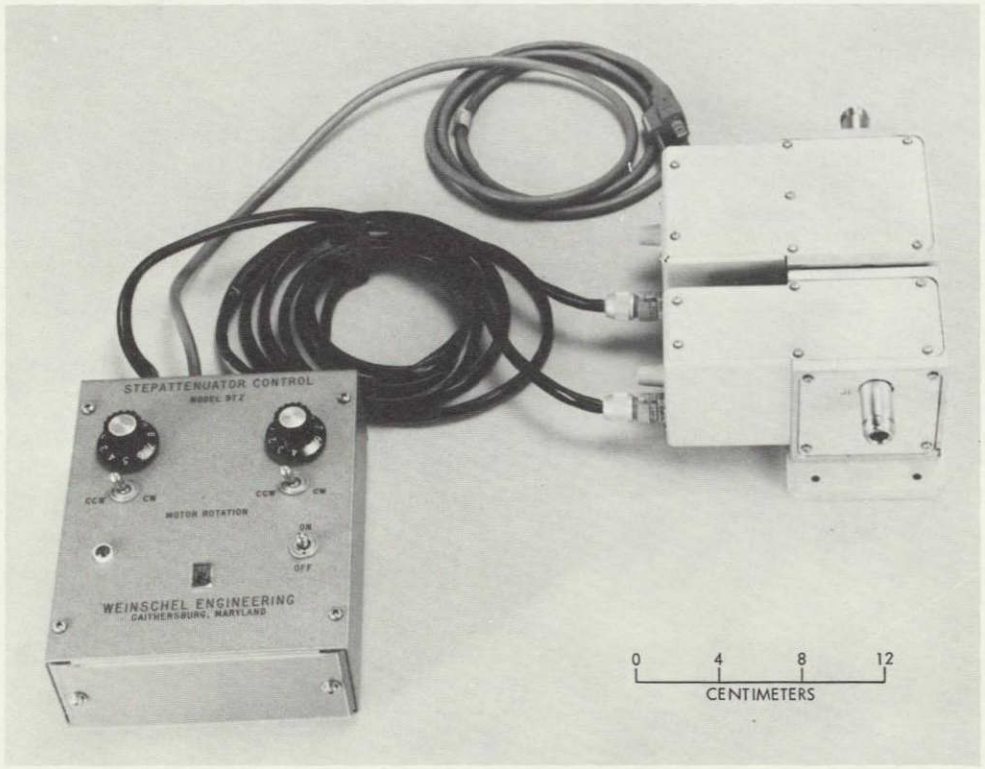

Fig. 3. Remotely controllable coaxial step attenuator, Weinschel Engineering Model AE 97-69-3

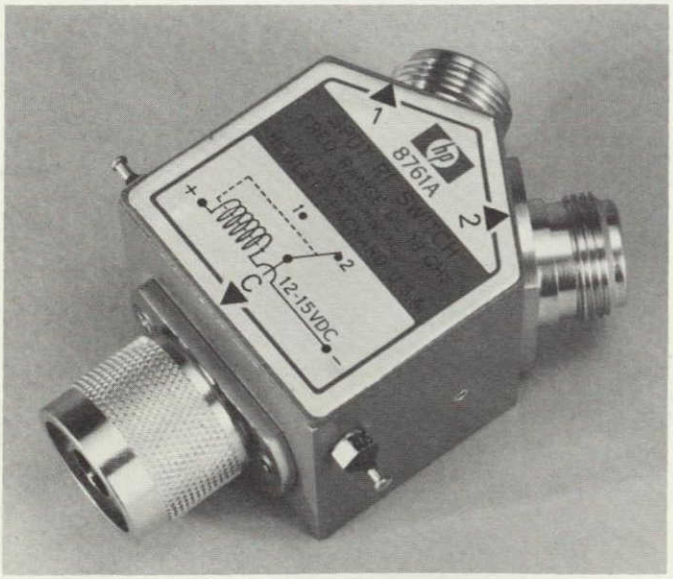

Fig. 4. Remotely controllable coaxial switch, Hewlett-Packard Model HP 8761A

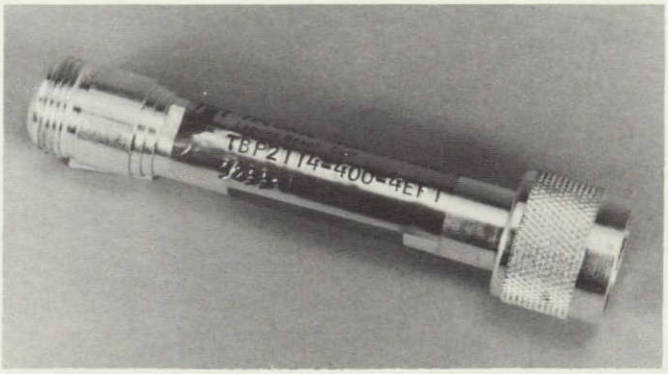

Fig. 5. Coaxial 2113-MHz bandpass filter, Telonic Industries Model TBP 2114-400-4EF1

Reprinted from *The Deep Space Network Progress Report*, Technical Report 32-1526, Vol. XV, June 15, 1973, pp. 84–87.

S/X-Band Experiment: Zero-Delay-Device Step Attenuator Evaluation

T. Y. Otoshi
Communications Elements Research Section

Test results are presented for a coaxial step attenuator to be used in the zero delay device for the S/X-band experiment. The test results at 182, 2113, 2295, 6302, and 8415 MHz indicate that the attenuator group delay changes about 0.07 ns over a 69-dB range. Tests made over a temperature range of 4.4°C (40°F) to 37.8°C (100°F) indicate that group delay and phase changes as a function of temperature are small.

I. Introduction

In Ref. 1, a zero delay device (ZDD) to be installed on the 64-m-diam antenna at DSS 14 was described. The ZDD is currently being developed for the S/X-band experiment to enable the group delay of the ground radio system to be calibrated, including the microwave antenna optics. Fig. 1 shows the step attenuator which will be used in the ZDD for purposes of varying signal levels. The attenuation of this device can be changed in 1-dB increments over a total dynamic range of 69 dB.

In the previous article (Ref. 1), some preliminary group delay and phase data were reported for the step attenuator at S- and X-band frequencies. Recently, the attenuator was also tested at 182 and 6302 MHz, which are the local oscillator frequencies for the S- and X-band mixers in the ZDD. This article will present these data, as well as data taken over a temperature range of 4.4°C (40°F) to 37.8°C (100°F).

II. Test Results

Table 1 shows a summary of the test results obtained on the step attenuator at 182, 2113, 2295, 6302, and 8415 MHz. The test data were obtained on a Hewlett-Packard 8542A Automatic Network Analyzer. The work was done by the Western Automatic Test Services of Palo Alto, California.

At higher attenuation settings in the region of 30 to 70 dB, it is known that the accuracy of the Automatic Network Analyzer becomes increasingly affected by noise. Therefore, it is not unusual to observe random fluctuations in the group delay data over the test frequency band. To overcome this problem, a least-squares linear fit was made to the phase data as a function of frequency over approximately 5% bandwidth frequency ranges. Group delay could then be calculated from the slope of the linear curve. This procedure was felt to be valid since it was already known (from data taken at

lower attenuation settings) that the step attenuator has very broadband properties.

The test data in Table 1 can be summarized as follows:

(1) The transmission coefficient phase data indicate that the attenuator becomes electrically longer as attenuation increases.

(2) Group delay tends to increase with attenuation setting, in agreement with the test results described above in (1). Group delay changes about 0.07 ns over the attenuation range of 0 to 69 dB.

(3) The group delay and phase data changes with temperature do not appear to be correlated. However, changes of group delay and phase appear to be reasonably small over the temperature range of 4.4°C (40°F) to 37.8°C (100°F).

(4) The incremental phase shift increases linearly with frequency. Therefore, the incremental phase shifts at two different frequencies are related by the frequency ratio.

To clarify (4), let the incremental phase shift for a 2-port variable attenuator be expressed as

$$\Delta\psi_{21} = \psi_{21}(A_{dB}) - \psi_{21}(0) \qquad (1)$$

where $\psi_{21}(A_{dB})$ and $\psi_{21}(0)$ are the transmission coefficient phases measured at an arbitrary attenuator setting A_{dB} and at a zero-dB setting, respectively. Then, if the incremental phase shift is known at one frequency, the incremental phase shift at another frequency can be calculated from the expression

$$(\Delta\psi_{21})_{f_1} = \frac{f_1}{f_2}(\Delta\psi_{21})_{f_2} \qquad (2)$$

For example, from Table 1e it is found that, at 8415 MHz and 21.1°C, the incremental phase shift at the 10-dB setting is

$$(\Delta\psi_{21})_{8415} = -47.8 - 28.8 = -76.6\,\text{deg}$$

Then, the corresponding incremental phase shift at 182 MHz as calculated from Eq. (2) is

$$(\Delta\psi_{21})_{182} = \frac{182}{8415}(-76.6) = -1.7\,\text{deg}$$

From Table 1a, the actual measured incremental phase shift at the 10-dB setting is

$$(\Delta\psi_{21})_{182} = -63.5 - (-61.9) = -1.6\,\text{deg}$$

which is in good agreement with the calculated value. The data at other test frequencies and attenuation settings are generally in good agreement with those predicted by Eq. (2).

III. Concluding Remarks

Group delay and phase data for the ZDD coaxial step attenuator have been presented. It was shown that the device becomes electrically longer by approximately 0.07 ns when the attenuation increases from 0 to 69 dB. The changes in group delay and phase as a function of temperature were found to be reasonably small over the temperature range of 4.4 to 37.8°C.

Reference

1. Otoshi, T. Y., and Batelaan, P. D., "S/X Band Experiment: Zero Delay Device," in *The Deep Space Network Progress Report for January and February 1973*, Technical Report 32-1526, Vol. XIV, pp. 73–80. Jet Propulsion Laboratory, Pasadena, Calif., Apr. 15, 1973.

Table 1. Test data for Weinschel model AE 97-69-3 step attenuator

Attenuator setting, dB	Group delay, ns			Transmission coefficient phase, deg		
	4.4°C	21.1°C	37.8°C	4.4°C	21.1°C	37.8°C
			(a) 182 MHz			
0	1.03	0.95	1.02	−61.1	−61.9	−61.1
10	1.02	0.96	1.01	−63.0	−63.5	−62.9
15	1.05	0.98	1.04	−63.7	−64.1	−63.6
30	0.97	0.97	0.98	−63.6	−63.8	−63.5
60	1.01	1.00	1.00	−65.8	−65.8	−65.4
69	—	1.01	—	—	−64.8	—
			(b) 2113 MHz			
0	0.95	0.94	0.96	7.4	3.8	7.4
10	1.02	0.97	1.03	−11.7	−15.5	−11.8
15	1.03	0.97	1.03	−17.8	−21.1	−17.3
30	0.98	0.97	0.98	−16.6	−20.0	−16.2
60	1.03	0.99	1.03	−33.2	−32.2	−32.7
69	—	1.00	—	—	−35.7	—
			(c) 2295 MHz			
0	0.95	0.91	0.94	−54.0	−58.0	−54.1
10	1.00	0.96	0.99	−75.0	−78.7	−75.1
15	0.99	0.98	0.98	−81.7	−84.7	−81.1
30	0.97	0.97	0.97	−80.3	−83.6	−79.9
60	0.97	0.96	0.99	−99.8	−97.5	−98.6
69	—	0.99	—	—	−103.3	—
			(d) 6302 MHz			
0	0.94	0.93	0.94	24.9	24.5	24.8
10	0.96	0.96	0.96	−32.5	−32.8	−33.0
15	0.97	0.97	0.98	−48.7	−48.6	−49.4
30	0.97	0.97	0.97	−47.7	−47.3	−47.7
60	1.01	0.99	0.98	−82.3	−80.5	−79.8
69	1.00	1.00	1.01	−96.8	−96.1	−93.9
			(e) 8415 MHz			
0	0.94	0.93	0.94	29.5	28.8	29.0
10	0.95	0.95	0.94	−47.5	−47.8	−48.3
15	0.98	0.98	0.98	−69.6	−69.5	−70.5
30	0.97	0.97	0.97	−69.6	−69.1	−69.6
60	1.01	1.01	1.02	−118.0	−115.5	−114.4
69	0.99	1.01	1.02	−136.8	−134.4	−132.3

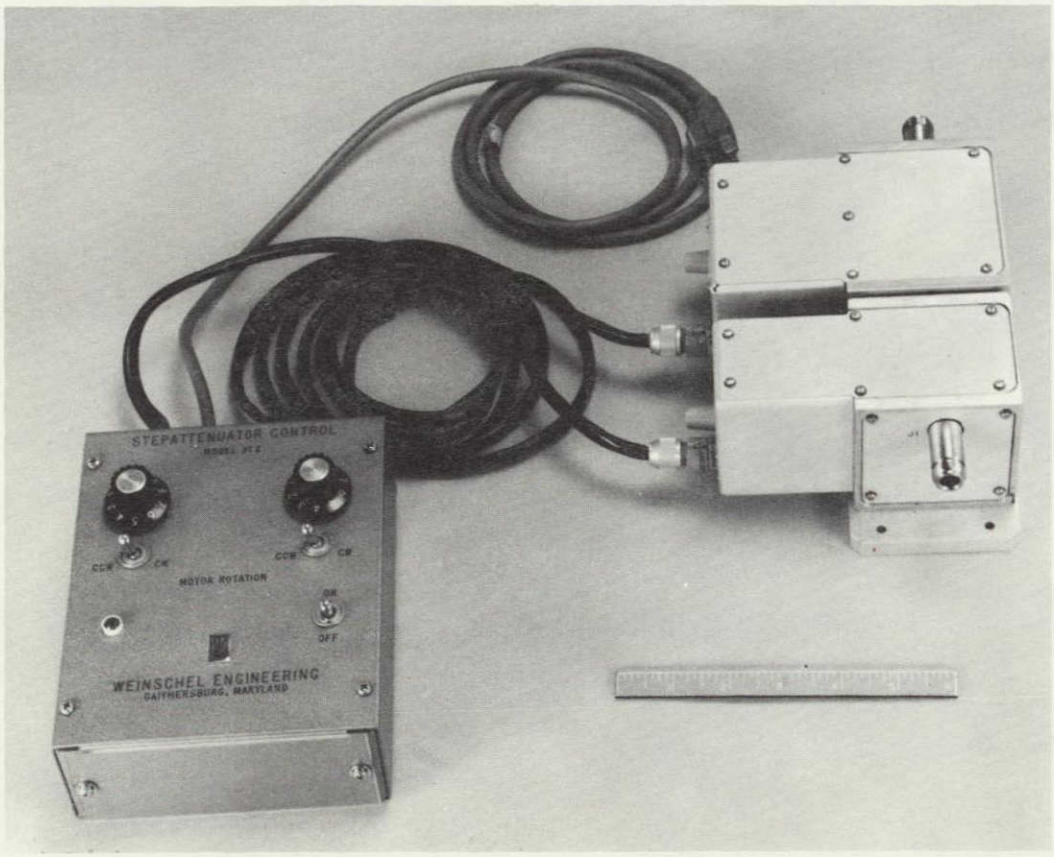

Fig. 1. Remotely controllable coaxial step attenuator, Weinschel Engineering Model AE 97-69-3

Reprinted from *The Deep Space Network Progress Report*, Technical Report 32-1526, Vol. XVII, Oct. 15, 1973, pp. 68–77.

S/X Experiment: Preliminary Tests of the Zero Delay Device

T. Y. Otoshi and P. D. Batelaan
Communications Elements Research Section

Preliminary testing of the zero delay device for the S/X experiment was performed at the Telecommunications Development Laboratory. The test setup consisted of a Block IV exciter, the zero delay device under test, a Block III receiver for S-band reception, a Block IV receiver for X-band reception, and a Mini-Mu ranging machine. Group delay through the system was measured as a function of received signal level and zero delay device temperature. The test results are presented and discussed.

I. Introduction

Fabrication of a zero delay device (ZDD), developed for the S/X experiment (Ref. 1), has recently been completed. This device will be installed on the side of the Mod-III section of the 64-m-diam antenna at DSS 14. The ZDD will simulate a spacecraft radio system mounted on the ground antenna itself. It is used for routine tracking precalibrations and will enable group delay and phase stability of the ground radio system to be calibrated as functions of antenna pointing coordinates and ambient temperatures. As was described in a previous article (Ref. 2), the ZDD in the operational configuration at DSS 14 will be used with a Block IV exciter, Block IV S-band receiver, Block IV X-band receiver, and a Mu-2 ranging system. Additional discussions on the principle of operation and detailed block diagrams of the ZDD may be found in Ref. 2.

II. Test Setup

The Block IV exciter/receiver systems and the Mu-2 ranging system are scheduled for installation at DSS 14 in October 1973. Owing to the unavailability of these systems, preliminary checkout of the ZDD assembly was attempted in the laboratory. The use of a Hewlett-Packard 5360A computing counter and other group delay measurement schemes was found to be only partially satisfactory.

It was suggested by L. Brunn of the Spacecraft Telecommunications Systems Section that preliminary ZDD tests be done at the Telecommunications Development Laboratory (TDL). The test equipment and setup at TDL were found to be ideally suited for testing the ZDD assembly. In addition to a Block III receiver for S-band testing, TDL was also equipped with a temperature-controlled test chamber, RF screen room, Mini-Mu ranging

machine, and an SDS 920 computer for both phase and group delay data processing. An engineering model Block IV exciter/receiver for X-band testing was made available by the R.F. Systems Development Section.

Figure 1 shows the ZDD placed in the TDL temperature-controlled test chamber. For these temperature tests, phase-stable cables (Flexco F182) were used for all critical RF transmission lines leading into and out of the temperature-controlled environment. A block diagram of the test setup is shown in Fig. 2. Some modifications made to the original ZDD block diagram (Ref. 2) to facilitate testing at TDL were (1) substitution of phase-stable cables for the S- and X-band horns, (2) removal of an S-band 45-dB pad, (3) substitution of a 2113-MHz bandpass filter by a 6-dB pad, and (4) substitution of a 40-dB X-band pad by a 3-dB pad. The substituted pads were chosen to make the received S/X signal levels be approximately the same as anticipated when the ZDD is used on the 64-m-diam antenna with the 400-kW transmitter turned on.

Tests were made by sequentially switching between the S-band Block III receiver and the X-band Block IV receiver. The following operating conditions existed for the calibrations at TDL:

S-band Block III receiver
Noise figure = 6.1 dB
RF bandwidth = 12 Hz
Threshold = −158 dBm

X-band Block IV receiver
Noise figure = 14 dB
RF bandwidth = 3 Hz
Threshold = −155 dBm

Uplink ranging modulation index = 69.2 deg

ZDD power levels: refer to Fig. 2

ZDD mixer oven temperature = 51.9°C

Group delay and phase data were obtained as functions of signal level and the physical temperature of the ZDD assembly. Signal levels were varied by means of the S- and X-band step attenuators on the ZDD assembly. The test chamber temperatures selected for the ZDD tests were 4, 21, and 34°C. The actual temperature extremes in the Mod III section, where the ZDD assembly will be installed, are expected to be well within the temperature range of 0 to 34°C.

III. Test Results and Discussion

Group delay ranging data and phase data were processed by means of special TDL computer programs written for the SDS 920 computer. Output data from the computer was provided every 20 or 30 seconds. However, these integration periods could be changed at the option of the operator. These output data were then averaged manually to obtain an overall mean and standard error applicable to the total integration time at a particular signal level setting or temperature. These mean values of group delay with standard error limits are shown plotted as functions of received signal levels and temperature for S- and X-band frequencies in Figs. 3 to 10.

It is of interest to note in Fig. 3 that at 21°C ambient temperature, the mean value for the S-band group delay changed about 1.6 ns when signal levels were varied over a 40-dB dynamic range. Figure 7 shows that the X-band group delay at 21°C changed about 4 ns when signal levels were varied over a 30-dB range. Similar observations of group delay changes at other temperatures are summarized in Table 1 for convenience of further study. The overall or worst case group delay change as functions of both temperature and signal level was found to be about 5 ns for S-band and 7 ns for X-band.

Table 2 is a summary of group delay repeatability tests at a particular strong signal level setting. The elapsed time between settings was 1 hour or more. The worst change or drift observed at 21°C was 0.77 ns for S-band and 1.56 ns for X-band.

The causes of the group delay changes at the stronger signal levels are not clearly understood at the present time. The changes should not be attributable to the ZDD attenuators because group delay changes of the individual attenuators are less than 0.05 ns over a 69-dB range and 4.4 to 37.8°C temperature range (Ref. 3). Repeatability of the ZDD attenuators was typically better than ±0.02 ns. Some of the group delay changes might be attributed to the ranging system itself. Changes of about ±2 ns have been previously observed on TDL ranging tests of spacecraft radio equipment (Ref. 4).

The data presented in this article should be considered to be preliminary and not necessarily applicable to the final installed configuration at DSS 14. Phase data which were also obtained on the ZDD assembly at TDL are currently being analyzed. The phase test results will be reported in a subsequent article.

Acknowledgments

The ZDD assembly was fabricated and assembled by R. B. Lyon of the Communications Elements Research Section. Jim Weese of the Spacecraft Telecommunications Systems Section and Boyd Madsen of The Boeing Company assisted with the TDL tests. The engineering model Block IV receiver was provided by H. Donnelly, C. Johns, and R. Weller of the R.F. Systems Development Section.

References

1. Levy, G. S., Dickinson, R., and Stelzried, C. T., "RF Techniques Research: S/X Band Experiment," in *Supporting Research and Advanced Development*, Space Programs Summary 37-61, Vol. III, pp. 93–95, Jet Propulsion Laboratory, Pasadena, Calif., Feb. 20, 1970.
2. Otoshi, T. Y., and Batelaan, P. D., "S/X Band Experiment: Zero Delay Device," in *The Deep Space Network Progress Report*, Technical Report 32-1526, Vol. XIV, pp. 73–80, Jet Propulsion Laboratory, Pasadena, Calif., Apr. 15, 1973.
3. Otoshi, T. Y., "S/X Band Experiment: Zero Delay Device Step Attenuator Evaluation," in *The Deep Space Network Progress Report*, Technical Report 32-1526, Vol. XV, pp. 84–87, Jet Propulsion Laboratory, Pasadena, Calif., June 15, 1973.
4. Brunn, L., private communication, June 1973.

Table 1. Summary of peak group delay changes observed as functions of signal level and temperature

Temperature, °C	Maximum, ns	Minimum, ns	Difference, ns
S-band mean values for signal levels 18 to 58 dB above threshold			
21.0	232.26	230.69	1.57
4.4	231.35	229.23	2.12
34.0	232.29	230.69	1.60
Postcalibration, 21.0	231.07	227.37	3.70
34°C for max; 21°C postcalibration for min	232.29	227.37	4.92
X-band mean values for signal levels 5 to 35 dB above threshold			
21.0	279.08	275.06	4.02
4.4	274.40	272.01	2.39
34.0	276.24	272.89	3.35
Postcalibration, 21.0	273.39	272.07	1.32
21°C for max; 4.4°C for min	279.08	272.01	7.07

Table 2. Summary of group delay system drift tests at strong signal level

Temperature, °C	Initial, ns	Final, ns	Change, ns	Elapsed time, h
S-band mean values for signal level 58 dB above threshold				
21.0	230.75	229.98	0.77	1.1
4.4	229.23	229.41	−0.18	1.3
34.0	230.76	230.60	0.16	1.5
Postcalibration, 21.0	229.32	229.17	0.15	1.3
X-band mean values for signal level 35 dB above threshold				
21.0	277.83	279.39	−1.56	2.1
4.4	273.65	274.40	−0.75	1.3
34.0	274.32	273.06	1.26	2.0
Postcalibration, 21.0	272.90	272.41	0.49	1.1

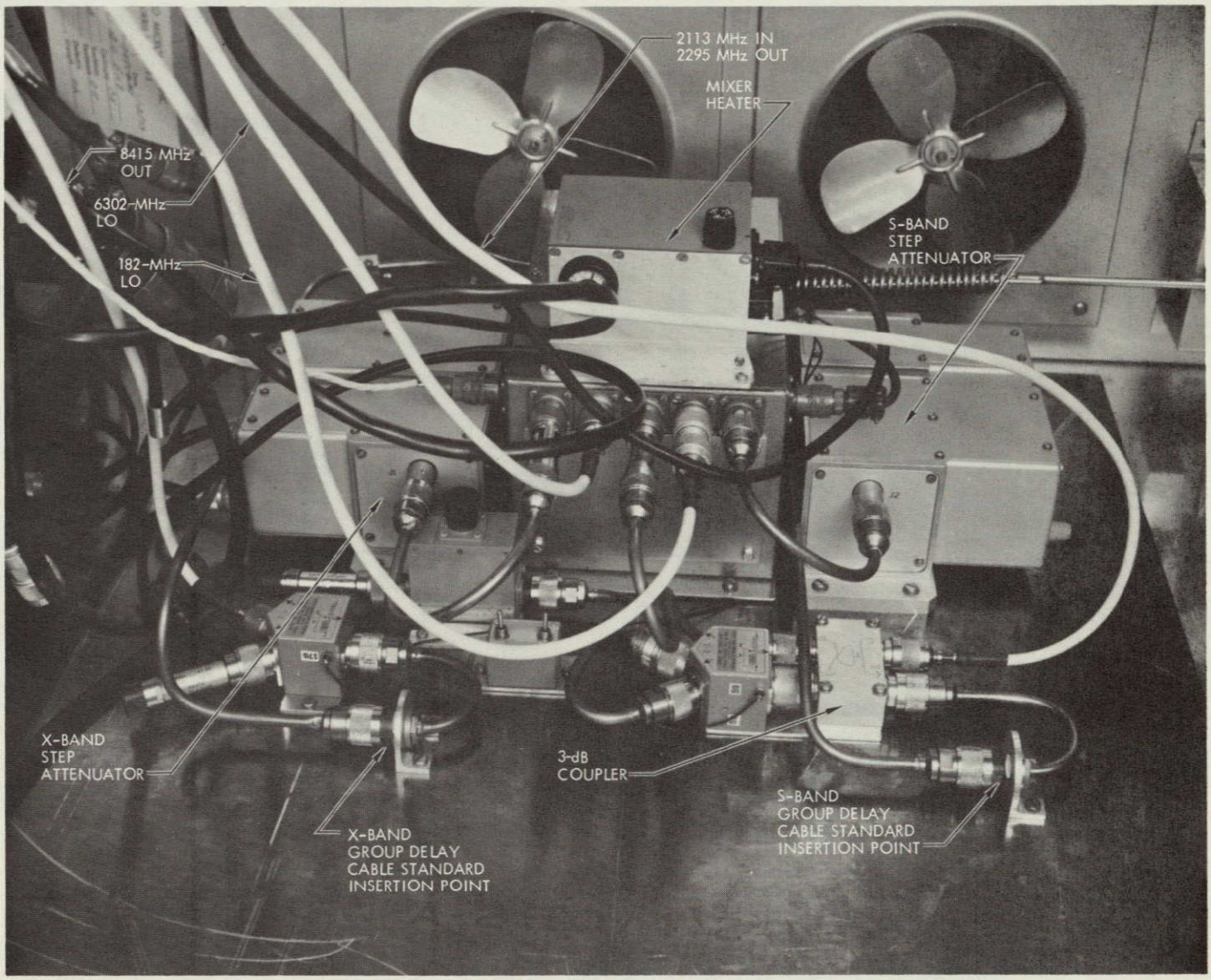

Fig. 1. Modified ZDD assembly in TDL temperature control chamber

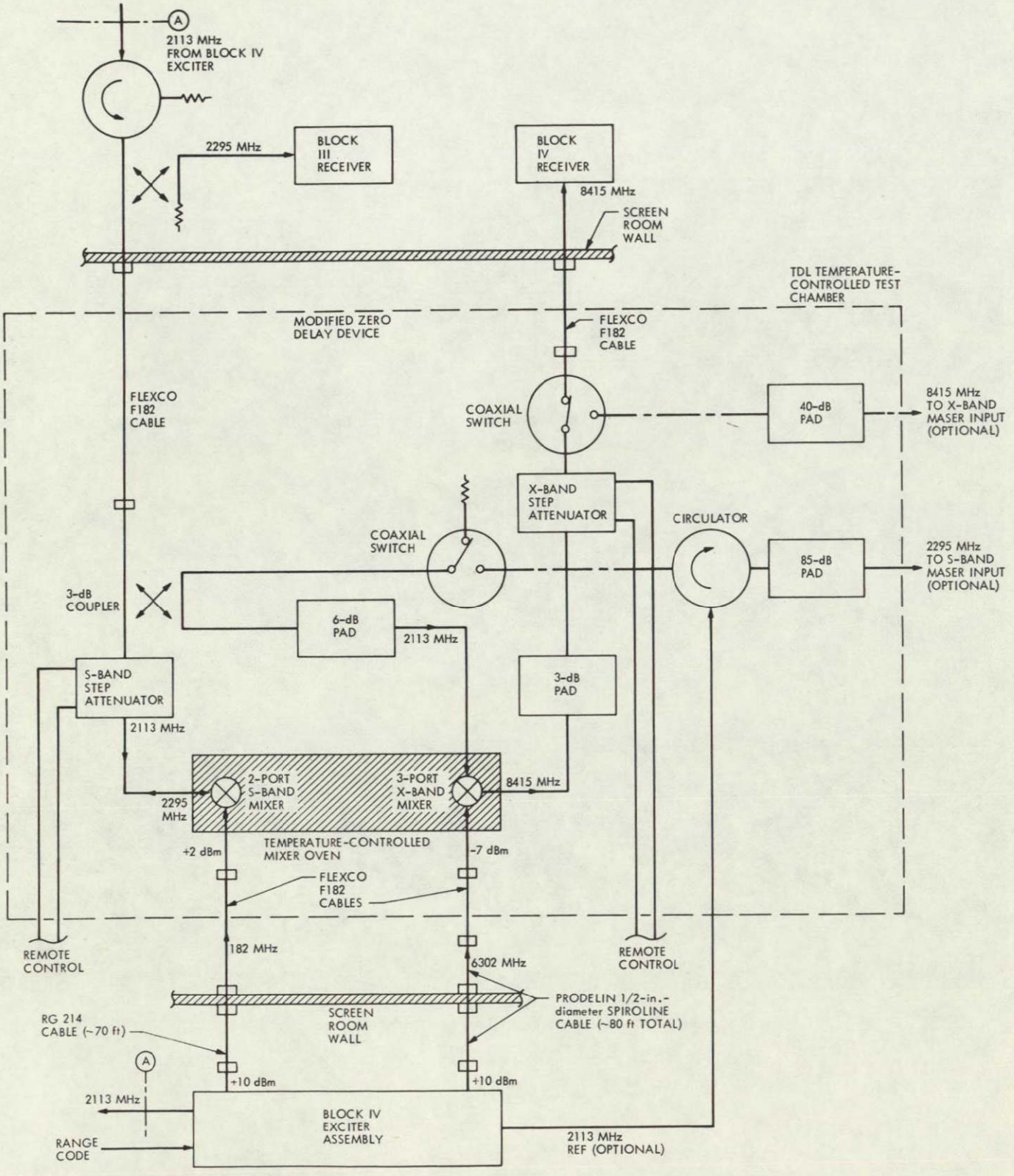

Fig. 2. Block diagram of test setup for ZDD tests at TDL

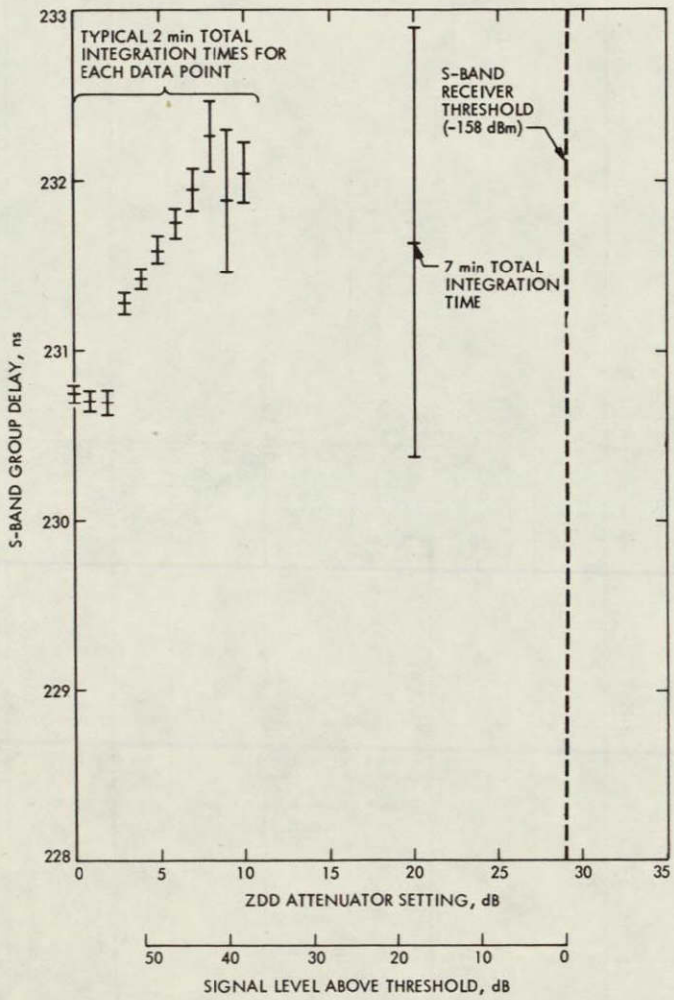

Fig. 3. Total system group delay via the 2113-MHz/2295-MHz path of the ZDD at 21°C

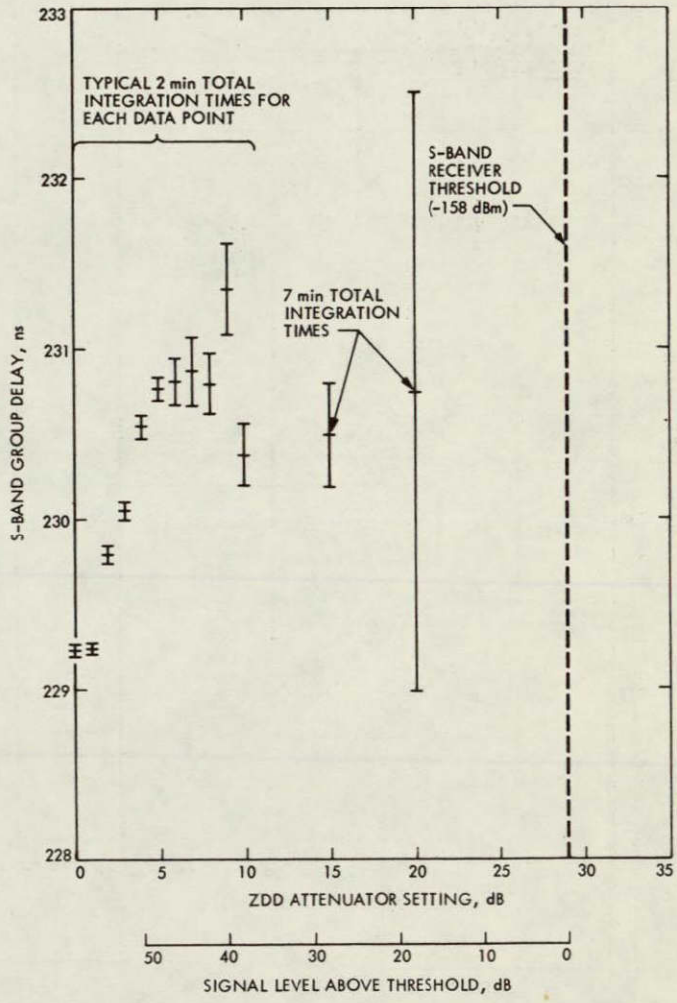

Fig. 4. Total system group delay via the 2113-MHz/2295-MHz path of the ZDD at 4.4°C

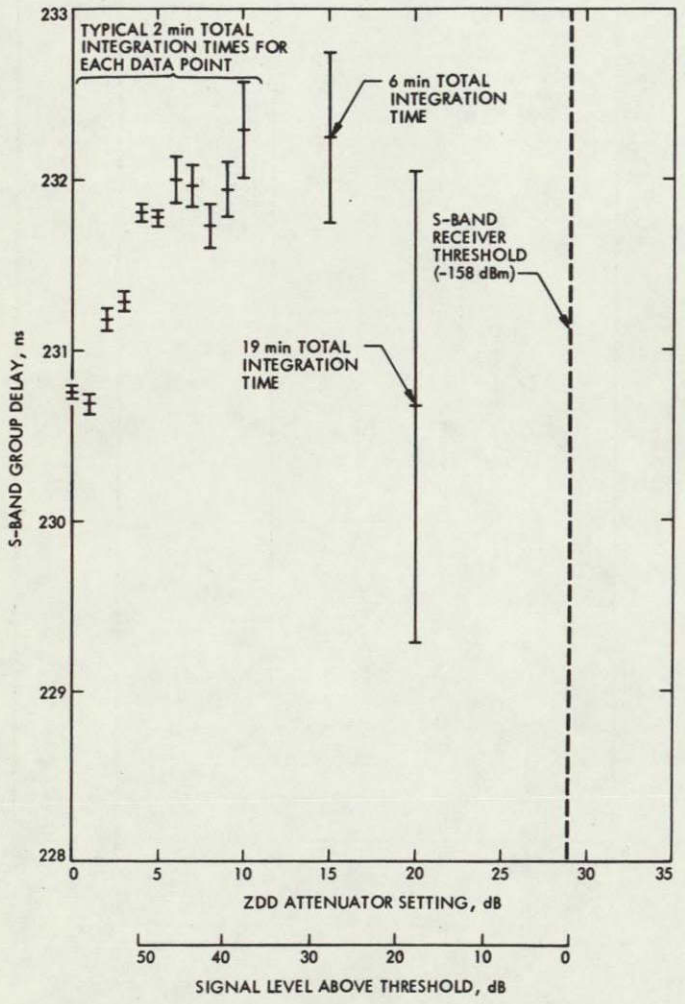

Fig. 5. Total system group delay via the 2113-MHz/2295-MHz path of the ZDD at 34°C

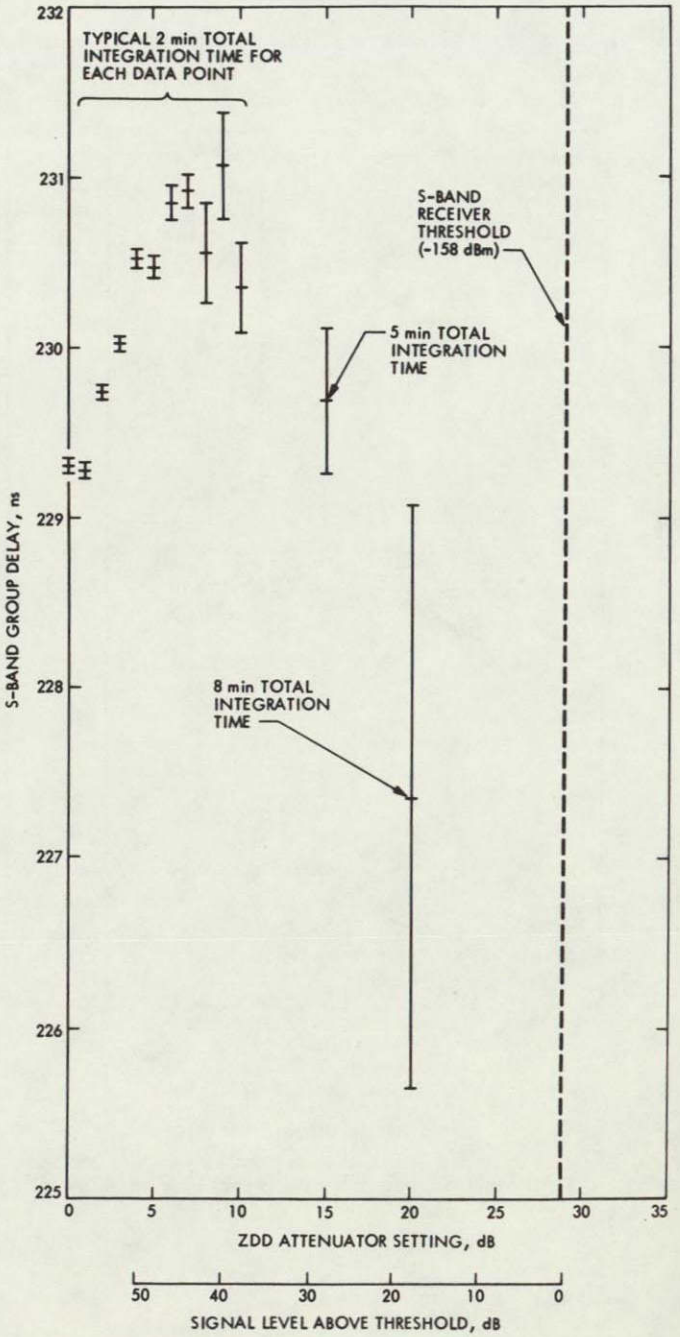

Fig. 6. Postcalibration of the total system group delay via the 2113-MHz/2295-MHz path of the ZDD at 21°C

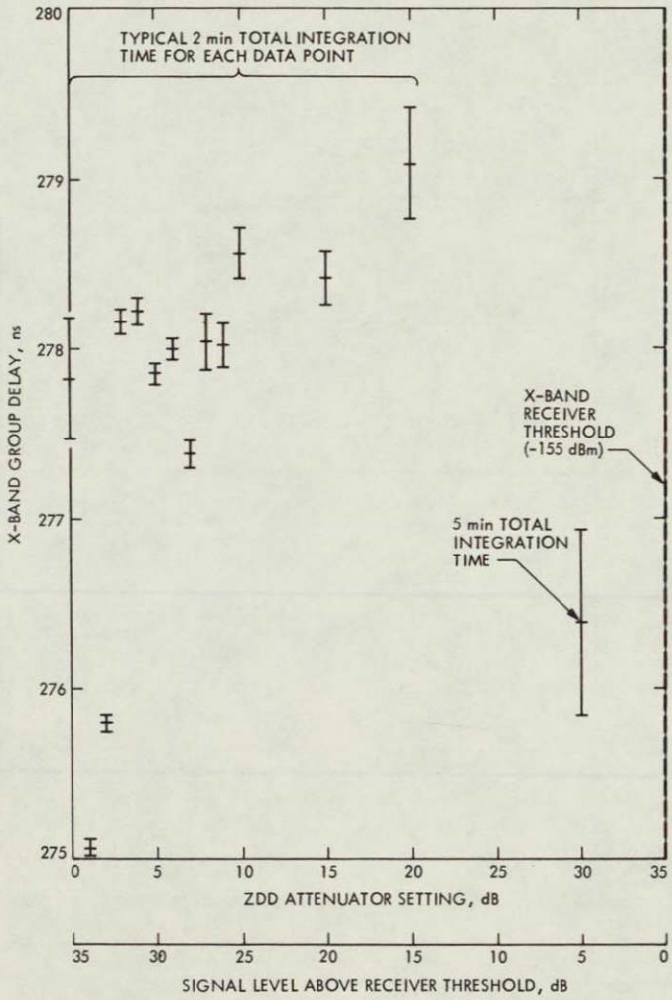

Fig. 7. Total system group delay via the 2113-MHz/8415-MHz path of the ZDD at 21°C

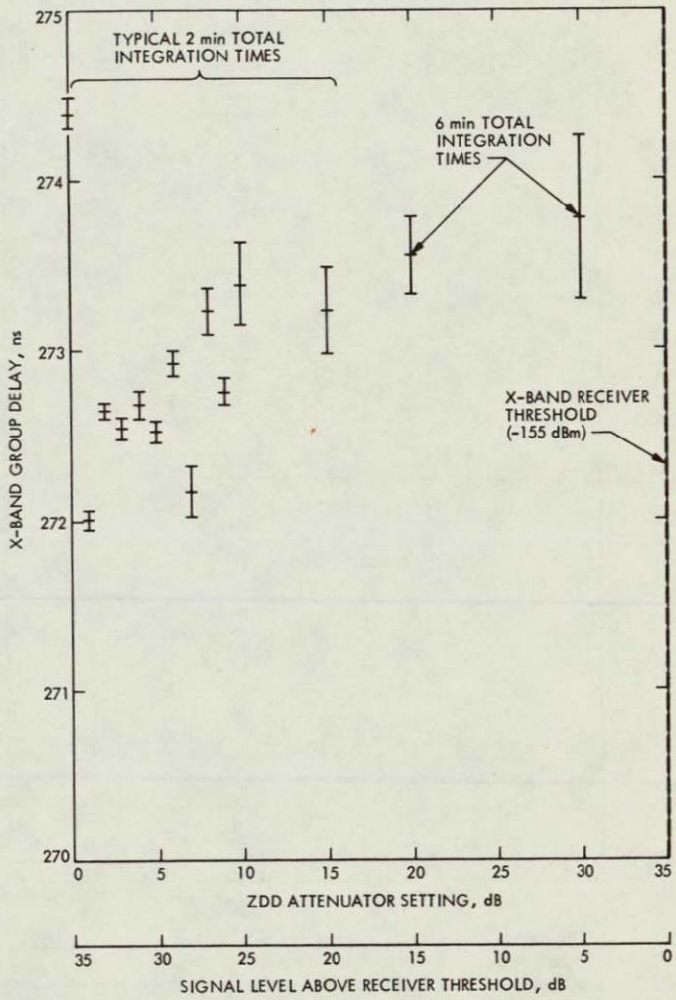

Fig. 8. Total system group delay via the 2113-MHz/8415-MHz path of the ZDD at 4.4°C

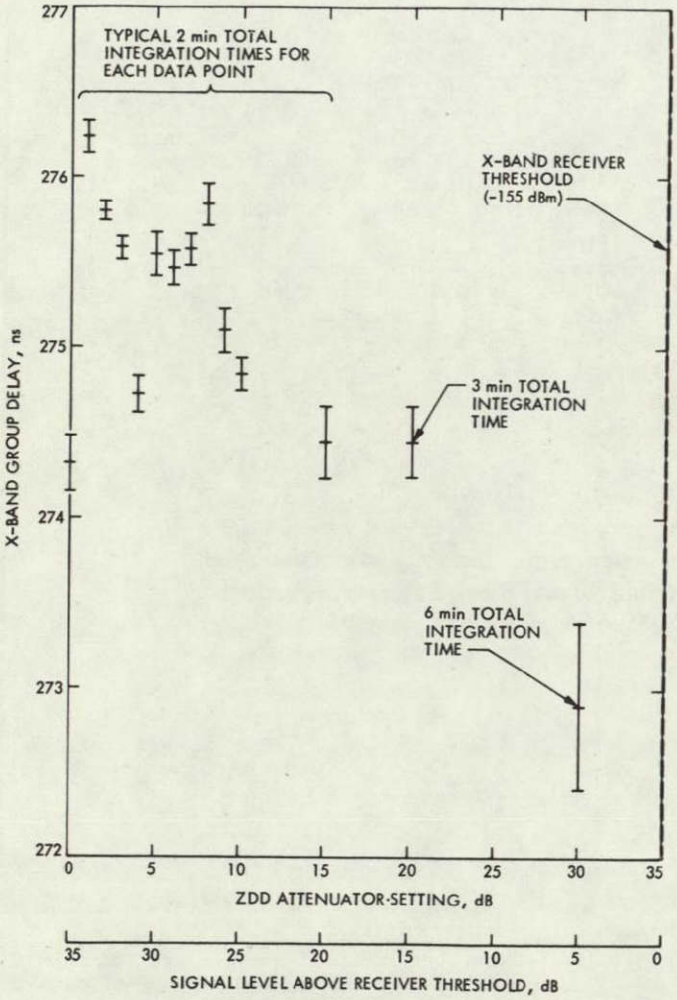

Fig. 9. Total system group delay via the 2113-MHz/8415-MHz path of the ZDD at 34°C

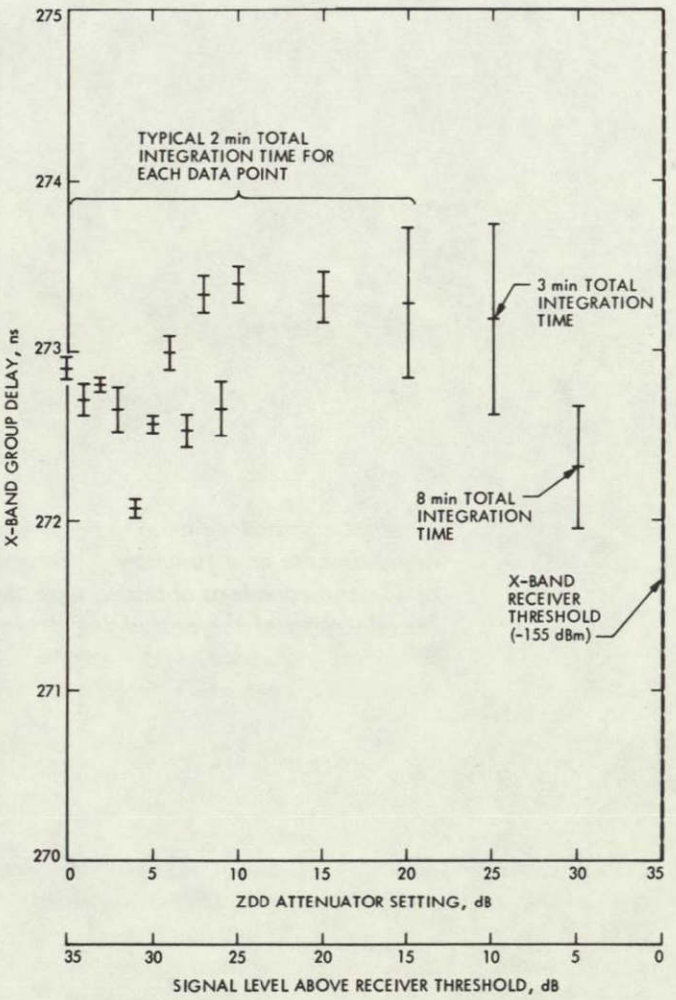

Fig. 10. Postcalibration of the total system group delay via the 2113-MHz/8415-MHz path of the ZDD at 21°C

Reprinted from *The Deep Space Network Progress Report 42-20*, Apr. 15, 1974, pp. 64–68.

S/X Band Experiment: Zero Delay Device Antenna Location

C. T. Stelzried, T. Y. Otoshi, and P. D. Batelaan
Communications Elements Research Section

Representative data are presented for the original Block 3 and Block 4 zero delay devices as a function of antenna elevation angle. Instabilities on the order of 33 nanoseconds as obtained with the original S-band Block 3 system are reduced by relocation of the zero delay device (ZDD) horn. However, unsatisfactory performance at X-band for the Mariner Venus/Mercury 1973 (MVM'73) S/X experiment ZDD requires a reconfiguration eliminating the horns and associated air path.

I. Introduction

The S/X-band experiment (Ref. 1) requires a zero delay device (ZDD) for routine calibrations and receiving system performance verification tests. The Block 4 ZDD (Ref. 2) developed for the S/X-band experiment is an antenna-mounted transponder that receives an uplink signal of 2113 MHz and reradiates downlink signals of 2295 and 8415 MHz. It utilizes the Mu-2 ranging and Block 4 receiving systems.

This article presents results of some preliminary tests at S-band made to determine the Block 3 ZDD range change sensitivity to antenna tipping and horn location. In addition, the Block 4 ZDD performance at both S- and X-band with antenna tipping is presented. Figure 1 shows the DSS 14 64-m antenna and indicates the various test locations for the ZDD on the dish surface (positions 1-3) and the ZDD installation exterior to the Mod 3 area (position 4).

II. Test Setup

A series of S-band tests was performed on the 64-m antenna at DSS 14 from August 1972 to January 1973 to evaluate the performance of the ZDD. Three test setups were as follows:

(1) The S-band Block 3 ZDD was used and consisted of an open-ended WR 430 waveguide/type N coaxial transition and a mixer diode. The local oscillator (LO) frequency of 181 MHz was supplied by the Block 3 receiver/exciter assembly, and ranging was done with the Mu-1 ranging system. The ZDD was first mounted on the 64-m antenna surface near the base of a quadripod leg (Fig. 1, position 1). This location has been used in conjunction with Mu-1 ranging for previous flight missions. The ZDD was then moved to other locations (Fig. 1, positions 2, 3) and tested. The polarization diversity S-band (PDS) cone diplex system and PDS maser were used for this test setup.

(2) The second test setup involved radiating from the PDS cone and receiving with several types of small antennas at a location exterior to the roof of the Mod 3 level (Fig. 1, position 4). Relative phase was measured with a network analyzer, and range was determined by a frequency variation method.

(3) The third test configuration may be seen in Fig. 2. In this test configuration the Block 4 ZDD is installed at a location exterior to the Mod 3 level, below and near the roof ladder access hatch (Fig. 1, position 4). The ZDD is enclosed in a special RF-shielded welded box with remotely controllable lid for RF noise burst suppression. The location for this configuration was selected on the basis of results obtained in the above test setups. This location has the added advantage that the source of the LO frequencies is physically close to the ZDD from the Mod 3 area, thus resulting in greater phase stability.

III. Test Results

Ranging stability using the Block 3 ZDD was found to be very sensitive to antenna elevation angle. Data were typically taken at 10-deg increments of elevation angle. A summary of the data is shown in Table 1. In addition, a test was performed using the Block 3 translator, which bypasses the transmitter and air path completely. Approximately 1 nanosecond of range change was measured with antenna tipping indicating good stability of the overall maser/receiver system. These data indicate that the location of the ZDD "antennas" is a key factor in determining the magnitude of the instabilities, which are presently assumed to be due to elevation-dependent multipath phenomena.

The comparable results for Tests 1 and 6 are to be noted in that they were made at different times with independent equipment and measurement setups but at the same location (Fig. 1, position 4).

Figure 3 shows the system ranging performance for the dual channel S- and X-band systems using Block 4 receivers and the Mu-2 ranging system with the ZDD mounted in the shielded box (Fig. 1, position 4) and with the S/X reflex feed system installed. Considering the large instability with elevation angle at X-band and the requirement to provide a stable calibration system for the MVM'73 S/X experiment, it was decided to modify the original ZDD block diagram. This was accomplished by bypassing the horns and providing the 2113 MHz from a directional coupler on the transmitter output and injecting the S (2295-MHz) and X (8415-MHz) signals directly into the respective masers via waveguide couplers and semirigid cables. This configuration eliminated the assumed multipath-originated range instabilities (Ref. 4).

IV. Conclusions

Tests for proper location of a ZDD were conducted only at S-band frequency and before installation of the S/X reflex feed mechanisms. These tests indicated that, under those conditions, the location exterior to the Mod 3 level would be satisfactory.

Based on these data, the Block 4 ZDD was installed at the Mod 3 location in the shielded RF box. After installation of the Block 4 receiver/exciter, Mu-2 ranging and the S/X reflex feed, tests showed that the location, while acceptable for S-band, was not acceptable for X-band. This required a reconfiguration eliminating the horns and associated air path.

References

1. Levy, G. S., et al., "RF Techniques Research: S/X Band Experiment," in *The Deep Space Network*, Space Programs Summary 37-61, Vol. III, p. 93, Jet Propulsion Laboratory, Pasadena, Calif., Feb. 1970.

2. Otoshi, T. Y., and Batelaan, P. D., "S/X Band Experiment: Zero Delay Device," in *The Deep Space Network Progress Report*, Technical Report 32-1526, Vol. XIV, pp. 73–80, Jet Propulsion Laboratory, Pasadena, Calif., Apr. 15, 1973.

3. Otoshi, T. Y., and Batelaan, P. D., "S/X Band Experiment: Preliminary Tests of the Zero Delay Device," in *The Deep Space Network Progress Report*, Technical Report 32-1526, Vol. XVII, pp. 68–77, Jet Propulsion Laboratory, Pasadena, Calif., Oct. 15, 1973.

4. Otoshi, T. Y., and Stelzried, C. T., "S/X Band Experiment: A New Configuration for Ground System Range Calibrations with the Zero Delay Device," in *The Deep Space Network Progress Report*, Technical Report 42-20, Jet Propulsion Laboratory, Pasadena, Calif., Apr. 15, 1974 (this issue).

Table 1. Summary of DSS 14 zero delay device performance in S-band antenna tipping tests

Test	Description	pk/pk range variation with antenna elevation angles between zenith and 11 deg, ns
1	Test setup 2 (Fig. 1, position 4)	<1
2	Test setup 1, Block 3 ZDD, original position (Fig. 1, position 1)	33
3	Test setup 1, Block 3 ZDD (Fig. 1, position 2)	6
4	Test setup 1 Block 3 ZDD (Fig. 1, position 3), 1.5 panels from antenna edge	15
5	Test setup 1, Block 3 ZDD, Mod 3 location (Fig. 1, position 4)	13
6	Test setup 1, same as Test 5 except pyramidal horn added to Block 3 ZDD	3

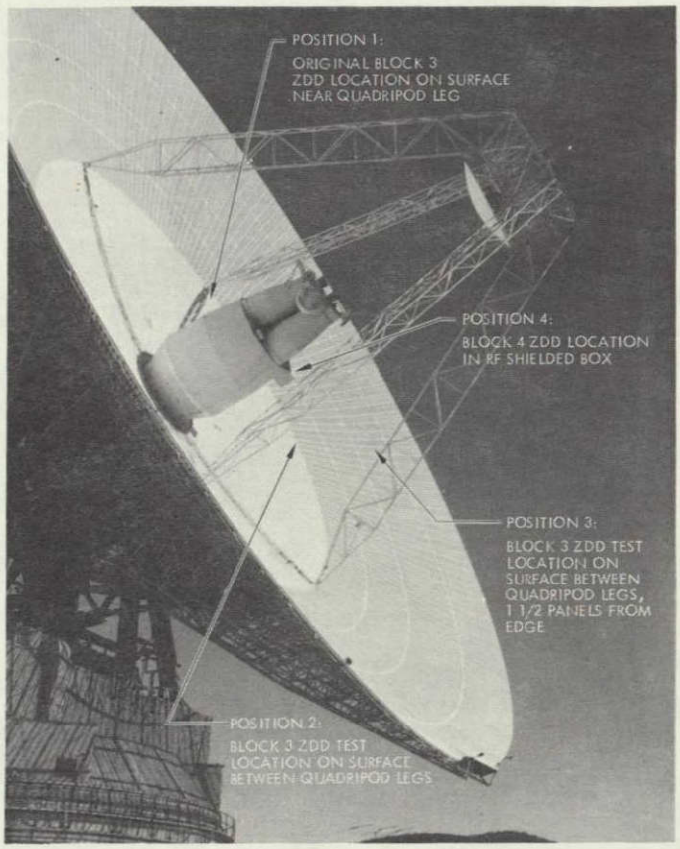

Fig. 1. DSS 14 64-m antenna showing various locations of ZDD test positions (1 through 3) and RF shielded box (position 4) used for the Block 4 ZDD installation

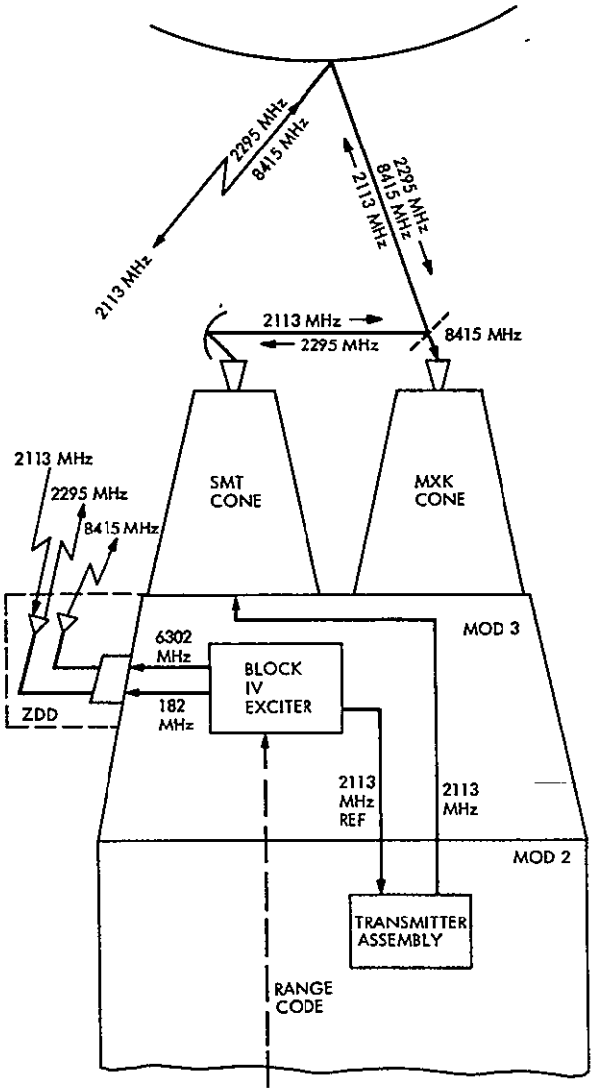

Fig. 2. Simplified block diagram of the original ZDD calibration system for S/X-band experiment

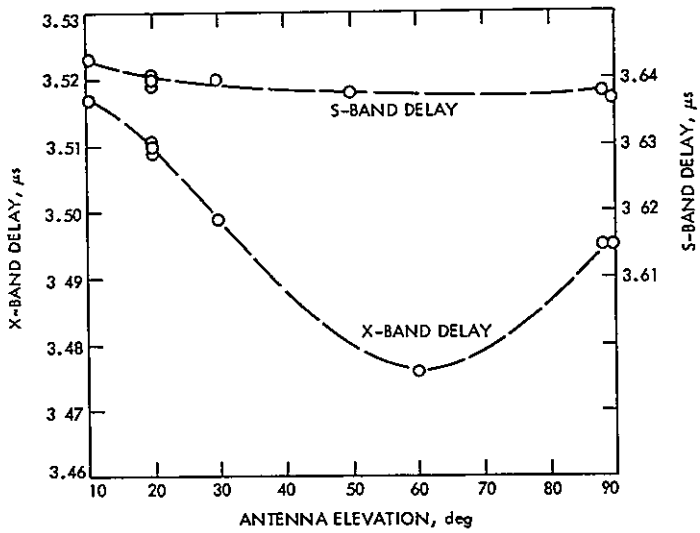

Fig. 3. DSS 14 dual-channel S/X-band ranging on the ZDD as a function of antenna elevation angle using the Block 4 ZDD (Fig. 1, position 4)

Reprinted from *The Deep Space Network Progress Report 42-20*, Apr 15, 1974, pp 57–63

S/X Experiment: A New Configuration for Ground System Range Calibrations With the Zero Delay Device

T. Y. Otoshi and C. T. Stelzried
Communications Elements Research Section

A new configuration for ground system range calibrations with the zero delay device (ZDD) was recently implemented at DSS 14 for the S/X experiment. In this new configuration, the original ZDD horns and associated air paths are eliminated. The uplink test signal is now coupled out of the transmitter waveguide path and brought directly to the ZDD by calibrated cables of known delays The downlink signals generated by the ZDD are injected directly into the masers via calibrated cables and waveguide couplers Preliminary tests on the new system indicate that, in the absence of the air path, the ground system range change as a function of antenna elevation angle is typically less than 3 ns at S-band and X-band.

I. Introduction

With the exception of DSS 14, all stations of the Deep Space Network use the conventional zero delay ranging configuration, in which the zero delay device (ZDD) is mounted on the dish surface A zenith range measurement to a dish-mounted ZDD and a simple Z-height correction (Ref 1) should provide all of the needed ground station information for determining the true range to the spacecraft However, as was pointed out in a separate article (Ref. 2) in this volume, results of tests showed that large changes in range occurred as a function of antenna elevation angle when a ZDD was placed on the 64-m antenna dish surface Since the changes could be due to a multipath phenomenon, one cannot assume that a zenith measured value is the correct value. It was further reported in Ref. 2 that a satisfactory location in the Mod-3 area was found for the ZDD at S-band, but the performance at X-band was unsatisfactory.

Because of the described problems with the conventional ZDD configuration, it was proposed by G. S. Levy that, for the S/X experiment, the ZDD horns and associated air paths be eliminated and replaced by semirigid cables This article describes the new configuration and presents results of some preliminary tests

II. New Configuration

A block diagram of the current ZDD calibration system at DSS 14 may be seen in Fig 1. This new configuration was installed on the 64-m antenna system at DSS 14 on January 12, 1974.[1] In this new configuration, the uplink 2113-MHz signal is now sampled from a directional coupler in the waveguide transmit line and carried directly to the ZDD by coaxial cables of known delay. The downlink signals of 2295 and 8415 MHz generated by the ZDD are carried by calibrated cables and injected directly into the respective S- and X-band masers via directional couplers. Figure 2 shows the block diagram of the ZDD assembly as presently modified for this new configuration. The original block diagram for the ZDD was previously shown in Refs 3 and 4

The main disadvantage of the new method is that, by elimination of the air path, one is not able to use the ZDD to detect problems which might occur in the microwave optics subsystem. With the new ZDD configuration, one is restricted to testing only the portion of the ground

[1]A previous similar configuration was installed on December 20, 1973, but is not described in this article This previous system could only be used with the 20-kW transmitter.

system that includes the transmitter, masers, Block 4 receivers, and associated waveguide and cable paths. A second disadvantage of the new method is that there is no longer just a simple Z-height correction that must be added to the measured ZDD range value. As described in an article elsewhere in this volume (Ref. 5), the new Z-correction now requires knowledge of range delays in all portions of the uplink and downlink signal paths that are not mutually common to the "Range-on-ZDD" path and "Range-on-Spacecraft" path as defined up to the antenna bench mark. Knowledge of these delays requires (1) group delay calibrations of cables to and from the ZDD, (2) group delay calibrations of portions of the transmit/receive waveguide paths, and (3) calculations of air path delays via the microwave optics path. A tabulation of the delays as calibrated with a phase-locked network analyzer system is presented in Table 1 for the DSS 14 ground system depicted in Fig. 1. It should be pointed out that any new equipment installation in the paths described in Table 1 will invalidate the calibrations.

The advantage of the new method is that the range and phase calibrations will be more stable and repeatable. As will be shown later, the range delay variation with antenna tipping is very small. A second advantage is that a theoretically calculated air path delay should be more accurate than a ZDD measured value which is apparently corrupted by multipath effects A theoretical analysis can account for the total integrated effects of a far-field illuminator and therefore more closely represent the actual spacecraft range configuration. The elevation angle dependence of range to quadripod blockage, reflector surface distortions and sagging, reflections from antenna-mounted structures, and subreflector defocussing can be studied analytically.

III. Test Results

Figures 3 and 4 show preliminary results of range tests on the new ZDD configuration using the 100- and 20-kW transmitters, respectively. It can be seen that the maximum range change with elevation angle was about 3 ns for S-band and X-band. Additional tests showed that insignificant changes of range occurred as functions of azimuth angles for either the S- or X-band system. These preliminary test results indicate that the group delays of the transmitters, masers, Block 4 receivers, and associated cabling are nearly insensitive to antenna motion.

The ZDD was also used to test the doppler phase stability of the S- and X-band systems as functions of antenna tipping The peak phase changes due to doppler phase jitter and antenna tipping were typically found to be less than ± 30 deg for S-band and X-band Some of the phase changes that were observed could be attributed to the quantization error of the S/X doppler resolvers. The peak error due to the resolvers is about ± 18 deg for a 5-MHz biased doppler. It should be pointed out again that the measured values do not include possible changes in the air path.

IV. Conclusions

The new ZDD configuration using cable paths rather than the air paths has been found to be virtually insensitive to antenna motion. This new configuration therefore appears to be superior to the original system in terms of repeatability. Since the new configuration does not include the air path, the effects of antenna sag on range and phase stability must now be determined theoretically.

At present the ZDD range values are being taken with the antenna at zenith during the precalibration and postcalibration periods of the Mariner 10 spacecraft tracking passes. Over a period of about 30 days, the differential S/X ZDD range appears to be stable to within 10 ns. The long-term absolute group delay instabilities are about two times greater. An attempt is being made to analyze the changes and correlate them with ambient temperature, maser gain, and Block 4 equipment modifications.

References

1. *TRK-2-8 Module of DSN System Requirements Detailed Interface Design Document 820-13, Rev. A*, Jet Propulsion Laboratory, July 1, 1973 (JPL internal document).

2. Stelzried, C. T., Otoshi, T. Y., and Batelaan, P. D., "S/X Band Experiment: Zero Delay Device Location," in *The Deep Space Network Progress Report*, Technical Report 42-20, Jet Propulsion Laboratory, Pasadena, Calif., Apr. 15, 1974 (this issue).

3. Otoshi, T. Y., and Batelaan, P. D., "S/X Band Experiment: Zero Delay Device," in *The Deep Space Network Progress Report*, Technical Report 32-1526, Vol. XIV, pp. 73–80, Jet Propulsion Laboratory, Pasadena, Calif., Apr. 15, 1973.

4. Otoshi, T Y , and Batelaan, P. D., "S/X Band Experiment: Preliminary Tests of the Zero Delay Device," in *The Deep Space Network Progress Report*, Technical Report 32-1526, Vol XVII, pp. 68–77, Jet Propulsion Laboratory, Pasadena, Calif , Oct 15, 1973.

5. Batelaan, P. D., "S/X Band Experiment: Zero Delay Device Z Corrections," in *The Deep Space Network Progress Report*, Technical Report 42-20, Jet Propulsion Laboratory, Pasadena, Calif , Apr. 15, 1974 (this issue).

Table 1. Summary of group delay measurements pertinent to DSS 14 Z-corrections for the new ZDD configuration implemented on January 12, 1974

Input port (Figs. 1 and 2)	Output port (Figs 1 and 2)	Measured group delay, ns
2′	A	42 35 ±0 09 (1σ)
A	B	14 11 ±0.76 (1σ)
B	4	87 38 ±0 12 (1σ)
A	C	9 49 ±0 80 (1σ)
C	7	70 63 ±0 10 (1σ)
2′	3	32 77 ±0 08 (1σ)
3	4	37 57 ±0.12 (1σ)
6	7	0 91 ±0.03 (1σ)

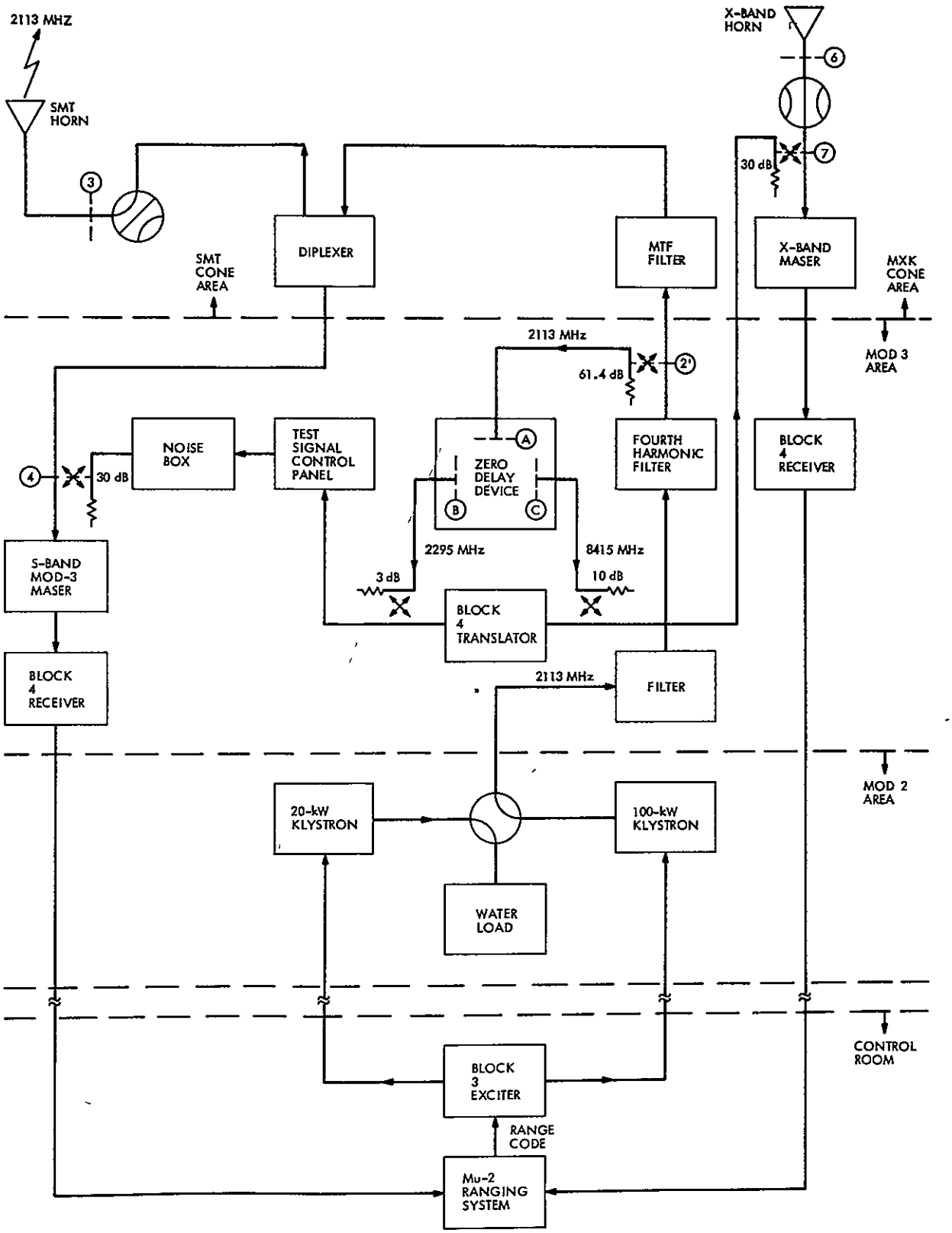

Fig. 1. Block diagram of the new configuration at DSS 14 for ground system range calibrations

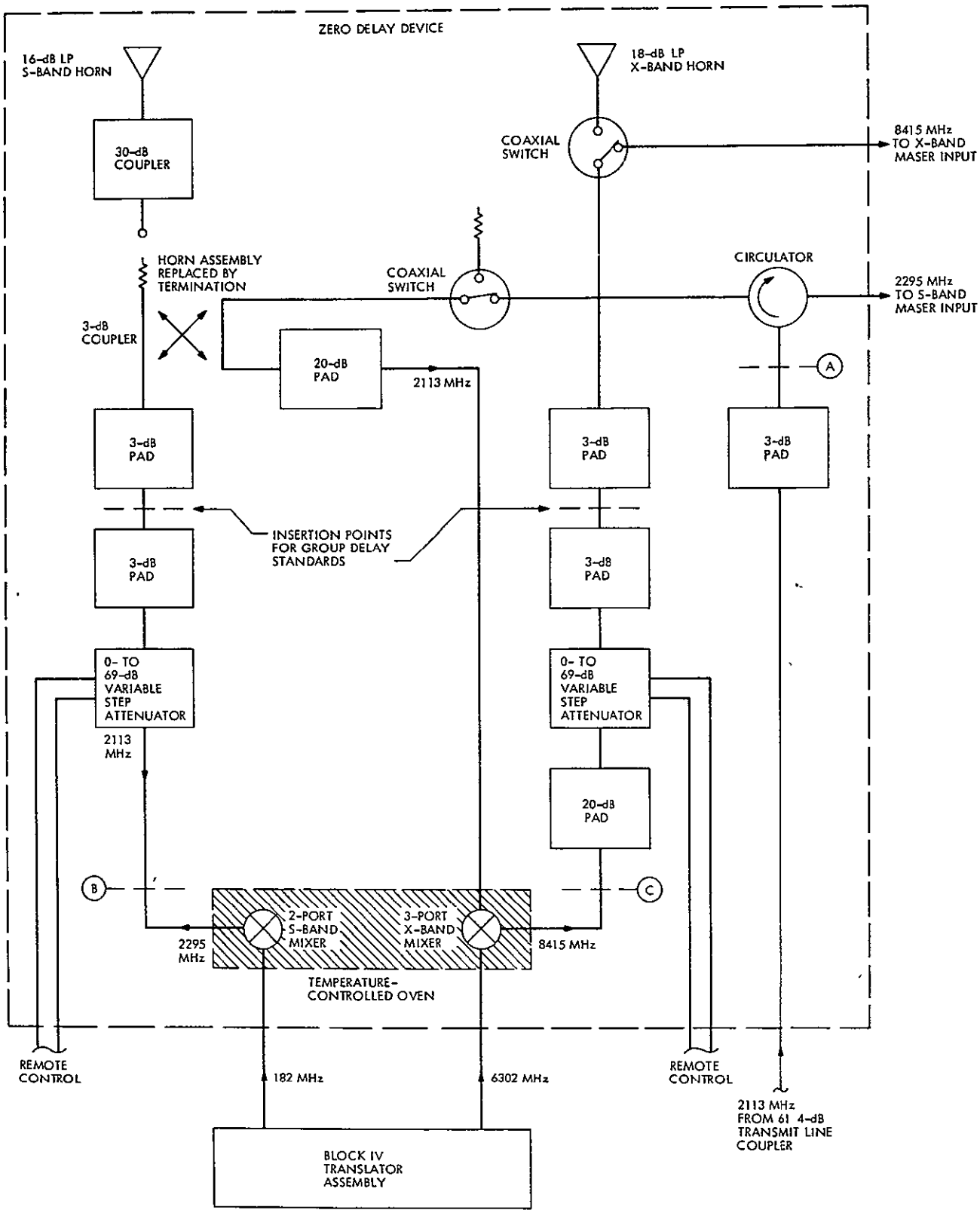

Fig. 2. Block diagram of the current zero delay device assembly at DSS 14

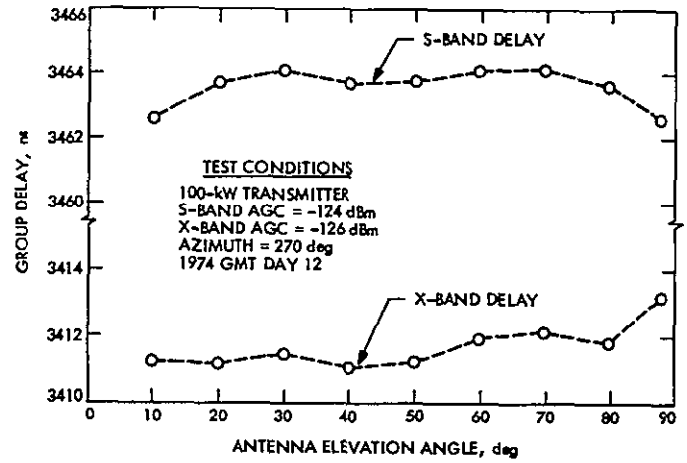

Fig. 3. Range delay as a function of elevation angle using the new ZDD configuration and the 100-kW transmitter

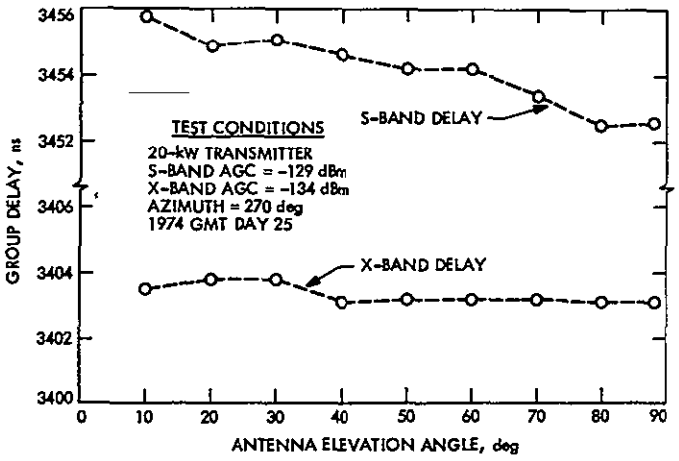

Fig. 4. Range delay as a function of elevation angle using the new ZDD configuration and the 20-kW transmitter

Reprinted from *The Deep Space Network Progress Report 42-20,* Apr 15, 1974, pp 78–83

S/X-Band Experiment: Zero Delay Device Z Correction

P. D. Batelaan
Communications Elements Research Section

A new dual-frequency (S-band and X-band) zero delay device (ZDD) was required for the MVM'73 S/X experiment at DSS 14 To properly utilize the "zero" calibration provided by the ZDD, an evaluation of the "Z" term in the ranging equations must be made An equation for this term is derived, and values are determined for several configurations

I. Introduction

A new dual frequency (S-band and X-band) zero delay device (ZDD) was required for the MVM'73 S/X experiment at DSS 14 (Refs 1, 2) [1] To properly utilize the "zero" calibration provided by the ZDD, an evaluation of the Z term in the ranging equations must be made (Ref 3) An equation for this term is derived and values are determined for several configurations

[1]Discussions of the preliminary location tests and calibration of this ZDD are presented by C. T Stelzried, et al and by T Y Otoshi and C T Stelzried elsewhere in this issue

II. Discussion

By referring to Figs. 1 and 2, it is possible to write an equation for the ranging machine "gross indicated" value of round-trip light time (RTLT) while tracking the spacecraft:

$$A_{S/C\,(S)} = [B_U + B'_U + C_U - D + E_S] + F_S + [E_S - D + C_{DS} + B'_{DS} + B_{DS}] \quad \text{(S-band)} \tag{1}$$

where

$A_{S/C}$ = ranging machine "gross indicated" round-trip light time while locked on the spacecraft (S/C), i.e., time for a signal to go from the ranging machine, through the complete system and back to the ranging machine[2]

B_U = time for a signal to travel from the ranging machine to the uplink sampling point for the ZDD

B'_U = time for a signal to travel from the uplink sampling point for the ZDD to the radio frequency (RF) ϕ center of the ground antenna feed horn

C_U = time for a signal to travel from the feed-horn phase center, through the dichroic feed system, subreflector and parabolic surface to the aperture plane of the paraboloid

D = distance (in equivalent time units) between the aperture plane and the antenna "bench mark"[3]

E = time for a signal to travel between the ground antenna bench mark and the spacecraft antenna aperture plane

F = two-way or round trip time for a signal to travel from the S/C antenna aperture plane, through the S/C radio subsystem and return to the S/C aperture plane

B'_D = time for a signal to travel from the RF ϕ center of the ground antenna feed horn to the ZDD simulated downlink injection point

B_D = time for a signal to travel from the ZDD simulated downlink injection point to the ranging machine

Subscripts U and D indicate uplink and downlink, respectively, and S indicates S-band X will indicate X-band Where no S or X designation appears, the terms are identical for S- and X-band signals.

A similar equation may be written for X-band·

$$A_{S/C\,(X)} = [B_U + B'_U + C_U - D + E_S] + F_X + [E_X - D + C_{DX} + B'_{DX} + B_{DX}] \quad \text{(X-band)} \tag{2}$$

[2]"Times" discussed here mean equivalent free-space light times

[3]For DSS 14, the "bench mark" designated here is the intersection of the azimuth and elevation axes

Similarly, equations can be written for the ranging machine "gross indicated" value of round-trip light time while "tracking" the ZDD:

$$A_{ZDD\,(S)} = [B_U + G_U] + H_S + [G_{DS} + B_{DS}] \tag{3}$$

$$A_{ZDD\,(X)} = [B_U + G_U] + H_X + [G_{DX} + B_{DX}] \tag{4}$$

where

A_{ZDD} = ranging machine "gross indicated" round-trip light time while locked on ZDD, i.e., time for a signal to go from the ranging machine, through the complete system and back to the ranging machine

G_U = time for a signal to travel from the uplink sampling point to the input port of the ZDD

H = two-way or round-trip time for a signal to travel from the ZDD input port through the ZDD and back to the appropriate output port

G_D = time for a signal to travel from the ZDD output port to the appropriate downlink injection point

Now, subtract Eq (3) from Eq (1) and combine terms

$$A_{S/C\,(S)} - A_{ZDD\,(S)} = B'_U + B'_{DS} + C_U + C_{DS} - 2D + E_S + E_S + F_S - [G_U + G_{DS} + H_S] \tag{5}$$

Rearrange

$$(E_S + E_S) = A_{S/C\,(S)} - A_{ZDD\,(S)} - F_S + [-(B'_U + B'_{DS} + C_U + C_{DS}) + 2D + G_U + G_{DS} + H_S] \tag{6}$$

The corresponding X-band equation is

$$(E_S + E_X) = A_{S/C\,(X)} - A_{ZDD\,(X)} - F_X + [-(B'_U + B'_{DX} + C_U + C_{DX}) + 2D + G_U + G_{DX} + H_X] \tag{7}$$

Now, compare Eqs. (6) and (7) with the R/D S/X ranging equation (repeated here for convenience) of Ref. 3.

$$RTLT = RU\frac{1}{(128)(48)F_T} + M\frac{64 \times 2^N}{3F_T} - BIAS_{DSN}\frac{1}{(128)(48)F_T} - BIAS_{S/C} + Z \tag{8}$$

The results of this comparison, term by term, are

$$(E + E) = \text{RTLT} \tag{9}$$

$$A_{S/C} = RU\frac{1}{(128)(48)F_T} + M\frac{64 \times 2^{\lambda}}{3F_T} \tag{10}$$

$$A_{ZDD} = BIAS_{DSN}\frac{1}{(128)(48)F_T} \tag{11}$$

$$F = BIAS_{S/C} \tag{12}$$

and finally,

$$[-(B'_U + B'_D + C_U + C_D) + 2D + G_U + G_D + H] = Z \tag{13}$$

(The frequency subscripts S and X have been omitted for convenience as the comparison applies to both frequencies.)

Some comments on the terms comprising the expression for Z are in order:

(1) The term C has the effect of moving the RF reference point from the ground antenna appropriate feed horn phase center to the aperture plane.

(2) Then, the term D further moves the resulting RF reference from the aperture plane to the "bench mark"

(3) The terms $(-B'_U + G_U)$ and $(-B'_D + G_D)$ compensate for the fact that the ZDD is not at the ground antenna feed horn phase center when taking a "zero delay" reading

(4) Finally, term H is exactly analogous to the S/C term F where each corrects for the signal turnaround time of its appropriate device.

The differential $(S) - (X)$ Z term can be determined simply by subtracting the S and X forms of equation (13), the Z equation:

$$Z_S - Z_X = -(B'_{DS} - B'_{DX} + C_{DS} - C_{DX} - G_{DS} + G_{DX} - H_S + H_X) \tag{14}$$

Notice that since uplink terms are common to both S- and X-band signals, virtually all of them have dropped out of the differential $(S) - (X)$ Z term

References

1. Otoshi, T. Y, and Batelaan, P D., *S/X-Band Experiment Zero Delay Device,* Technical Report 32-1526, Vol. XIV, pp. 78–80, Jet Propulsion Laboratory; Pasadena, Calif., Apr. 15, 1973
2. Otoshi, T. Y., and Batelaan, P. D, *S/X Experiment: Preliminary Tests of the Zero Delay Device,* Technical Report 32-1526, Vol. XVII, pp. 68–77, Jet Propulsion Laboratory, Pasadena, Calif., Oct. 15, 1973.
3 DSN System Requirements Document 820-13, Rev. A, Detailed Interface Design, TRK-2-8, pg. 20, paragraph 3
4. Otoshi, T. Y., and Stelzried, C T., "S/X Experiment: A New Configuration for Ground System Range Calibrations with the Zero Delay Device," (this issue).
5. Private communication, D. Bathker to P. Batelaan, 1/11/74.
6. Private communication, Smoot Katow to P. Batelaan, 11/14/73.

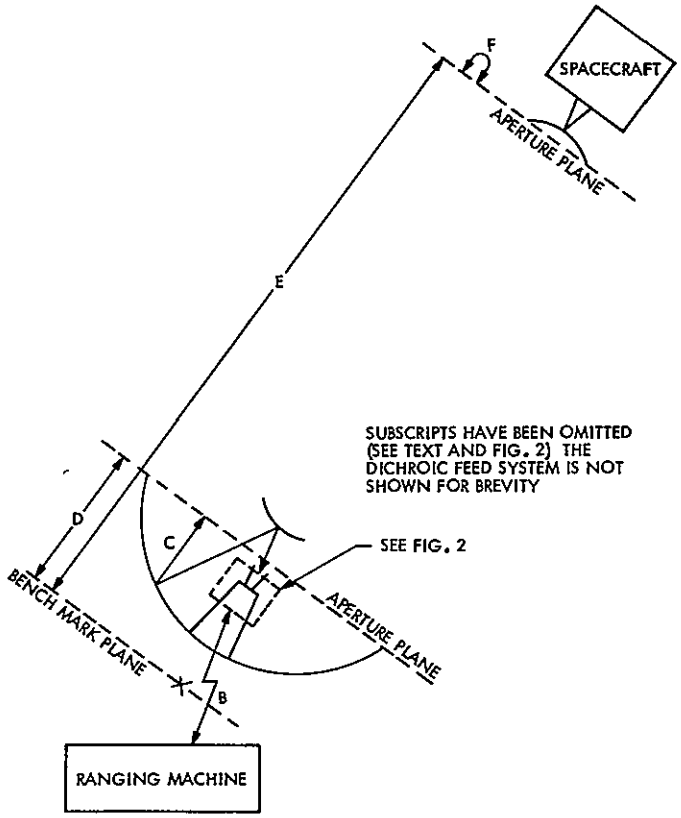

Fig. 1. Overall ranging path

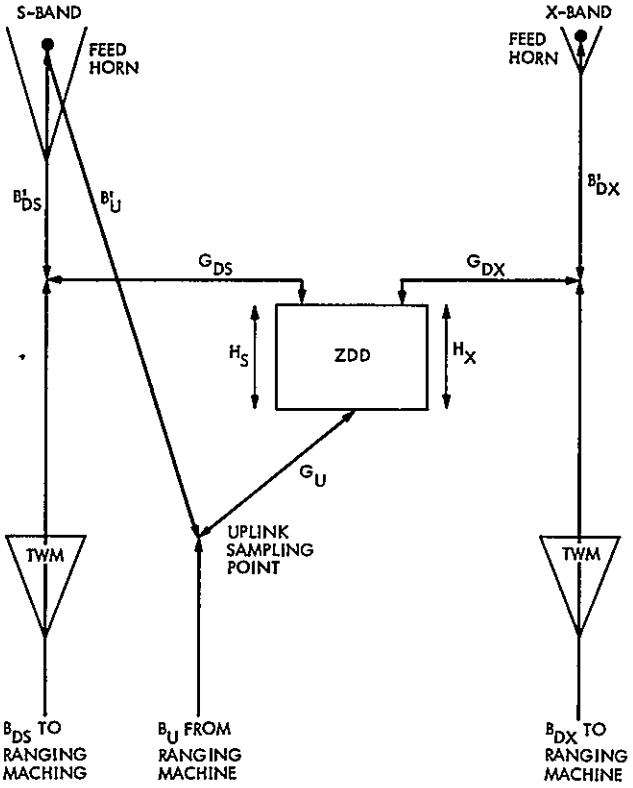

Fig. 2. Detail ranging path

Appendix A
Values of Z_S and Z_X for DSS 14 for the Period 12/21/73 Through 1/12/74

Values of Z_S and Z_X for DSS 14 for the period 12/21/73 through 1/12/74 are:

$$Z_S = -169.00 \pm 0\ 86\ \text{ns},\ 1\sigma$$

$$Z_X = -137.58 \pm 0\ 86\ \text{ns},\ 1\sigma$$

These numbers were arrived at by evaluating the appropriate forms of Eq. (13) with the values in Table A-1 substituted for the various indicated parameters (they do not, however, include the effects of the instabilities described in the articles of footnote 1)

Table A-1. Values of parameters

Parameter		Value, ns	Source
B'_U	=	91.29 ±0 26	τ_{23} (Ref 4) + τ (2113 feed and components) (Ref 5)
B'_{DS}	=	47.37 ±0 28	τ_{34} (Ref 4) + τ (2295 feed and components) (Ref 5)
B'_{DX}	=	3 52 ±0 08	τ_{67} (Ref. 4) + τ (8415 feed and components) (Ref. 5)
C_U	=	168.95 ±0 02	Ray optics tracing of path from S-band feed horn to aperture plane via dichroic system, subreflector and paraboloid
C_{DS}	=	168.95 ±0.02	Ray optics tracing of path from S-band feed horn to aperture plane via dichroic system, subreflector and paraboloid
C_{DX}	=	160 01 ±0 06	Ray optics tracing of path from X-band feed horn to aperture plane via dichroic system, subreflector and paraboloid
D	=	58.62 ±0.01	Ref 6 and print 9437255
G_U	=	88.83 ±0 09	τ_{2A} (Ref. 4)
G_{DS}	=	87 38 ±0.12	τ_{B4} (Ref. 4)
G_{DX}	=	70.63 ±0 10	τ_{C7} (Ref 4)
H_S	=	14 11 ±0.76	τ_{AB} (Ref. 4)
H_X	=	9.49 ±0 80	τ_{AC} (Ref 4)

Appendix B
Values of Z_S and Z_X for DSS 14 for 1/14/74 and Later

On 1/13/74 the uplink sampling point was moved from the 10/20 kW transmitter in the MOD II area to the junction of the megawatt transmitter filter (MTF) and the 4th harmonic filter in the MOD III area. This was done so that the sampling point would be independent of which transmitter was in use: 10, 20, 100 or 400 kW. Because of this relocation, the values of Z_S and Z_X have changed to:

$$Z_S = -166\,50 \pm 0.86 \text{ ns}, 1\sigma$$

$$Z_X = -135\,08 \pm 0\,86 \text{ ns}, 1\sigma$$

These numbers were arrived at by evaluating the appropriate forms of Eq. (13) with the values in Table B-1 substituted for the various indicated parameters.

Table B-1. Values of parameters

Parameter		Value, ns	Source
B'_U	=	42 31 ±0 26	$\tau_{2'3}$ (Ref 4) + τ (2113 feed and components) (Ref. 5)
B'_{DS}	=	47 37 ±0 28	τ_{34} (Ref. 4) + τ (2295 feed and components) (Ref 5)
B'_{DX}	=	3 52 ±0 08	τ_{67} (Ref 4) + τ (8415 feed and components) (Ref. 5)
C_U	=	168 95 ±0.02	Ray optics tracing of path from S-band feed horn to aperture plane via dichroic system, subreflector and paraboloid
C_{DS}	=	168.95 ±0.02	Ray optics tracing of path from S-band feed horn to aperture plane via dichroic system, subreflector and paraboloid
C_{DX}	=	160 01 ±0 06	Ray optics tracing of path from X-band feed horn to aperture plane via dichroic system, subreflector and paraboloid
D	=	58 62 ±0 01	Ref 6 and print 9437255
G_U	=	42 35 ±0 09	$\tau_{2'A}$ (Ref 4)
G_{DS}	=	87.38 ±0.12	τ_{B4} (Ref 4)
G_{DX}	=	70 63 ±0 10	τ_{C7} (Ref. 4)
H_S	=	14.11 ±0 76	τ_{AB} (Ref 4)
H_X	=	9.49 ±0 80	τ_{AC} (Ref 4)

Reprinted from *The Deep Space Network Progress Report 42-22*, Aug 15, 1974, pp 81–89.

S/X Experiment: DSS 14 Pre- and Post-Track Ranging Calibrations for Mariner 10 Tracking Passes and Associated Problems

T Y. Otoshi
Communications Elements Research Section

Ground system ranging calibration data for DSS 14 are presented for 1974 Day 12 through Day 150. Associated ranging problems are discussed and recommendations for calibration improvements are presented.

I. Introduction

Ranging calibrations on the ground system at DSS 14 are currently being performed with the Zero Delay Device (ZDD) in the cable configuration that was described in Ref. 1. The ranging calibrations are normally done during pre- and post-calibration periods of Mariner 10 tracking passes at the signal levels and frequencies applicable to the particular tracking pass. These ZDD pre- and post-calibration data are used along with the ground station Z-correction (Ref. 2) and spacecraft radio system bias correction to enable determination of the true range to the spacecraft (Ref 3)

For purposes of observing the long-term performance of the ZDD, pre- and post-track calibration data have been systematically tabulated at DSS 14 as functions of ambient temperature, signal levels, and other range-dependent parameters. This article presents some of these data in plotted form for convenient reference purposes

II. Calibration Data

Systematic tabulation of ranging calibration data for the S/X system at DSS 14 was begun after 1974 Day 12 when the new ZDD cable configuration was installed (see Ref. 1). Figures 1 through 10 show plots of the S/X ground system ranging calibrations for Mariner 10 tracking passes from 1974 Day 12 through Day 150.

From Day 47 through Day 85, unexpected Block 4 doppler instability problems made accurate ranging values very difficult to obtain. In this period many system configuration and component changes were implemented by a "Tiger Team" that was formed to investigate and correct the source of the Block 4 receiver doppler instabilities The doppler instability problem was solved on Day 85, after which the DSS 14 ranging configuration was left virtually unchanged.

From the plotted results, it can be seen that during periods when the range configuration was left unaltered

and the same transmitter used, the peak-to-peak range variations were typically within 10 ns for S-band and X-band It is of interest to observe that the jitter in the data noticeably decreased around the time of Mariner 10 Venus and Mercury encounters, which were Days 36 and 88, respectively

It can be seen that a significant change of range occurs whenever different transmitters (klystron amplifiers) are used. The ground system S- or X-band group delay is anywhere from 5 ns to 18 ns longer when the 100-kW transmitter is used rather than the 20-kW transmitter Based on data on the configuration after Day 82, it was found that, when Receiver 3 is used for S-band instead of Receiver 4, the S-band group delay through the DSS 14 ground system is about 28 ns longer. When Receiver 4 is used for X-band instead of Receiver 3, the X-band range delay through the DSS 14 ground system is about 19 ns shorter.

The ground station range delay using the Block 4 system has recently been found to be strongly dependent on received signal level. Variations of delay with signal level have been reported in the following article of this volume (T. Y. Otoshi and P. D. Batelaan, "S/X Experiment: DSS 14 S/X Ground System Ranging Tests). This signal level change is a long-term effect, however, and does not explain the short-term peak-to-peak variations Some of the short-term variation is correlated with ambient temperature changes. The dependence on temperature, however, is not conclusive because this effect appears to be nonlinear and only a limited amount of reliable data has been available

III. Discussion of Ranging Problems and Recommendations

It has been found that many variables or factors can affect the ranging calibration values on a day-to-day basis Therefore, it is important that the ZDD ranging calibration data be applied only for the particular tracking pass for which calibrations were done. Use of some average value for the station delay can result in significant error.

In summary, some of the known major factors that can change ranging calibrations or introduce errors are.

(1) Interchanging transmitters (20-kW or 100-kW klystron).

(2) Interchanging receivers (Receiver 3 or 4 for S or X).

(3) Interchanging exciters (Block 3 or Block 4). The Block 4 exciter is not currently used during pre- and post-calibrations or tracking passes.

(4) Maser gain and tuning

(5) Ambient temperature.

(6) Replacement of components or cables in the signal path

(7) Received signal level.

(7) Antenna sag and subreflector defocusing. (This effect cannot be evaluated at DSS 14 with present cable configuration.)

(9) Incorrect range modulation setting. (This effect has not been completely investigated)

(10) Improper calibration configuration (if there is more than one signal path)

(11) Incorrect voltage-controlled oscillator (VCO) frequency typed into ranging machine by operator

(12) Reporting acquisition range instead of updated range.

Note that since many of the above factors cannot be controlled or always be known, it is important that pre- and post-calibration data be used for the same day's tracking pass only. The station configuration should not be altered during the tracking pass after calibrations have been performed. Operator errors described by factors (9) through (11) can be minimized only by operator care and long-term familiarity and training of DSS operators on the new S/X system and Mu-2 ranging machine Data improvement would result from operator verification of correlation voltages Data with bad correlation voltages should not be reported. Calibrations not within 10 ns or 0 010 μs of previous calibrations indicate a need for recalibration.

It should be possible to eliminate inaccuracies due to factors (11) and (12) by using the Engineering Cal Program[1] (DOI-5399-SP) during the pre- and post-calibration periods This program contains most of the features of the Monitor Program (DOI-5046-OP), with the addition that doppler phase and ranging calibration processing is done in real time at the station This calibration program is applicable to the Block 3/PRA and Block 4/Mu-2 configurations. Data from this program can be sent

[1]This program was written by Harvey Marks of Informatics Inc, Canoga Park, California

to the Mission Control and Computing Center (MCCC) via the high-speed data line. The program is currently in the DSN program library and is now at all stations in the DSN including CTA 21

It is recommended that for long-term study of ranging and doppler stability data, S/X tests be done at all stations of the DSN with the Engineering Cal Program (DOI-5399-SP).

Acknowledgments

Ray Allis and Ed Cole of the Philco-Ford Corporation performed most of the systematic calibrations and tabulations of data presented in this article. The ranging data were obtained from the teletyped output of the Mu-2 ranging machine which was developed by Warren Martin and programmed by Art Zygielbaum of Section 331

References

1. Otoshi, T. Y, and Stelzried, C T, "S/X Experiment A New Configuration for Ground Range Calibrations With the Zero Delay Device," in *The Deep Space Network Progress Report 42-20*, pp. 57–63, Jet Propulsion Laboratory, Pasadena, Calif., Apr. 15, 1974.

2 Batelaan, P D, "S/X-Band Experiment: Zero Delay Device Z Correction," in *The Deep Space Network Progress Report 42-20*, pp. 78–83, Jet Propulsion Laboratory, Pasadena, Calif., Apr. 15, 1974

3 *TRK-2-8 Module of DSN System Requirements Detailed Interface Design Document 820-13, Rev. A*, July 1, 1973 (JPL internal document).

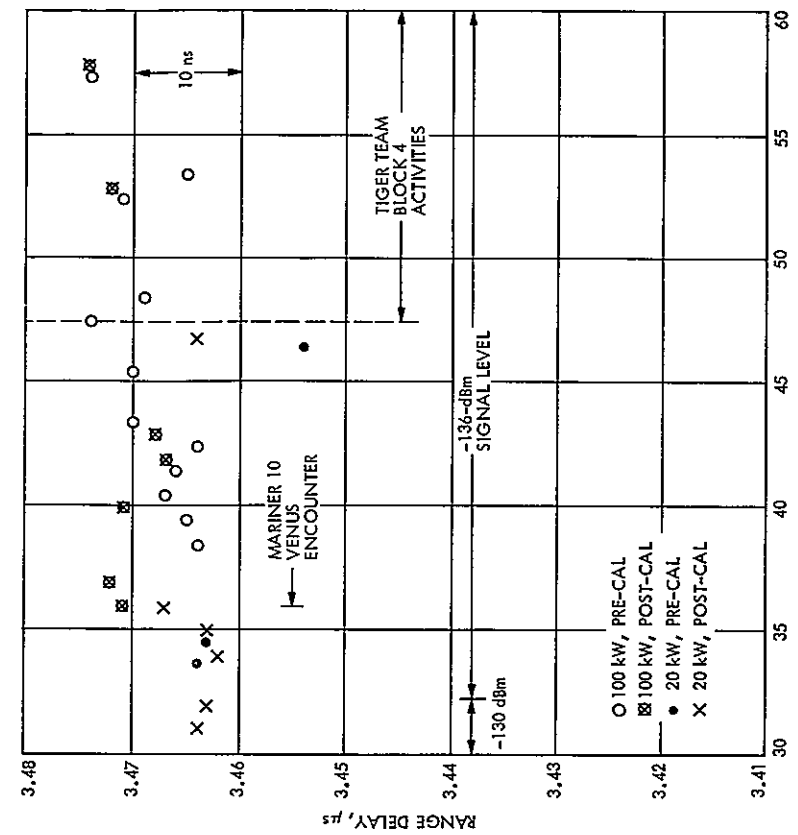

Fig. 2. S-band zero delay range, 1974 Day 30–60 (Jan 30–Mar 1)

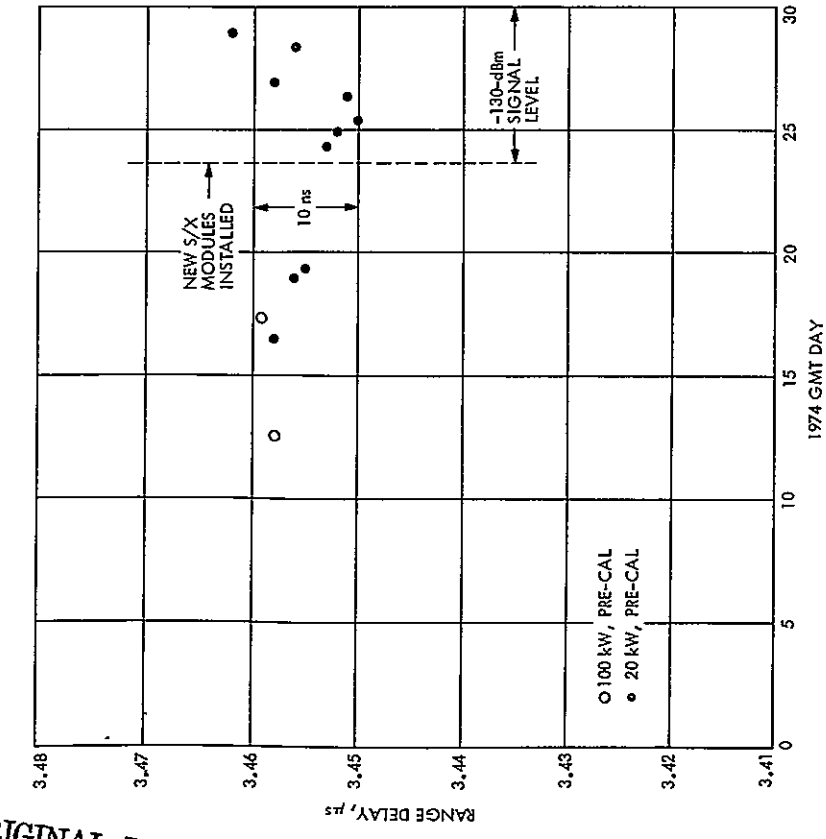

Fig 1. S-band zero delay range, 1974 Day 1–30 (Jan 1–30)

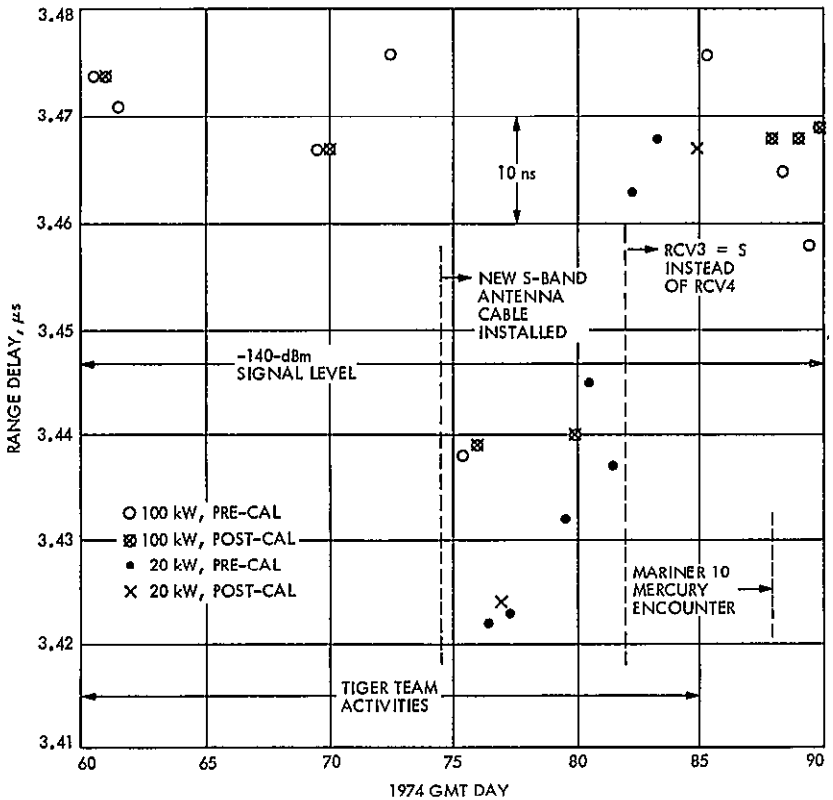

Fig. 3. S-band zero delay range, 1974 Day 60–90
(Mar 1–Mar 31)

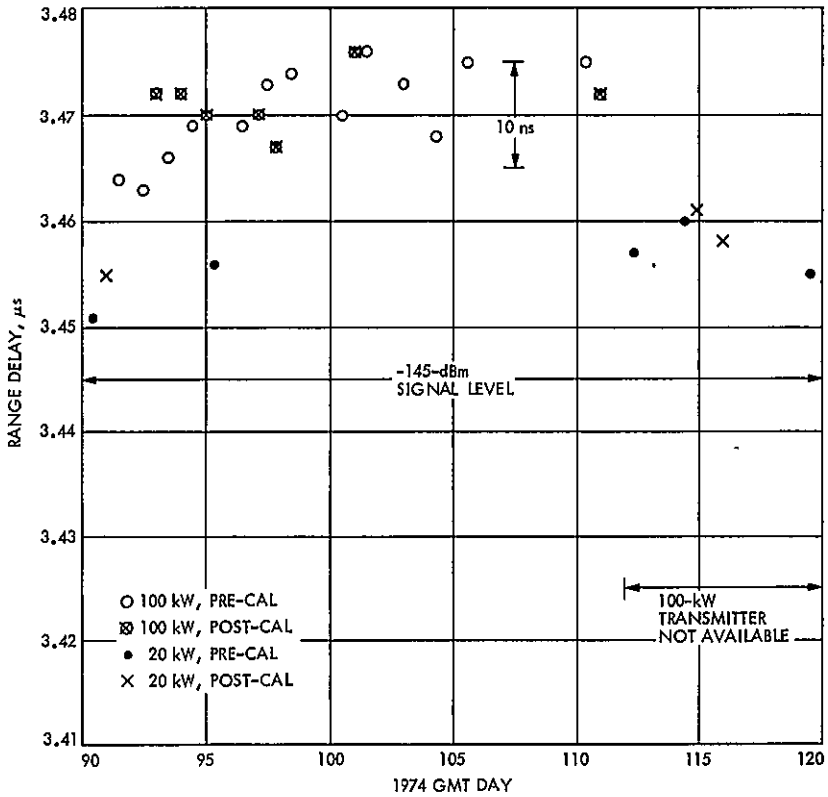

Fig. 4. S-band zero delay range, 1974 Day 90–120
(Mar 31–Apr 30)

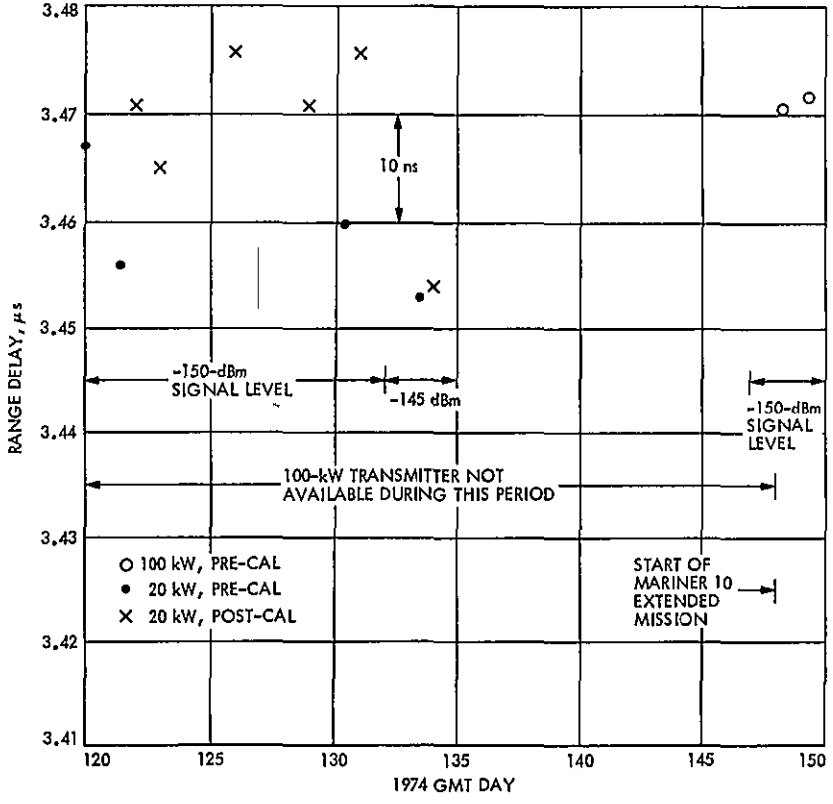

Fig. 5. S-band zero delay range, 1974 Day 120–150 (Apr 30–May 30)

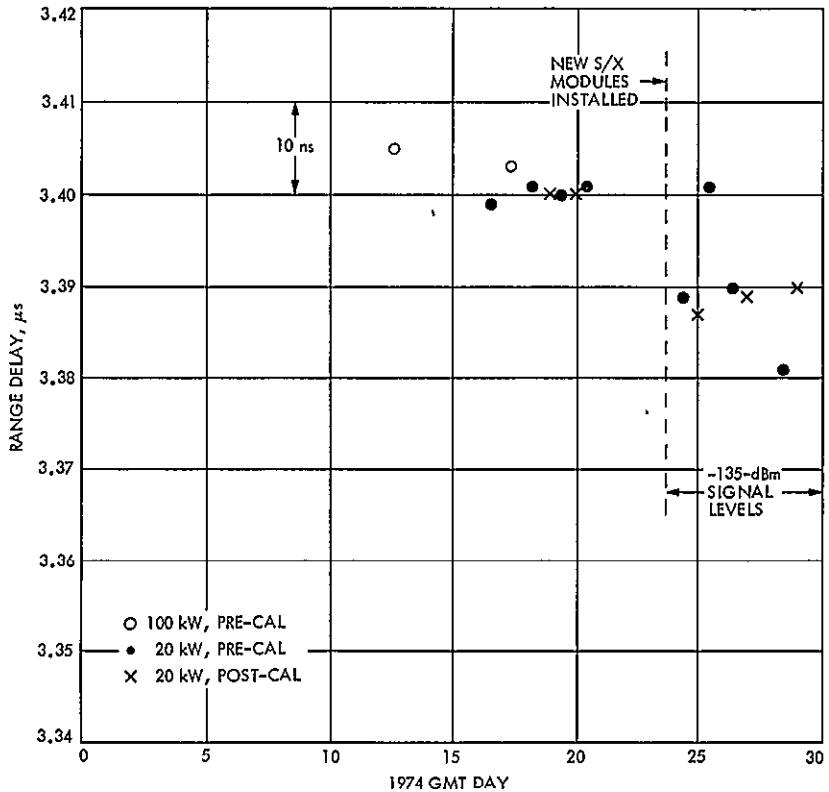

Fig 6. X-band zero delay range, 1974 Day 1–30 (Jan 1–30)

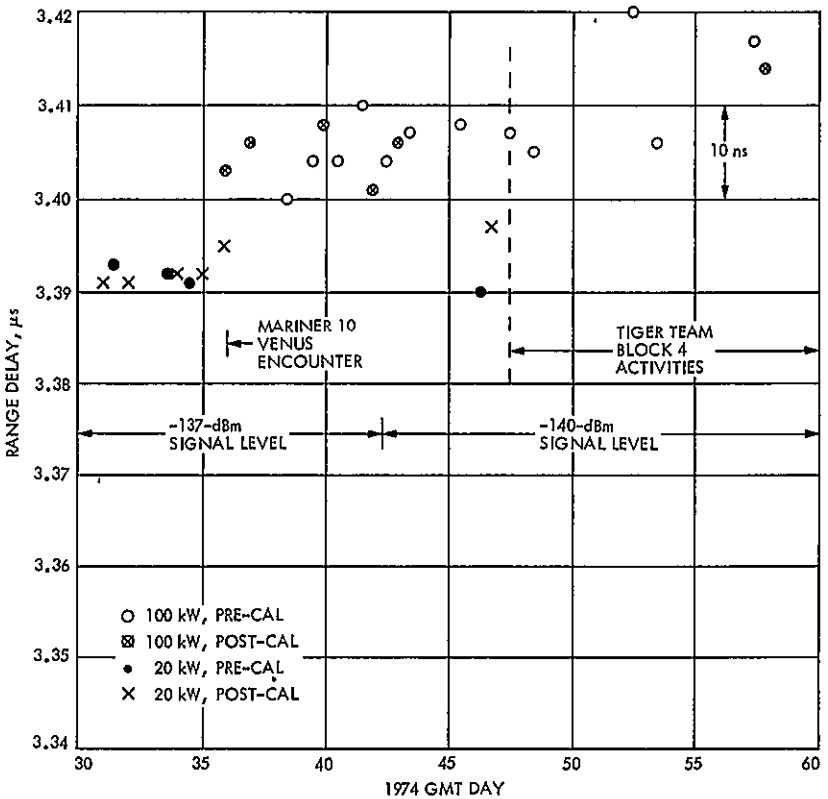

Fig. 7. X-band zero delay range, 1974 Day 30–60 (Jan 30–Mar 1)

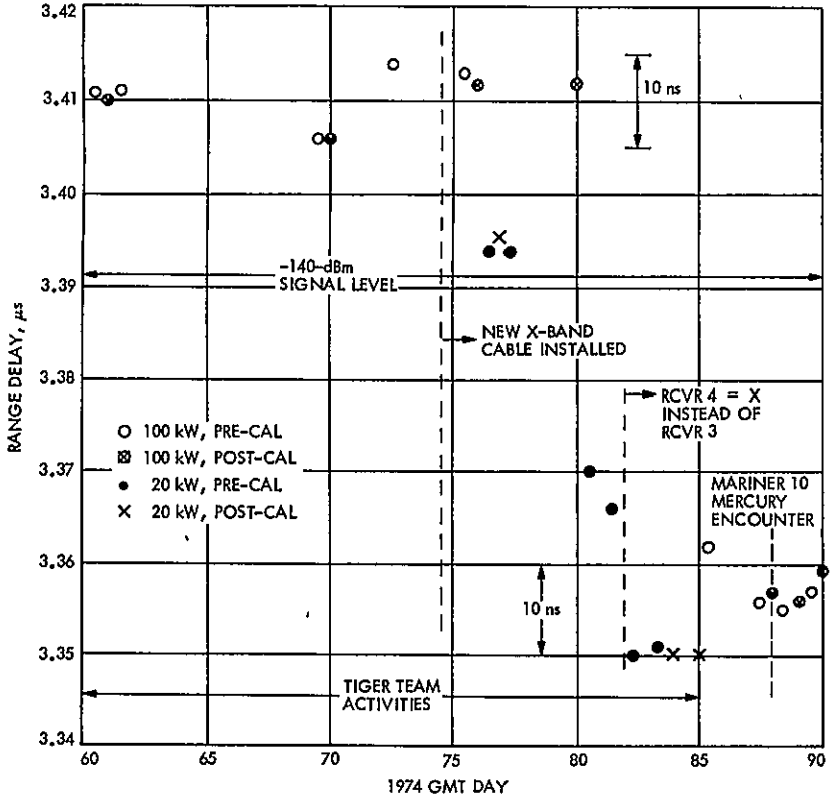

Fig. 8. X-band zero delay range, 1974 Day 60–90 (Mar 1–Mar 31)

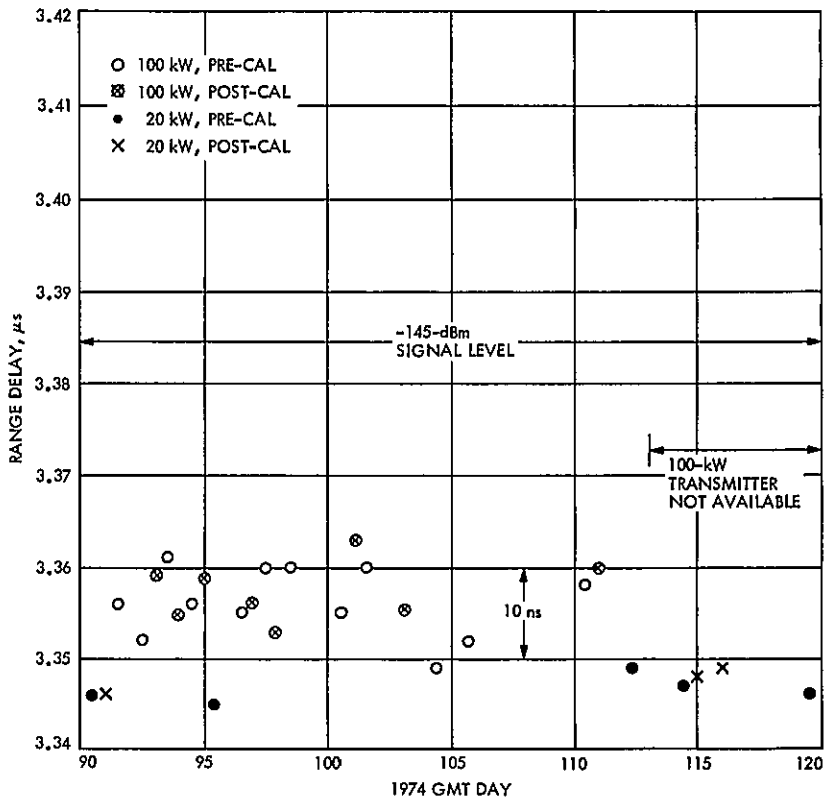

Fig. 9. X-band zero delay range, 1974 Day 90–120 (Mar 31–Apr 30)

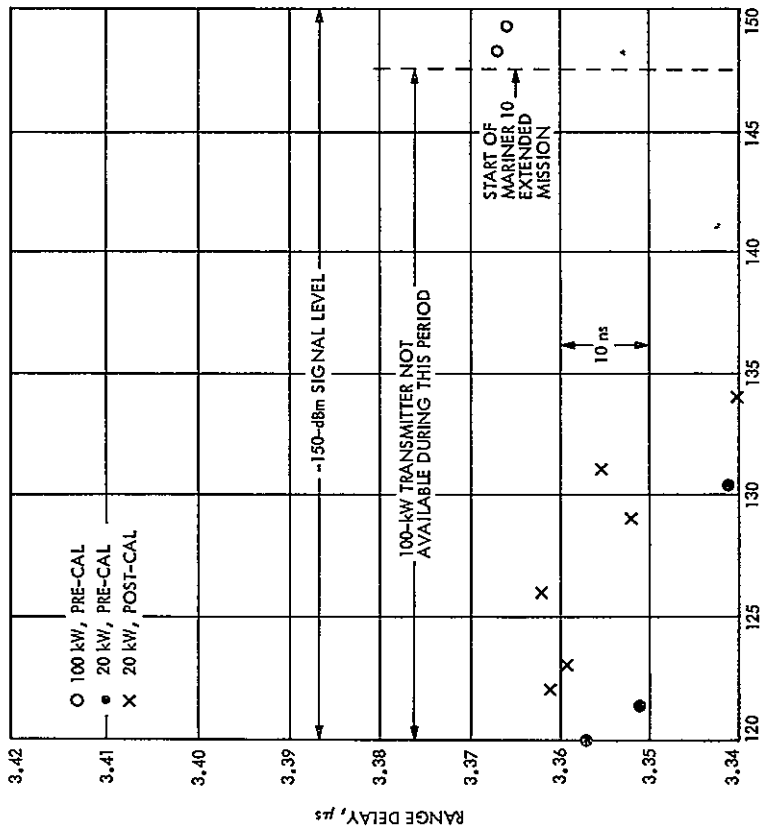

Fig. 10. X-band zero delay range, 1974 Day 120–150 (Apr 30–May 30)

Reprinted from *The Deep Space Network Progress Report 42-22*, Aug 15, 1974, pp 90–100

S/X Experiment: DSS 14 S/X Ground System Ranging Tests

T. Y. Otoshi and P. D. Batelaan
Communications Elements Research Section

This article presents special ranging test data obtained on the S/X ground system at DSS 14. The test data consist of ground system range as functions of (1) uplink 100-kW transmitter power, (2) downlink S- and X-band signal levels, and (3) antenna elevation and azimuth angles via the cable path and via the airpath

I. Introduction

On 1974 Day 12, a new configuration was installed at DSS 14 for ground system ranging calibrations As described in Ref. 1, this new configuration differs from the conventional one in that the zero delay device (ZDD) uplink and downlink signals are transmitted through calibrated cables instead of through the airpath. Some limited amount of range calibration data on this new configuration was previously reported in Ref. 1.

Due to unexpected doppler stability problems with the Block 4 receiver system during the period 1974 Day 47 through 85, it was difficult to perform useful ranging tests on the S/X system until after the Mariner 10 Mercury encounter on 1974 Day 88.

This article presents results of some recent ranging tests made on the S/X ground system at DSS 14 as functions of various ground station parameters. Pre- and post-track calibration data for the Mariner 10 tracking passes and discussion of S/X calibration problems are discussed in the preceding article of this volume (T. Y. Otoshi, "S/X Experiment: DSS 14 Pre- and Post-Track Ranging Calibration for Mariner 10 Tracking Passes and Associated Problems).

II. Test Configuration

A block diagram of the present ZDD configuration for the S/X ground system calibrations at DSS 14 may be seen in Fig. 1 As was described in Ref. 1, the ZDD is a ground station antenna-mounted transponder that samples the uplink 2113 MHz from the transmitter and generates coherent downlink S- and X-band test signals of 2295 MHz and 8415 MHz. Transmission of these test signals to the respective masers is possible either through a cable path or a microwave airpath by means of an internal coaxial switch in the ZDD assembly.

As may be seen in Fig 1, the present ground system configuration being calibrated at DSS 14 consists of the Block 3 exciter, the 100- or 20-kW transmitters, the S/X masers, Block 4 receivers, and the Mu-2 ranging machine Test data were reduced in real time at DSS 14 by means of the Engineering Calibration Program (DOI-5399-SP), which was specially developed for the S/X Experiment [1] A sample output from the program may be seen in Fig. 2 This program has many of the features of the Monitor Program (DOI-5046-OP), and can be used to test range and cumulative doppler phase at any DSN station having the Block 3/Planetary Ranging Assembly (PRA) ranging or Block 4/Mu-2 ranging systems The program is currently in the DSN Program Library and copies of tapes and documentation have been sent to all stations in the DSN including CTA 21.

III. Test Results

Special tests were performed to investigate range as functions of (1) uplink 100-kW transmitter power, (2) downlink S/X signal levels, and (3) antenna elevation and azimuth angles.

Data from special tests obtained with the Engineering Cal Program are presented in graphical form in Figs 3 through 14 Figures 3 and 4 show plots of round-trip range delay as functions of uplink power from the 100-kW transmitter It can be seen that the variation of delay is less than 2 ns for either the S- or X-band system when the transmitter power is varied from 75 kW to 100 kW.

Figures 5 through 8 show round-trip range delays as a function of received signal level as defined at the input to the Mod 3 S-band maser and X-band maser. Range is found to be significantly dependent upon signal level when Receiver 4 of the Block 4 system is used for either S- or X-band and less dependent when Receiver 3 is operated for either S- or X-band. In the signal level range of -135 dBm to -145 dBm, the range change is approximately 0 3 ns/dB for Receiver 3 and 0 8 ns/dB for Receiver 4 Tests with the signals injected behind the respective S- and X-band masers showed the same type response and therefore ruled the masers out as possible causes of range change with signal level. Further tests on the Mu-2 ranging machine as well as manual gain control (MGC) tests on the Block 4 receivers resulted in the isolation of the Block 4 automatic gain control (AGC) loop as being the source of the range changes.

Special tests were also made to study the effects of antenna elevation and azimuth movement on range. The results of these tests for the cable path configuration may be seen in Figs 9 through 12. The variations of 6 ns as functions of elevation angles in the S-band cable path are larger than reported previously (see Ref. 1). The variations could be due to changes somewhere in the 100-kW Klystron Amplifier Assembly This fact can be verified in the future by performing a similar test with both the Block 4 translator and the ZDD and comparing the results. This test should give a valid indication since the ZDD samples the uplink signal after the Klystron Amplifier, while the Block 4 translator obtains the uplink signal from the exciter assembly in front of the Klystron Amplifier.

Figures 13 and 14 show the results of range tests with the ZDD in the airpath configuration. The large variation of about 25 ns in the airpath for the X-band is about the same as was reported previously in Ref 2. The cause of this change in range is still not known Several tests were made to isolate possible multipath signals in the airpath One test involved the temporary installation of an RF screen that interconnected the rooftops of the three cones mounted on the Tricone Support Structure This screen covered the open area between the three cones and blocked potential S- and X-band leakage signals. A small improvement was noticed at S-band and a small (but insufficient) improvement at X-band was also obtained. Another screen placed around the dichroic plate assembly support structure resulted in no further improvement at X-band. Another test showed that the performance of the X-band airpath range could be improved significantly by axial focusing of the subreflector at each elevation angle for optimum antenna gain at X-band. However, optimizing for X-band seriously affected the S-band performance. Although the strange behavior in the airpath is not clearly understood at present, it is felt that airpath tests are still useful for trouble shooting potential problems in the S/X reflex feed system.

IV. Conclusion

Data from special ranging tests on the S/X system at DSS 14 have been presented. These data may be useful for indicating improvement areas needed on the ground

[1]This program was written by Harvey Marks of Informatics, Inc., Canoga Park, California

system for future missions such as Viking '75. In addition, these data could be helpful in explaining some of the ranging anomalies seen during the Mariner 10 mission (Refs. 3 and 4). It has been reported that part of the structured noise in the differenced range versus integrated doppler (DRVID) data seen in the Mariner Venus/Mercury 1973 mission was correlated to ground station received signal level changes (Ref. 5).

References

1. Otoshi, T. Y, and Stelzried, C. T., "S/X Experiment: A New Configuration for Ground System Range Calibrations With the Zero Delay Device," in *The Deep Space Network Progress Report 42-20*, pp. 57–63, Jet Propulsion Laboratory, Pasadena, Calif., Apr. 15, 1974.
2. Stelzried, C T., Otoshi, T. Y., and Batelaan, P. D., "S/X Band Experiment. Zero Delay Device Antenna Location," in *The Deep Space Network Progress Report 42-20*, pp. 64–68, Jet Propulsion Laboratory, Pasadena, Calif., Apr. 15, 1974.
3. Spradlin, G., *Simultaneous Two-Way/Three-Way DRVID Tests*, IOM 421G-74-197, May 17, 1974 (JPL internal document)
4. Chaney, W. D., *Range Calibration Discrepancies During MVM-73*, IOM NSE-74-105, May 8, 1974 (JPL internal document).
5. Rourke, K H., *Viewgraphs from DRVID Investigation Initial Phase Report*, IOM 391-8-180, June 5, 1974 (JPL internal document).

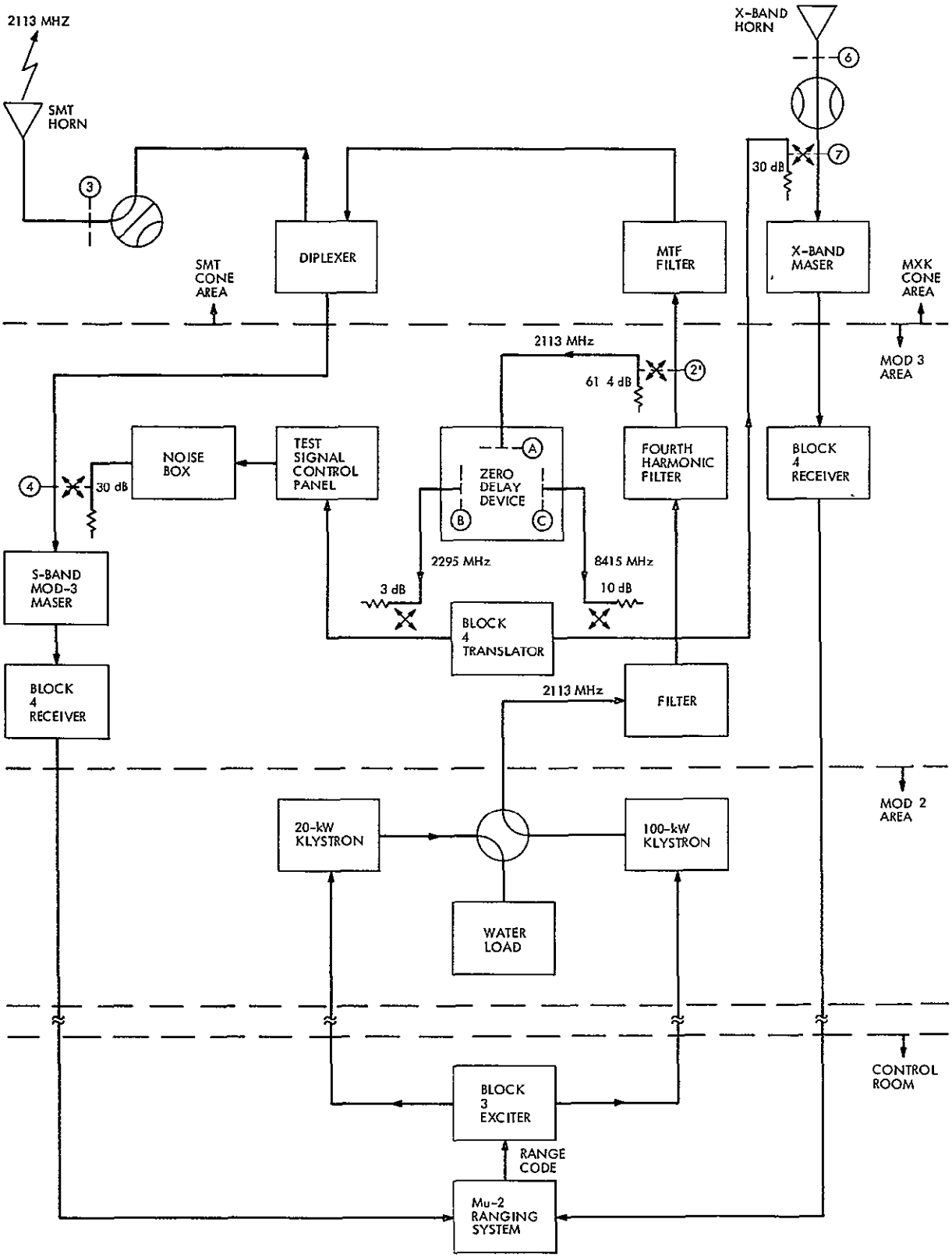

Fig. 1. Block diagram of the new configuration at DSS 14 for ground system range calibrations

ZUO CABLE CONFIG

DAY 157	AZ[DEG]	EL[DEG]	SD[USEC]	XD[USEC]	SR[USEC]	XR[USEC]	DR[USEC]	SP[DEG]	XP[DEG]	DP[DEG]
01:24:07	219.998	10.002	-.0031	.0060	3.4677	3.3656	.1022	.0	18.0	-4.9
01:24:12	219.998	10.002	-.0031	.0060	3.4677	3.3656	.1022	18.0	18.0	13.1
01:24:17	219.998	10.002	-.0031	.0060	3.4677	3.3656	.1022	18.0	54.0	3.3
01:24:22	219.998	10.002	-.0031	.0060	3.4677	3.3656	.1022	.0	18.0	-4.9
01:24:27	219.998	10.002	-.0027	.0061	3.4679	3.3655	.1025	.0	18.0	-4.9
01:24:32	219.998	10.002	-.0027	.0061	3.4679	3.3655	.1025	18.0	18.0	13.1
01:24:37	219.998	10.002	-.0027	.0061	3.4679	3.3655	.1025	.0	18.0	-4.9
01:24:42	219.998	10.002	-.0027	.0061	3.4679	3.3655	.1025	18.0	36.0	8.2
01:24:47	219.998	10.002	-.0040	.0075	3.4680	3.3655	.1025	18.0	.0	18.0
01:24:52	219.998	10.002	-.0040	.0075	3.4680	3.3655	.1025	.0	36.0	-9.8
01:24:57	219.998	10.002	-.0040	.0075	3.4680	3.3655	.1025	.0	36.0	-9.8
01:25:02	219.998	10.002	-.0040	.0075	3.4680	3.3655	.1025	.0	72.0	-19.6
01:25:07	219.998	10.002	-.0032	.0068	3.4681	3.3655	.1026	18.0	54.0	3.3
01:25:12	219.998	10.002	-.0032	.0068	3.4681	3.3655	.1026	.0	54.0	-14.7
01:25:17	219.998	10.002	-.0032	.0068	3.4681	3.3655	.1026	-18.0	18.0	-22.9
01:25:22	219.998	10.002	-.0032	.0068	3.4681	3.3655	.1026	.0	36.0	-9.8
01:25:27	219.998	10.002	-.0035	.0058	3.4682	3.3654	.1028	18.0	36.0	8.2
01:25:32	219.998	10.002	-.0035	.0058	3.4682	3.3654	.1028	.0	18.0	-4.9
01:25:37	219.998	10.002	-.0035	.0058	3.4682	3.3654	.1028	.0	18.0	-4.9
01:25:42	219.998	10.002	-.0035	.0058	3.4682	3.3654	.1028	.0	.0	.0
01:25:47	219.998	10.002	-.0035	.0065	3.4683	3.3654	.1029	18.0	.0	18.0
01:25:52	219.998	10.002	-.0035	.0065	3.4683	3.3654	.1029	.0	36.0	-9.8
01:25:57	219.998	10.002	-.0035	.0065	3.4683	3.3654	.1029	.0	36.0	-9.8
01:26:02	219.998	10.002	-.0035	.0065	3.4683	3.3654	.1029	18.0	18.0	13.1
01:26:07	219.998	10.002	-.0042	.0060	3.4683	3.3653	.1030	-18.0	18.0	-22.9
01:26:12	219.998	10.002	-.0042	.0060	3.4683	3.3653	.1030	.0	18.0	-4.9
01:26:17	219.998	10.002	-.0042	.0060	3.4683	3.3653	.1030	18.0	18.0	13.1
01:26:22	219.998	10.002	-.0042	.0060	3.4683	3.3653	.1030	18.0	18.0	13.1
01:26:27	219.998	10.002	-.0052	.0062	3.4682	3.3653	.1029	.0	36.0	-9.8
01:26:32	219.998	10.002	-.0052	.0062	3.4682	3.3653	.1029	.0	18.0	-4.9
01:26:37	219.998	10.002	-.0052	.0062	3.4682	3.3653	.1029	.0	36.0	-9.8
01:26:42	219.998	10.002	-.0052	.0062	3.4682	3.3653	.1029	.0	18.0	-4.9
01:26:47	219.998	10.002	-.0036	.0064	3.4683	3.3653	.1030	.0	18.0	-4.9
01:26:52	219.998	10.002	-.0036	.0064	3.4683	3.3653	.1030	.0	36.0	-9.8
01:26:57	219.998	10.002	-.0036	.0064	3.4683	3.3653	.1030	.0	18.0	-4.9
01:27:02	219.998	10.002	-.0036	.0064	3.4683	3.3653	.1030	18.0	36.0	8.2
01:27:07	219.998	10.002	-.0035	.0060	3.4684	3.3652	.1032	.0	36.0	-9.8

Fig. 2. Sample printout page from Engineering Cal Program (DOI-5399-SP) showing S/X DRVIDs, S/X updated ranges, and S/X doppler phases (DSS 14 test data on 1974 Day 157)

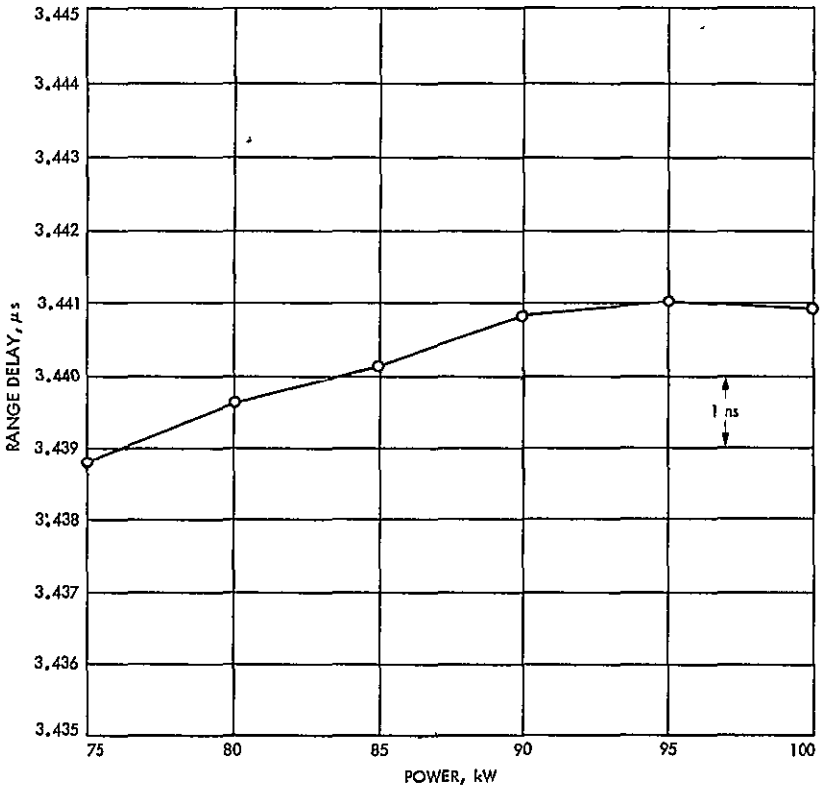

Fig 3 100-kW transmitter power vs ZDD S-band range on 1974 Day 75

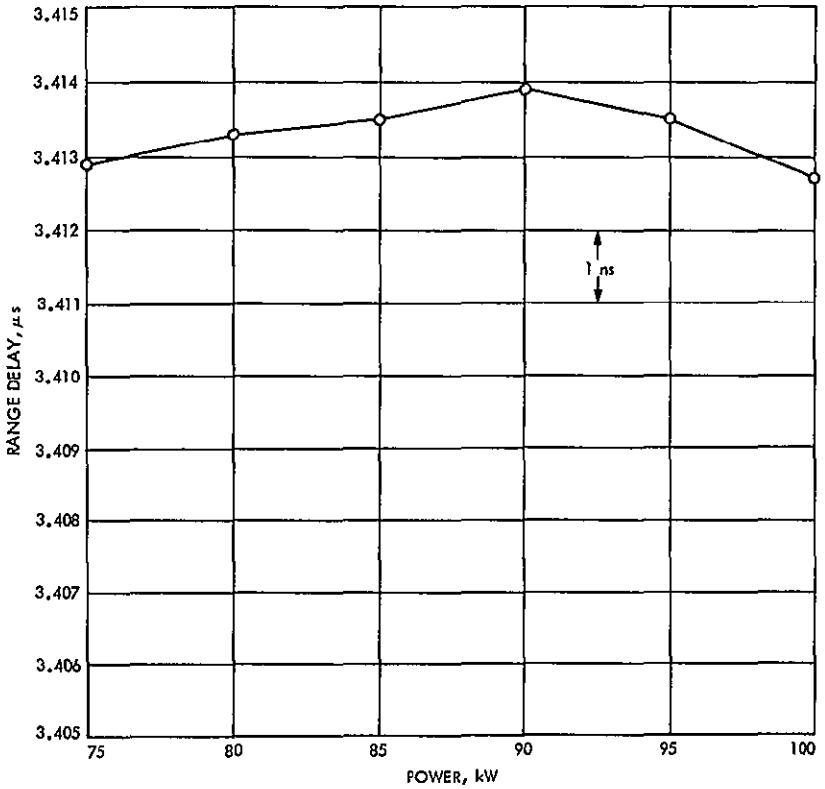

Fig. 4. 100-kW transmitter power vs ZDD X-band range on 1974 Day 75

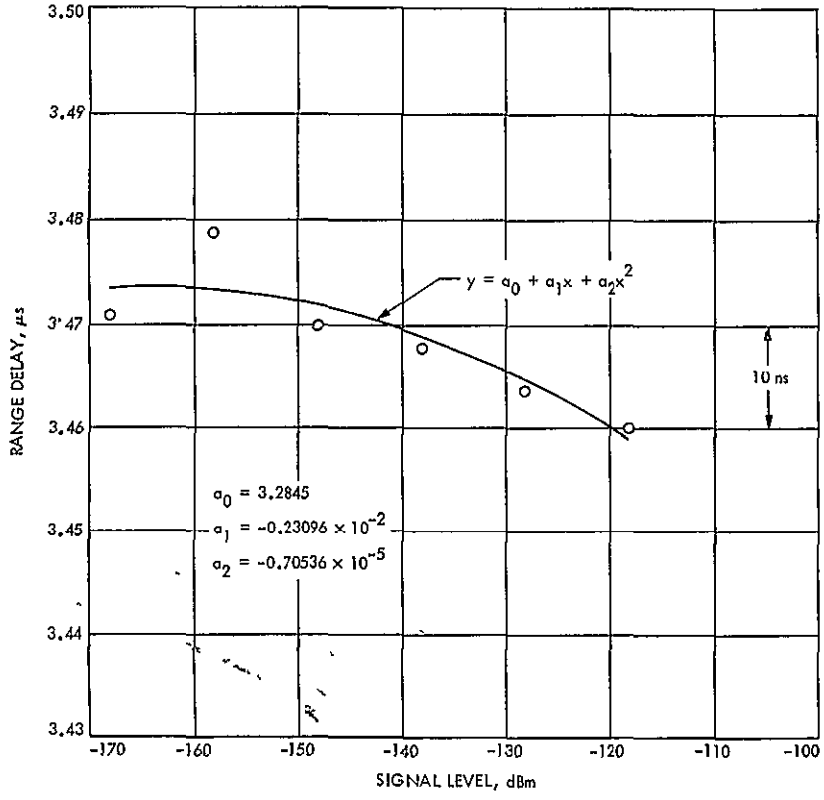

Fig 5. Signal level vs S-range, 100 kW, ZDD test 1 with RCV3 = S, 1974 Day 110

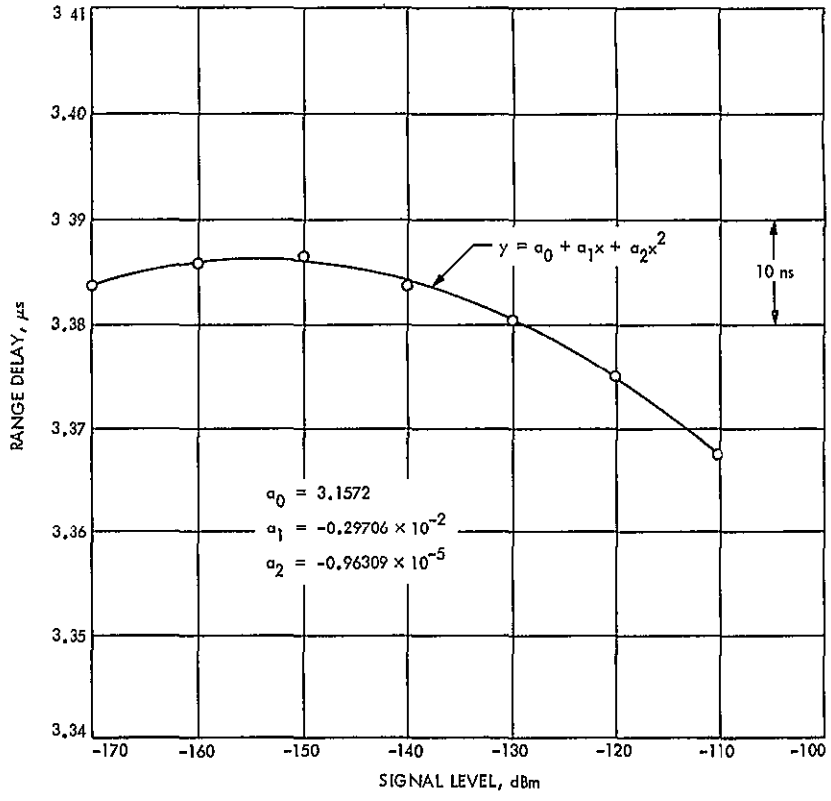

Fig 6. Signal level vs X-range, 100 kW, ZDD test 2 with RCV3 = X, 1974 Day 110

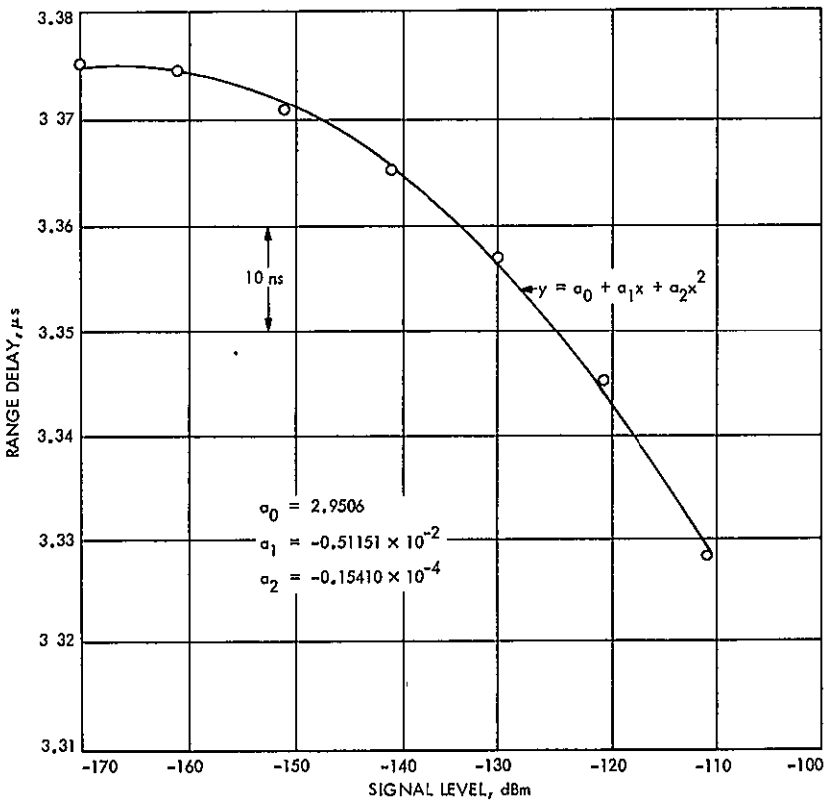

Fig. 7. Signal level vs X-range, 100 kW, ZDD test 1 with RCV4 = X, 1974 Day 110

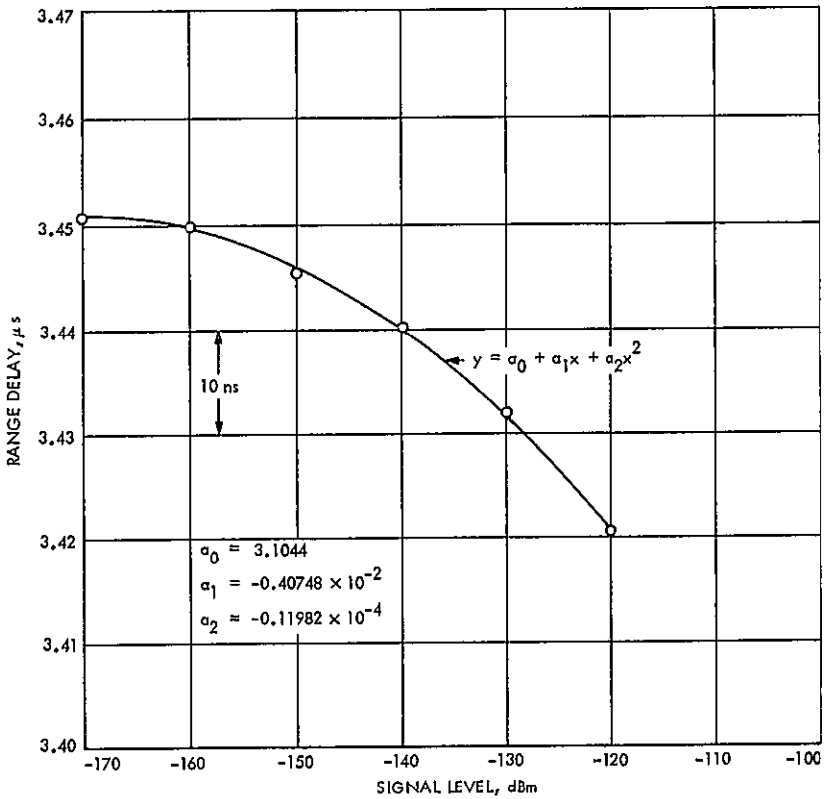

Fig. 8. Signal level vs S-range, 100 kW, ZDD test 2 with RCV4 = S, 1974 Day 110

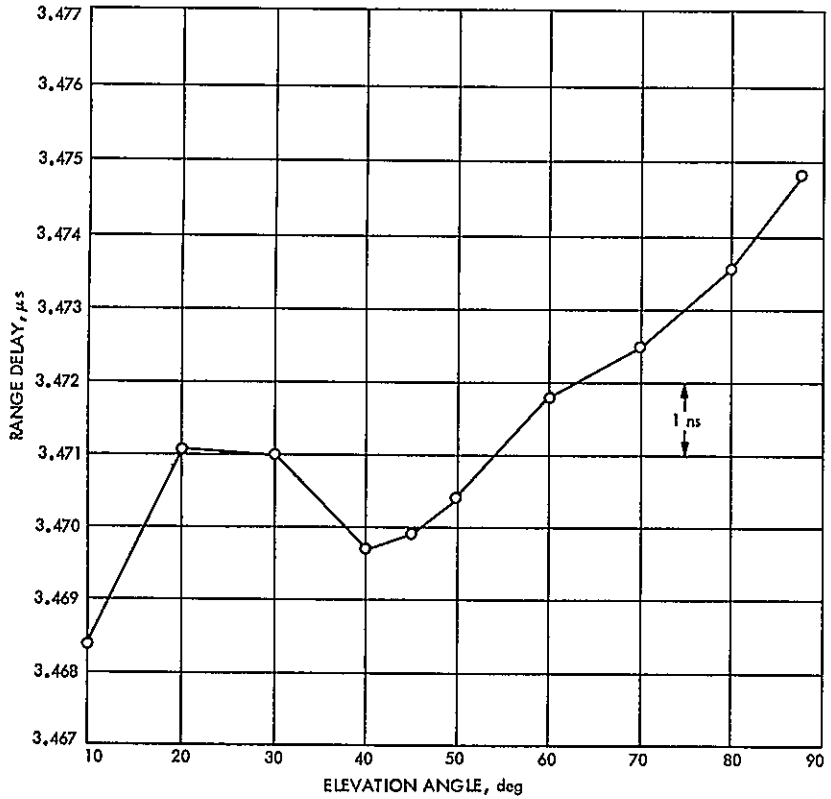

Fig. 9. S-range vs elevation angle via ZDD cable configuration, AZ = 220 deg, 100 kW, RCV3 = S, 1974 Day 157

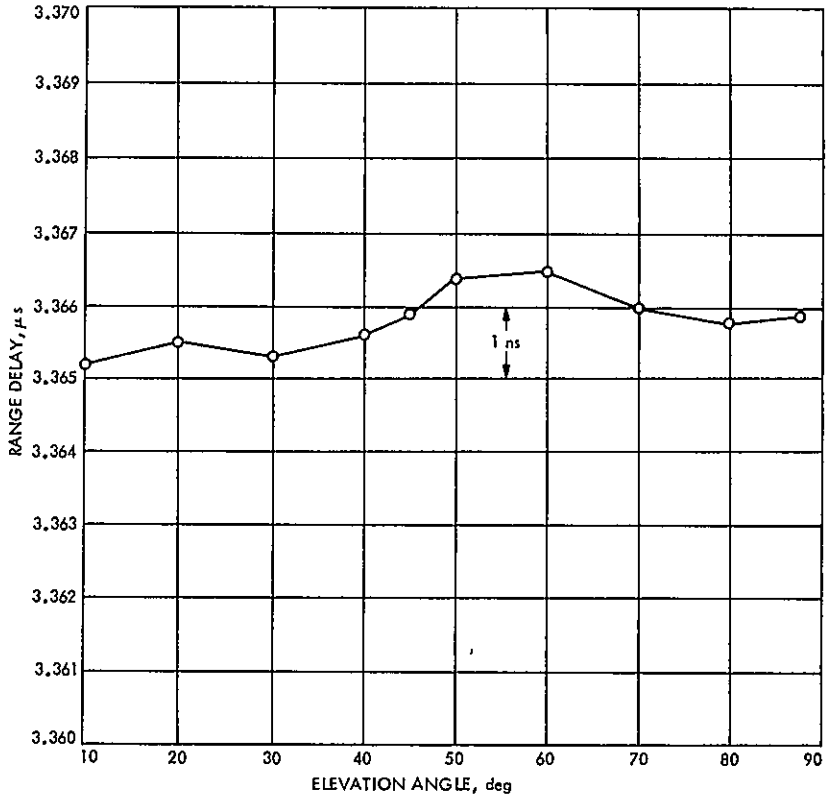

Fig. 10 X-range vs elevation angle via ZDD cable configuration, AZ = 220 deg, 100 kW, RCV4 = X, 1974 Day 157

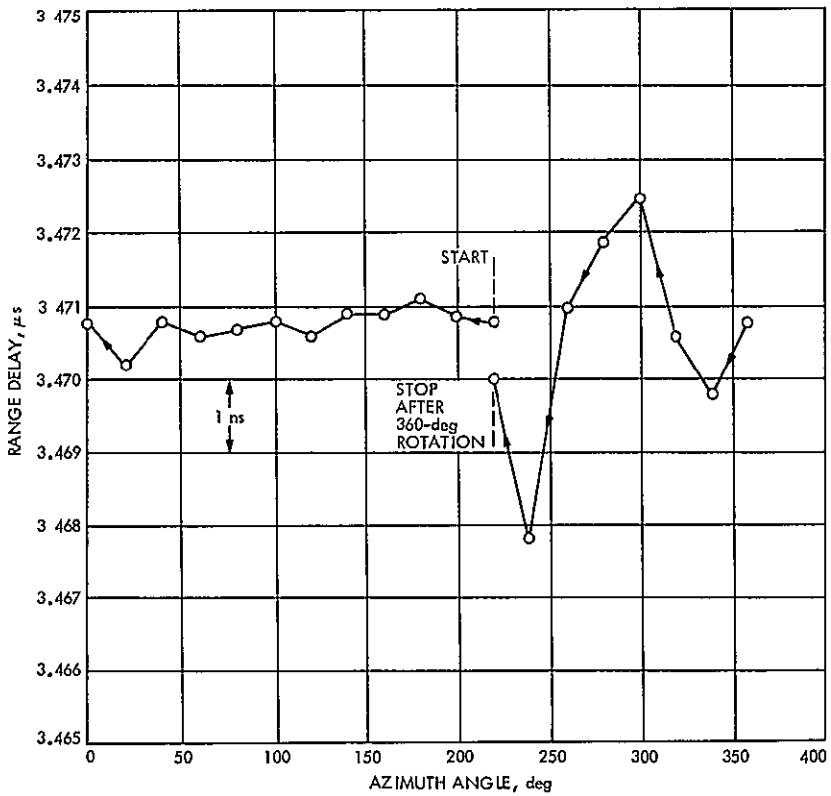

Fig. 11. S-range vs azimuth angle via ZDD cable configuration, EL = 45 deg, 100 kW, RCV3 = S, 1974 Day 157

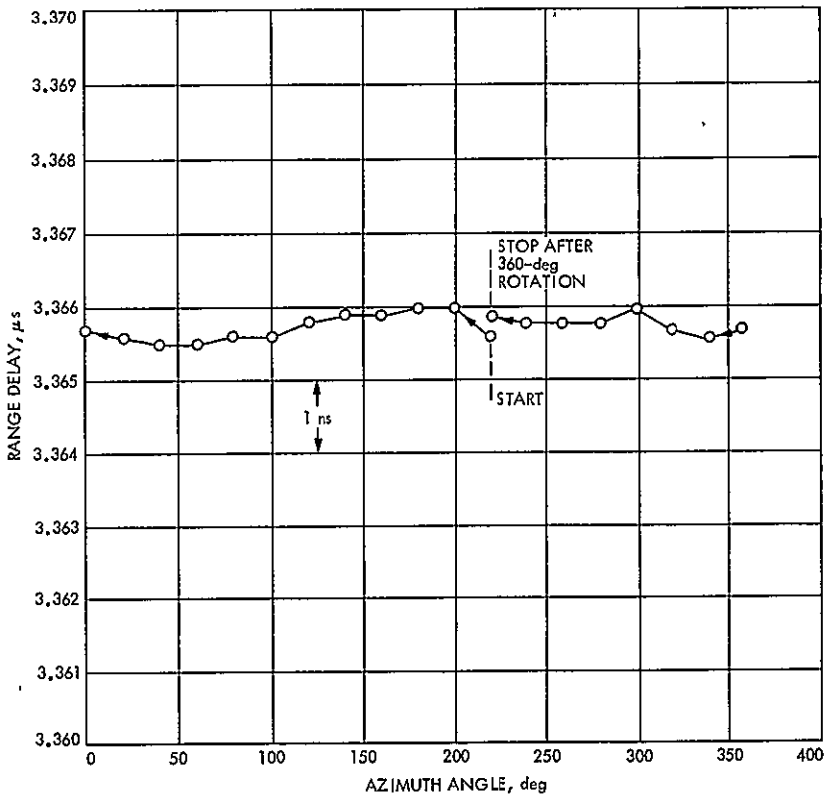

Fig 12. X-range vs azimuth angle via ZDD cable configuration, EL = 45 deg, 100 kW, RCV4 = X, 1974 Day 157

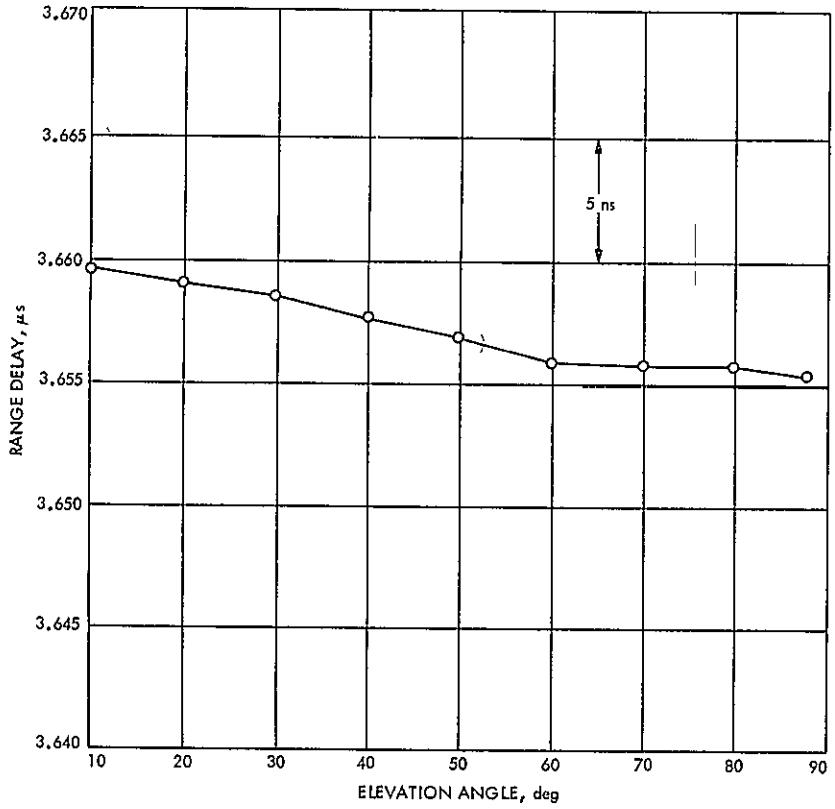

Fig. 13. S-range vs elevation angle via ZDD airpath, 1974 Day 114

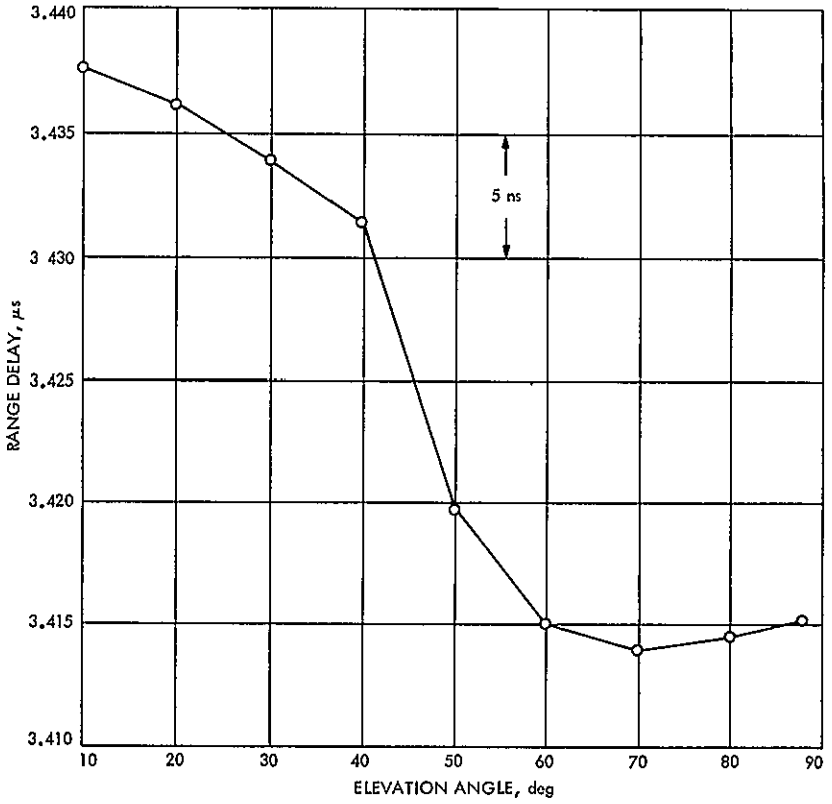

Fig 14 X-range vs elevation angle via ZDD airpath (X-maser by-passed), 1974 Day 114

Reprinted from *The Deep Space Network Progress Report 42-23*, Oct 15, 1974, pp 45–51

S/X Experiment: A Study of the Effects of Ambient Temperature on Ranging Calibrations

T Y. Otoshi
Communications Elements Research Section

A study has been made of the effects of the outside air temperature at DSS 14 on ground system range calibrations Some correlation was found on range data obtained with the 20-kW transmitter system configuration, but no correlation was found for the 100-kW transmitter system configuration

I. Introduction

In a previous report (Ref. 1), Mariner 10 pre- and post-tracking pass range calibration data were presented for 1974 Day 12 through Day 150 A cursory examination of the data showed that differences between pre- and post-calibration data for the same day's track could be attributed to ambient temperature changes. Since outside air temperatures at DSS 14 have been tabulated in the ranging calibration log book, it was possible to perform a correlation analysis of these data This article presents the result of this study.

II. Calibration Configuration

Ranging calibrations on the ground system at DSS 14 are currently being performed with the zero delay device (ZDD) in the cable configuration that was described in Ref. 2. The ranging calibrations are normally done during pre- and post-calibration periods of Mariner 10 tracking passes at the signal levels and frequencies applicable to the particular tracking pass. These ZDD pre- and post-calibration data are used along with the ground station Z-correction (Ref 3) and spacecraft radio system bias correction to enable determination of the true range to the spacecraft (Ref 4)

A block diagram of the present ZDD configuration for the S/X ground system calibrations at DSS 14 is shown in Fig 1. As was described in Ref 2, the ZDD is a ground station antenna-mounted transponder that samples the uplink 2113 MHz from the transmitter and generates coherent downlink S- and X-band test signals of 2295 and 8415 MHz These test signals are transmitted to the respective masers through calibrated cables of known delay.

Figures 2 and 3 show the ZDD in the cable configuration as it is currently installed in the Mod-3 section of the 64-m antenna at DSS 14. Since this ZDD assembly is located in the air-conditioned environment of the Mod-3 area, this portion of the range calibration system should not be affected by outside air temperature changes It is believed that most of the range changes attributed to outside air temperature changes will occur in the uplink and downlink cables between the tricone

area and the control room. Only about 97.5 m (320 ft) round trip cable length is actually exposed to the outside air temperature environment Most of this cable run is Spiroline RG 252 cable, but about 12.2 m (40 ft) of round trip RG 214 cable is used in the elevation cable wrapup.

III. Test Results

As was discussed in previous reports (Refs. 1 and 5), the Block 4 range calibration data are also a function of signal level and differ when using the 20-kW or the 100-kW transmitters. Therefore, it was necessary to group the data as those belonging to either the 20-kW or 100-kW transmitter calibrations. Through the use of range change versus signal level curves presented in Ref 5 it was possible to correct the data and normalize them to a common signal level reference, which was arbitrarily chosen to be −145 dBm Only calibration data from 1974 Day 85 to Day 172 were used; it was only after Day 85 when both the doppler and system configurations were left unaltered.

The ranging calibration data are shown plotted as functions of outside air temperature in Figs. 4 through 7. It can be seen that some correlation of range change to temperature is evident for the 20-kW transmitter system for both S- and X-band.

For the purposes of comparison, X-band group delay data as a function of temperature are shown in Figs. 8 and 9 for 3 05-m (10-ft) lengths of Spiroline RG 252 and RG 214 cables, respectively. These data were obtained in a temperature-controlled oven and group delay measured by a phase versus frequency measurement technique with a network analyzer. It can be seen that the Spiroline RG 252 characteristics are similar to those measured for the 20-kW data. As was mentioned previously, most of the DSS 14 ranging system cable run consists of RG 252 cable

No correlation was seen for the data plotted for the 100-kW transmitter system data. This lack of correlation for the 100-kW transmitter data is difficult to explain. It is possible that there are more random noise and range changes associated with the 100-kW transmitter itself. The effect on connector and cable mismatches could also cause departure from expected trends.

IV. Discussion and Conclusions

The results presented in this article show that some correlation of range change with ambient temperature changes was found However, the results should be interpreted to show trends only and not be used as a correction curve. The data quality is understandably poor for this type of analysis since it is based on two data points a day for a period of about three months. Many systematic and random errors could easily be introduced. It would have been preferable to obtain ranging stability data in one continuous run over a period of about 12 hours. This test should begin in the early morning hours and continue to nighttime hours so as to include the large temperature change periods.

Although time at DSS 14 had been scheduled for performing some of this type of testing, other system problems and test requirements made it difficult to obtain a long continuous run of good ranging stability data.

References

1 Otoshi, T Y., "S/X Experiment DSS 14 Pre- and Post-Track Ranging Calibrations for Mariner 10 Tracking Passes and Associated Problems," in *The Deep Space Network Progress Report 42-22*, pp 81–89, Jet Propulsion Laboratory, Pasadena, California, August 15, 1974.

2. Otoshi, T Y, and Stelzried, C T., "S/X Experiment: A New Configuration for Ground Range Calibrations With the Zero Delay Device," in *The Deep Space Network Progress Report 42-20*, pp 57–63, Jet Propulsion Laboratory, Pasadena, California, April 15, 1974.

3. Batelaan, P. D., "S/X-Band Experiment: Zero Delay Device Z Correction," in *The Deep Space Network Progress Report 42-20,* pp 78–83, Jet Propulsion Laboratory, Pasadena, California, April 15, 1974.

4. "TRK-2-8 Module of DSN System Requirements Detailed Interface Design Document 820-13, Rev. A.," July 1, 1973 (JPL internal document).

5. Otoshi, T. Y., and Batelaan, P. D., "S/X Experiment: DSS 14 S/X Ground System Ranging Tests," in *The Deep Space Network Progress Report 42-22,* pp. 90–100, Jet Propulsion Laboratory, Pasadena, California, August 15, 1974.

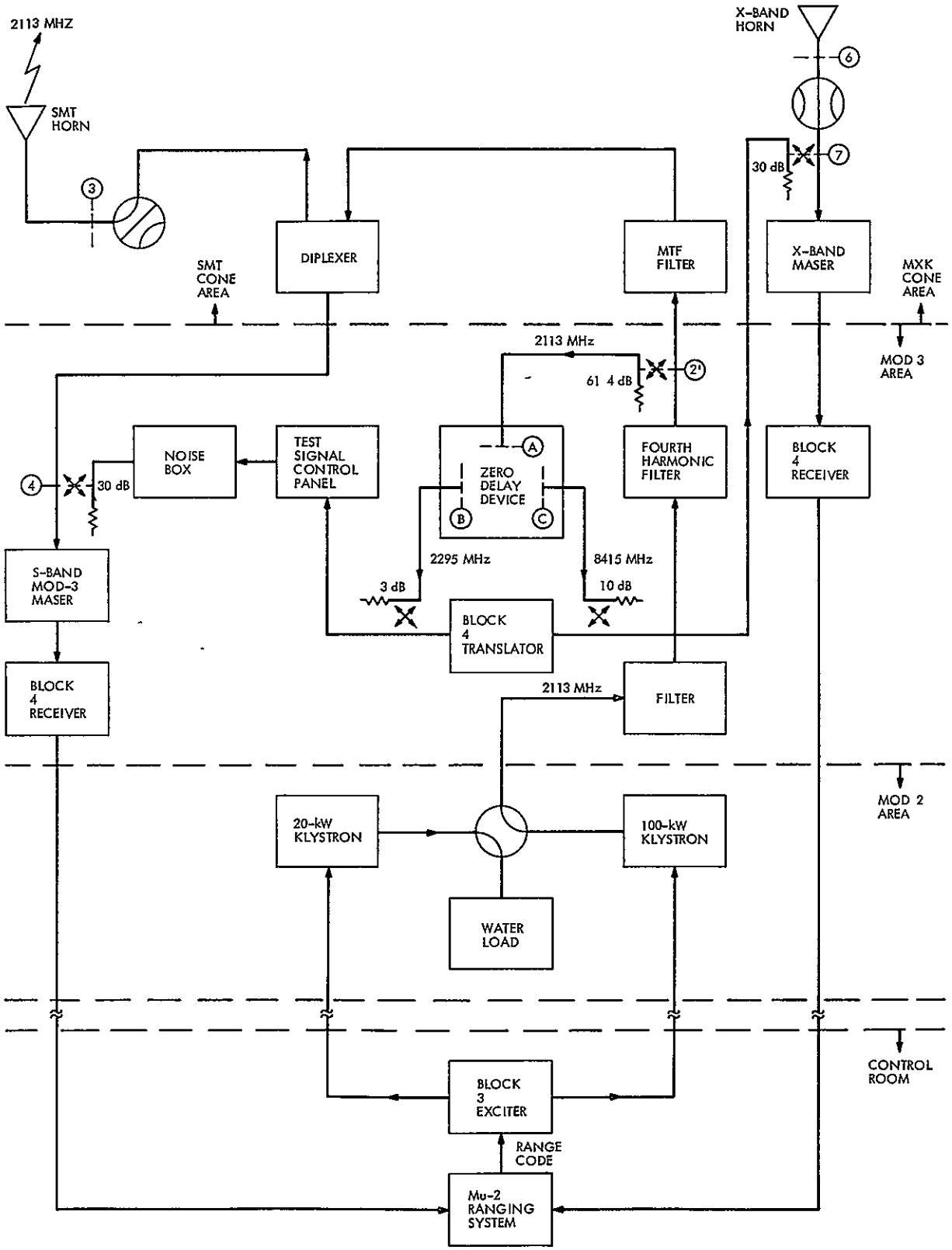

Fig 1. Block diagram of the new configuration at DSS 14 for ground system range calibrations

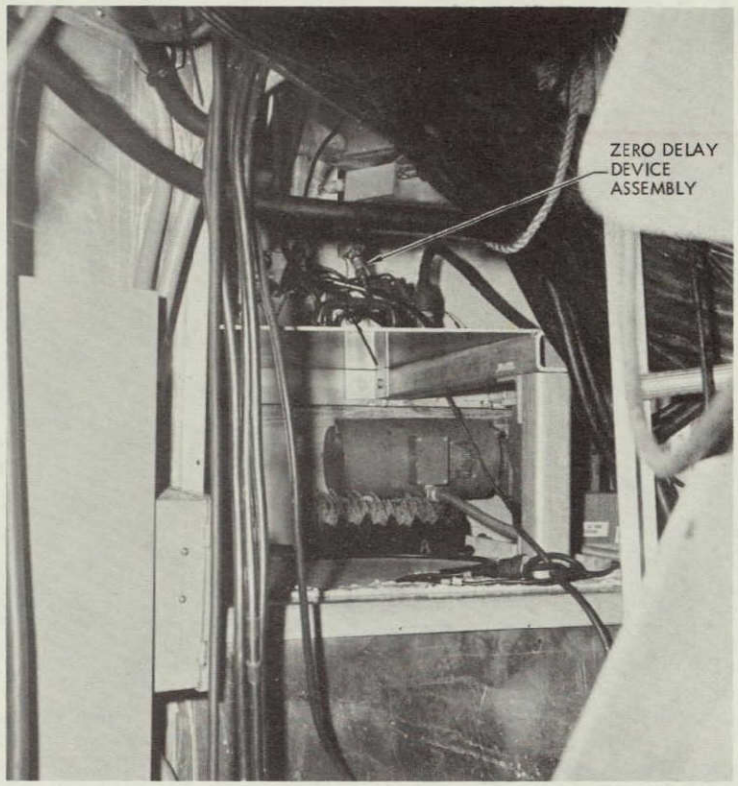

Fig. 2. Zero delay device assembly as seen inside the Mod 3 area

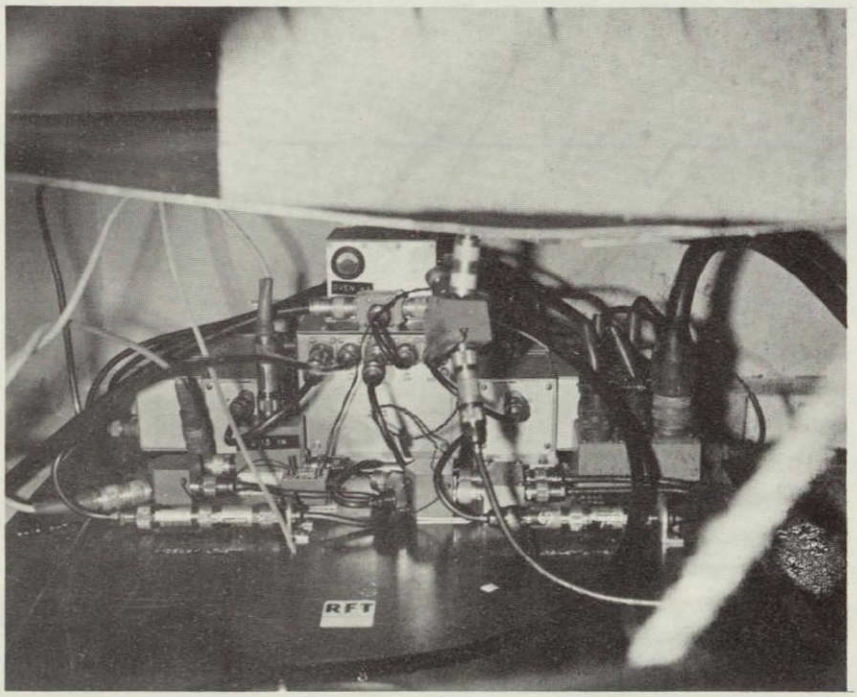

Fig. 3. Closeup view of the zero delay device assembly as currently installed in the Mod 3 area

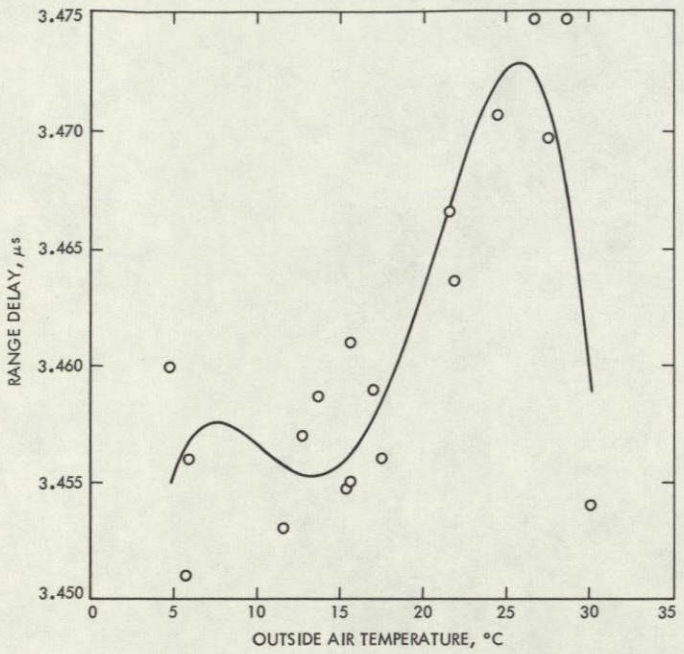

Fig. 4. S-band range as a function of outside air temperature at DSS 14. Data taken after 1974 Day 85 for 20-kW transmitter configuration and corrected to the −145-dBm signal level

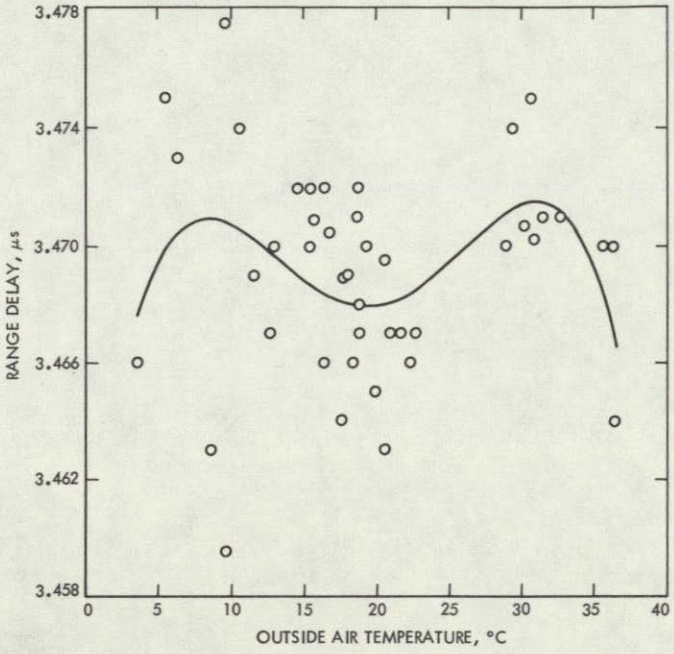

Fig. 6. S-band range as a function of outside air temperature at DSS 14. Data taken after 1974 Day 85 for 100-kW transmitter configuration and corrected to the −145-dBm signal level

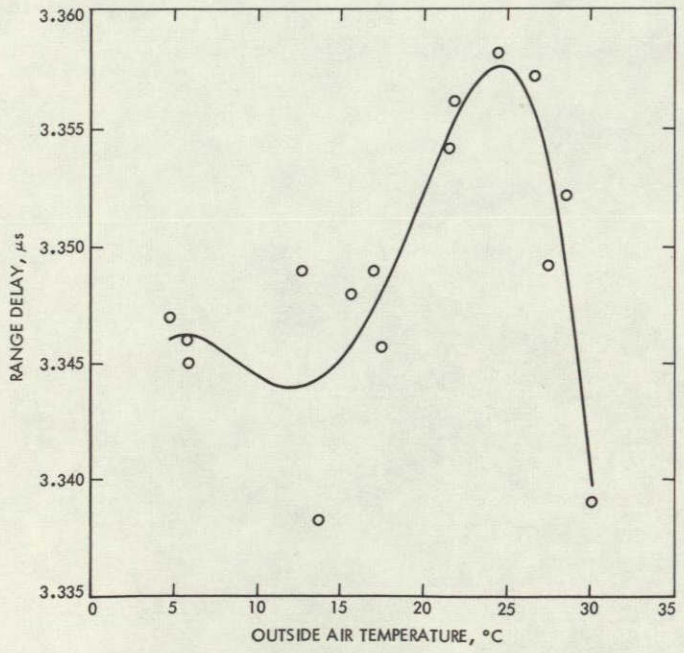

Fig. 5. X-band range as a function of outside air temperature at DSS 14. Data taken after 1974 Day 85 for 20-kW transmitter configuration and corrected to the −145-dBm signal level

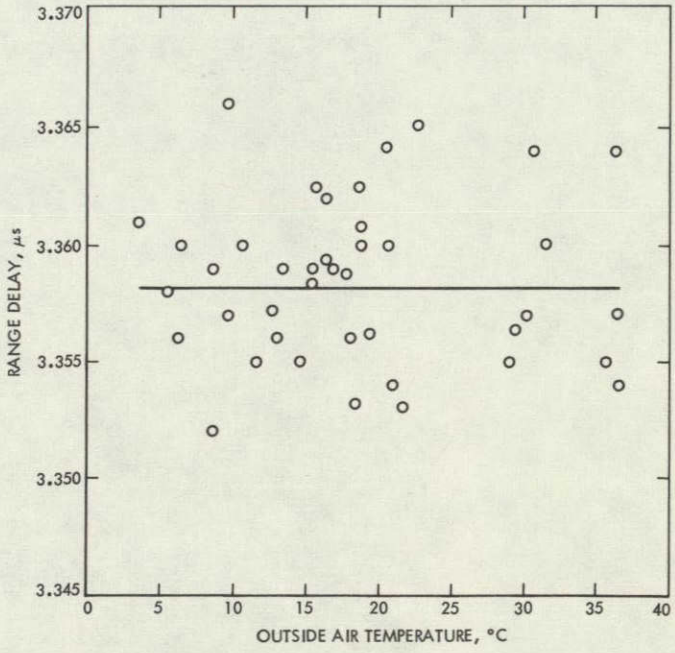

Fig. 7. X-band range as a function of outside air temperature at DSS 14. Data taken after 1974 Day 85 for 100-kW transmitter configuration and corrected to the −145-dBm signal level

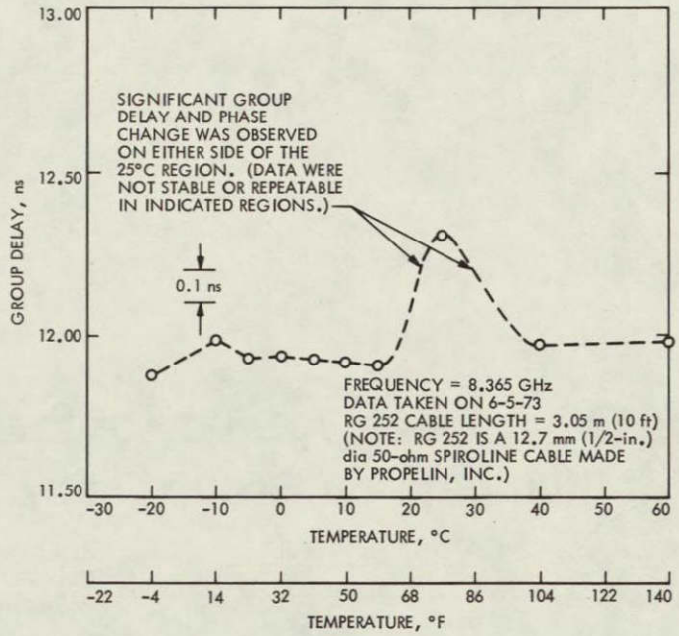

Fig. 8. X-band group delay as a function of temperature for 3.05-m (10-ft) length of Spiroline RG 252 cable

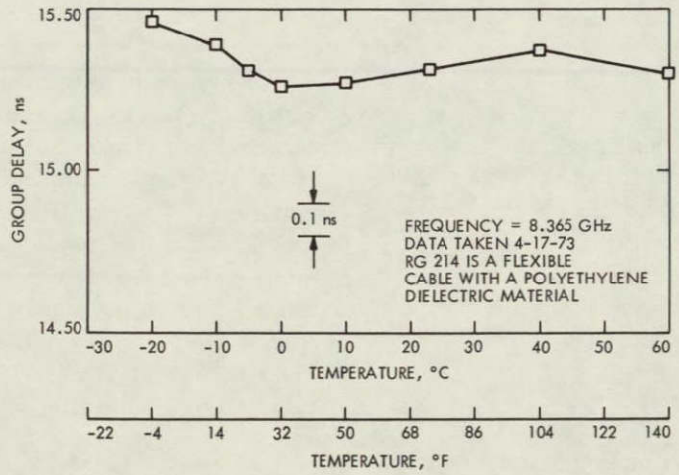

Fig. 9. X-band group delay as a function of temperature for 3.05-m (10-ft) length of RG 214 cable

Reprinted from *The Deep Space Network Progress Report 42-24*, Dec. 15, 1974, pp. 40–50.

S/X-Band Experiment: A Study of the Effects of Multipath on Group Delay

T. Y. Otoshi
Communications Elements Research Section

An analytical expression is presented for calculating the effects of multipath on group delay. The expression was experimentally verified by tests made at the Telecommunications Development Laboratory using the Mariner Venus/Mercury 1973 Radio Frequency Subsystem, Block 3 receiver and the Mu 1 ranging machine.

I. Introduction

With the exception of DSS 14, all stations of the Deep Space Network use the conventional zero-delay ranging configuration, in which the zero-delay device (ZDD) is mounted on the dish surface. A zenith range measurement via the airpath to a dish-mounted ZDD and a Z-height correction (Ref. 1) provide needed ground station information for determining the true range to the spacecraft.

Results of airpath tests at DSS 14 showed that large changes in range occurred as a function of antenna elevation angle when a ZDD was mounted on the 64-m antenna dish surface (Ref. 2). This characteristic was also observed on the 64-m antenna systems at DSS 43 and DSS 63 (Ref. 3). Since the range dependence on elevation angle could be due to a multipath phenomenon, one cannot assume that a zenith measured value is the correct value.

Other airpath tests made on the 64-m antenna S/X system at DSS 14 showed that large-range changes also occurred when small changes were made in axial focusing of the hyperbola. Another unexplained airpath phenomenon observed was a 53-ns discrepancy between the theoretical and experimental values of S-band zero delay range when the dichroic plate/ellipsoid assembly was retracted and the system was operated for S-band only (Ref. 4). Because of the described airpath problems, the ZDD configuration at DSS 14 has been operated in a cable configuration (Ref. 5) since January 12, 1974.

Although it had been suspected that some of the airpath problems could be due to multipath, other system testing priorities made it difficult to perform further airpath tests to isolate the source of the problems. It was also thought that multipath could not generate errors of the magnitudes which were observed. Recently, the study of the multipath effect was reinitiated and resulted in the

derivations of two theoretical expressions which showed that surprisingly large errors on range measurements could be caused by multipath. One expression derived by J. R. Smith (Refs. 6, 7) is based on the phase shift produced on the envelope of a carrier that is phase-modulated with a square-wave. The analysis was done for the range-clock modulation and detection processes actually employed by the Planetary and Mu-Ranging systems. The second expression, which was derived independently by this author, is based on the conventional definition of group delay where the output phase of a carrier wave is differentiated with respect to frequency. It was shown by Smith (Ref. 7) that for low range-clock modulation frequencies, the two independent derivations reduced to the same mathematical expression.

This article presents the theoretical expression derived by this author and the test data obtained at the Telecommunications Development Laboratory (TDL), showing good agreement between theory and experiment.

II. Summary of Theoretical Expressions

Figure 1 shows the multipath configuration for which the theory was derived. Path 1 is the primary path, and path 2 is the leakage path. The group delay (in seconds) for a signal to travel from the input port to the output port can be expressed as

$$t_g = t_{g1} + \epsilon_g \tag{1}$$

where t_{g1} is the group delay which would be observed in the absence of multipath, and ϵ_g is the deviation from t_{g1} caused by multipath. As derived in the Appendix, this error term is given by

$$\epsilon_g = A(t_{g2} - t_{g1})\left[\frac{A + \cos\theta}{1 + 2A\cos\theta + A^2}\right] \tag{2}$$

where

$$\theta = -(\beta_2 \ell_2 - \beta_1 \ell_1) \tag{3}$$

and where

A = ratio of the magnitude of the leakage wave to the magnitude of the primary wave

β_1, β_2 = phase constants, respectively, of paths 1 and 2, rad/m

ℓ_1, ℓ_2 = physical path lengths, respectively, of paths 1 and 2, m

t_{g1} = group delay of the primary wave traveling through path 1 only, s

t_{g2} = group delay of the leakage wave traveling through path 2 only, s

It is also shown in the Appendix that the carrier phase delay in seconds is

$$t_p = t_{p1} + \epsilon_p \tag{4}$$

where

$$\epsilon_p = -\frac{1}{\omega}\tan^{-1}\left[\frac{A\sin\theta}{1 + A\cos\theta}\right] \tag{5}$$

The differenced range versus integrated doppler (DRVID) can be calculated from (See Ref. 8)

$$\text{DRVID} = t_g - t_p \tag{6}$$

and relative carrier amplitude in dB from

$$20\log_{10}\left|\frac{E_{\text{out}}}{E_{\text{in}}}\right| = 20\log\left|\frac{E_1}{E_{\text{in}}}\right| + 20\log_{10}|1 + A\,e^{j\theta}| \tag{7}$$

Assuming that $t_{g2} > t_{g1}$, and $\theta = -2\pi m$ where m is a positive integer, the group delay and amplitude errors simultaneously reach their upper bounds while the phase delay error given by Eq. (5) goes to zero. When $\theta = -(2n - 1)\pi$ where n is a positive integer, the group delay and amplitude errors simultaneously go to their lower bounds while the phase delay error goes to zero. However, in the case where $t_{g2} < t_{g1}$, the group delay error and carrier amplitude simultaneously reach *opposite* bounds. The expressions for upper and lower bounds on phase delay, group delay, and carrier amplitude are given in the Appendix.

Figure 2 shows plots of the upper and lower bounds of group delay in a free-space media for cases where $t_{g2} > t_{g1}$. The upper bound is obtained when the leakage and primary waves are in phase. The lower bound is obtained when the signals are out of phase. If $t_{g2} < t_{g1}$, the opposite polarity must be assigned to the $\Delta\ell$ and error-bound values of Fig. 2. For this latter case, the new upper bound will be reached when the signals are out of phase rather than in phase. (See Case 2 in the Appendix.) The signal level ripple shown on the plot is the peak-to-peak carrier signal level change as observed when θ is varied 360 deg or less. The ripple was calculated from

$$\Delta_{\text{dB}} = 20\log_{10}\frac{|E_{\text{out}}|_{\max}}{|E_{\text{out}}|_{\min}} = 20\log_{10}\left(\frac{1 + A}{1 - A}\right) \tag{8}$$

The curves shown on Fig. 2 may be useful for isolating possible sources of leakage waves on the 64-m antenna. Possible leakage can result from scattering of waves from the quadripod legs, tricone, or the dichroic plate/ellipsoid assembly support structures. Some of the differential path lengths of leakage and primary waves on the 64-m antenna can be of the order of 30 m.

III. Experimental Setup

Figure 3 shows a multipath device that was fabricated for purposes of verifying the theoretical equations presented above. Figure 4 is a block diagram of this device. To obtain the desired differential delay between path 1 and path 2, appropriate length cables can be inserted into either path 1 or path 2. The amplitude and phase of the signal in path 2 is adjusted with the variable attenuator and phase shifter, respectively. Repeatable coaxial switches were used to permit measurements of the amplitude and group delay of the signals in the individual paths.

The ranging tests were performed at the TDL in JPL Building 161. The TDL tests were performed with a 516-kHz square wave phase-modulating the uplink signal of 2113 MHz that was transmitted to an MVM'73 Radio Frequency Subsystem (RFS). After receiving the range-coded uplink, the RFS then generated a coherent 2295-MHz downlink signal that was transmitted to the Block 3 receiver through coaxial cables. The multipath device was inserted into this downlink path and therefore, adjustments made on the multipath device resulted in one-way range changes only. Measurements of absolute two-way range as well as one-way range changes were achieved with the Mu-1 ranging machine.

The initial TDL test parameters were as follows:

MVM'73 Radio Frequency Subsystem
Radio mode 022
Uplink signal level total power = −115 dBm
Block 3 Receiver
Mu-1 ranging machine
Carrier suppression = 9 dB
Integration time = 30 s

IV. Test Results

Table 1 shows a summary of the ranging test results obtained with the multipath device. Appropriate length cables were inserted into path 2 of the multipath device to create differential path lengths of 23 ns (Case A) and 93.2 ns (Case B). For each case, the signal in path 2 was adjusted to be approximately −21, −11, and −6 dB relative to the primary signal. More precise post-calibration measurements showed the leakage and primary signals to be at the relative dB levels indicated in the table. The maximum and minimum received signal levels shown in Table 1 are in reasonably good agreement with those predicted by Eqs. (A-10a) and (A-10b). The tabulated received signal levels as obtained from automatic gain control (AGC) calibrations are estimated to be accurate to ±0.2 dB.

Theoretical range change values were calculated from Eqs. (A-23a) and (A-23b). The agreement between theory and experimental range change value was typically within 1 ns. The large discrepancy of 14 ns for the last case in Part B of Table 1 could possibly be due to an error in setting the attenuator so that the relative signal level was actually −6 dB instead of the relative level of −5.5 dB on which the theoretical calculations were based. It is also possible that the discrepancy was caused by the fact that the theoretical value is valid only at a single frequency. The measured value applies to a carrier wave that is phase-modulated with a 516 kHz square wave. Therefore, for severe multipath cases it might be more appropriate to make comparisons with a theoretical value that is averaged over an effective finite bandwidth. For example, see Footnote b in Table 1.

V. Summary and Conclusions

Theoretical equations have been derived for studying the effects of multipath (or leakage) on group delay measurements. The theory was developed for group delay but is applicable to analysis of envelope delay when distortion is small. In general, very good agreement was obtained between theory and experiment.

The theory can be applied to ZDD test data to help isolate possible sources of leakage waves on the 64-m antenna. This type of analysis was done by J. R. Smith (Refs. 6, 7) for the Mariner 10 spacecraft antenna system. He showed a correlation of range change to amplitude change and isolated one of the major causes as being a multipath signal reflecting from a solar panel on the Mariner 10 spacecraft.

In this article, only one-way range error was analyzed. In a telecommunications system, the range change can be

caused by a two-way effect (uplink and downlink). The two-way range error analysis is somewhat more involved and too lengthy to include in this article. Test data on the effects of multipath on two-way range has been obtained and will be reported in a subsequent issue of this publication.

Acknowledgements

This experimental work at TDL was supported and made possible by D. L. Brunn of the Spacecraft Radio Section. M. M. Franco of the Communications Elements Research Section fabricated the multipath device.

References

1. *TRK-2-8 Module of DSN System Requirements Detailed Interface Design Document 820-13, Rev. A*, Jet Propulsion Laboratory, July 1, 1973 (JPL internal document).

2. Stelzried, C. T., Otoshi, T. Y., and Batelaan, P. D., "S/X Band Experiment: Zero Delay Device Antenna Location," in *The Deep Space Network Progress Report 42-20*, Jet Propulsion Laboratory, Pasadena, Calif., Apr. 15, 1974, pp. 64–68.

3. Schlaifer, R., "Planetary Ranging Station Delays," IOM 421-PF-TRK040, March 4, 1974 (JPL internal document).

4. Otoshi, T. Y., "Operational Support for Proposed Ranging Experiment to Resolve Range Anamolies in DSS-14 S/X System," IOM 3333-74-106, May 14, 1974 (JPL internal document).

5. Otoshi, T. Y., and Stelzried, C. T., "S/X Experiment: A New Configuration for Ground System Range Calibrations With the Zero Delay Device," in *The Deep Space Network Progress Report 42-20*, pp. 57–63, Jet Propulsion Laboratory, Pasadena, Calif., Apr. 15, 1974.

6. Smith, J. R., "Viking Ranging Investigation Team," IOM 3382-74-064, July 22, 1974 (JPL internal document).

7. Smith, J. R., "Viking Ranging Investigation Team," IOM 3382-74-076, July 30, 1974 (JPL internal document).

8. MacDoran, P. F., "A First-Principles Derivation of the Differenced Range Versus Integrated Doppler (DRVID) Charged-Particle Calibration Method," in *The Deep Space Network, Space Programs Summary 37-62, Vol. II*, pp. 28–34. Jet Propulsion Laboratory, Pasadena, Calif., Mar. 31, 1970.

9. Ramo, S., and Whinnery, J. R., "Fields and Waves in Modern Radio," John Wiley & Sons, Inc., New York, N.Y., 1953, pp. 46–48.

10. Collin, R. E., "Foundations for Microwave Engineering," pp. 132–137, McGraw-Hill Book Company, New York, N.Y., 1966.

Table 1. Results of one-way range tests with the multipath device (frequency = 2.295 GHz)

Test conditions	Phase shifter setting, deg	Approx. received signal level, dBm	Range change, ns		
			Average measured value[a]	Theoretical value	Measured minus theoretical
A. Measured delay via path 2 alone is 23.0 ns longer than path 1 alone					
1. Attenuator adjusted to make leakage signal be −21 dB relative to primary signal					
Phase shifter adjusted to obtain maximum received signal	−224.9	−89.6	1.7	1.9	− 0.2
Phase shifter adjusted to obtain minimum received signal	− 45.9	−91.2	− 2.5	− 2.3	− 0.2
2. Attenuator adjusted to make leakage signal be −10.8 dB relative to primary signal					
Phase shifter adjusted to obtain maximum received signal	−224.9	−88.1	4.8	5.1	− 0.3
Phase shifter adjusted to obtain minimum received signal	− 45.9	−93.5	−10.1	− 9.3	− 0.8
3. Attenuator adjusted to make leakage signal be −5.65 dB relative to primary signal					
Phase shifter adjusted to obtain maximum received signal	−224.9	−86.7	7.3	7.9	− 0.6
Phase shifter adjusted to obtain minimum received signal	− 45.9	−97.0	−26.4	−25.1	− 1.3
B. Measured delay via path 2 alone is 93.2 ns longer than path 1 alone					
1. Attenuator adjusted to make leakage signal be −20.7 dB relative to primary signal					
Phase shifter adjusted to obtain maximum received signal	−397.0	−89.5	7.6	7.8	− 0.2
Phase shifter adjusted to obtain minimum received signal	−218.0	−91.1	− 9.2	− 9.4	0.2
2. Attenuator adjusted to make leakage signal be −10.7 dB relative to primary signal					
Phase shifter adjusted to obtain maximum received signal	−397.0	−88.0	20.5	21.1	− 0.6
Phase shifter adjusted to obtain minimum received signal	−218.0	−93.3	−36.6	−38.7	2.1
3. Attenuator adjusted to make leakage signal be −5.5 dB relative to primary signal					
Phase shifter adjusted to obtain maximum received signal	−397.0	−86.6	31.1	32.3	− 1.2
Phase shifter adjusted to obtain minimum received signal	−218.0	−97.0	−91.2	−105.2[b]	14.0

[a]Number of 30-sec integration data points used to obtain average value was typically 20. The calculated standard error associated with the average was typically ± 0.2 ns.

[b]The average theoretical range change over the frequency range of 2295.0 ± 0.5 MHz is −96.4 ns.

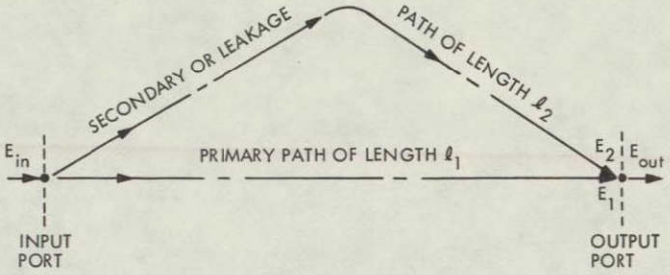

Fig. 1. Geometry for multipath analysis

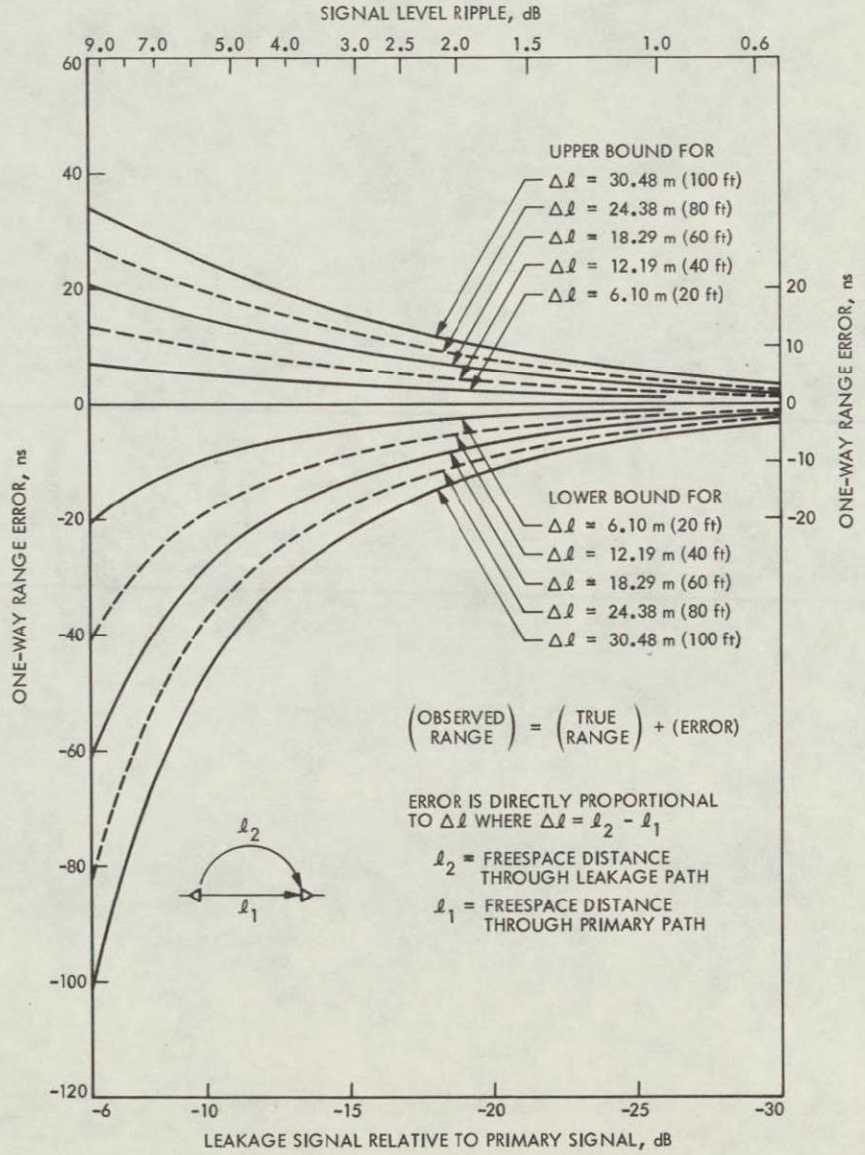

Fig. 2. Limits of one-way range error due to multipath in a free-space media

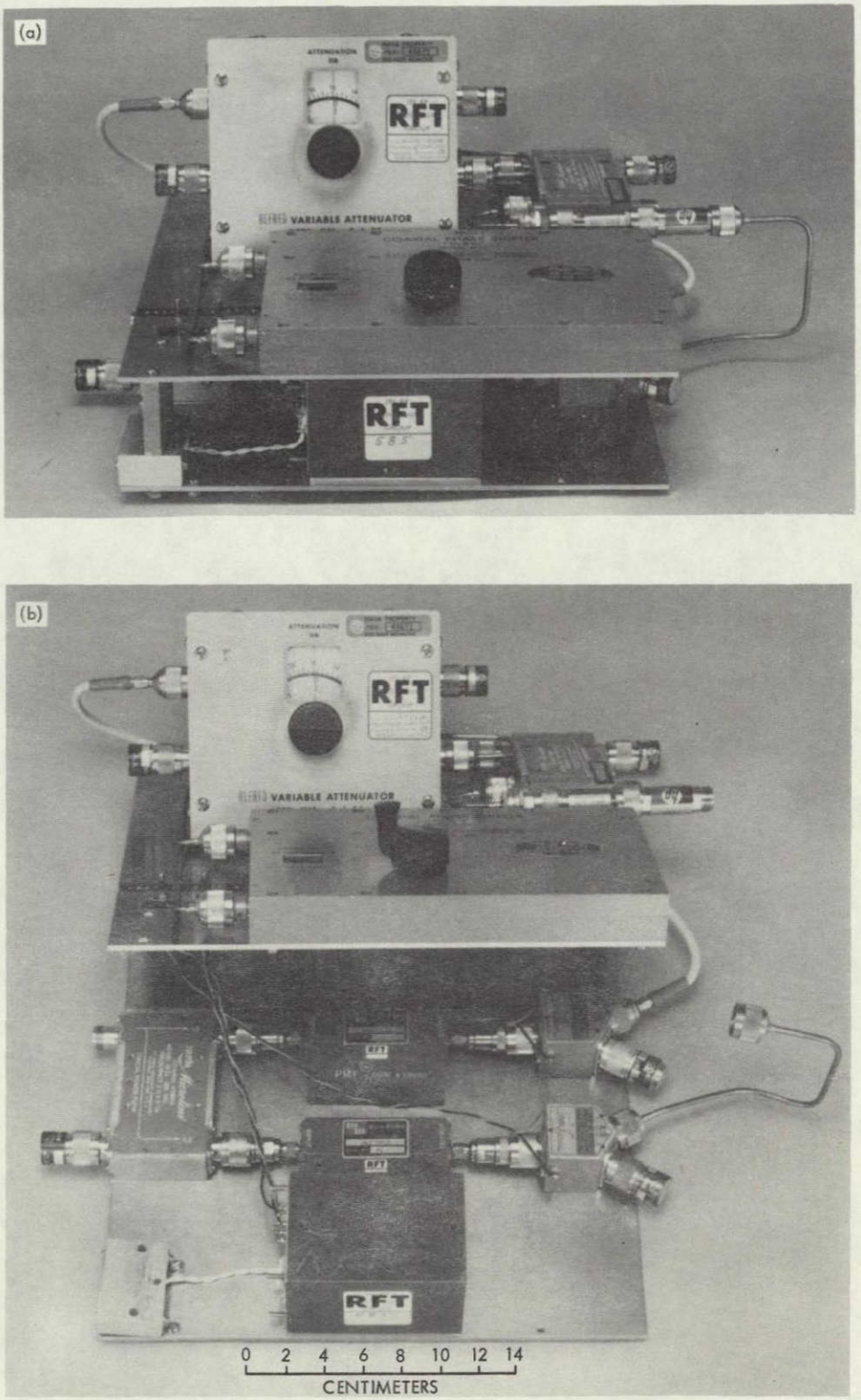

Fig. 3. Multipath device for experimental verification of theoretical derivations: (a) completely assembled, (b) partially disassembled

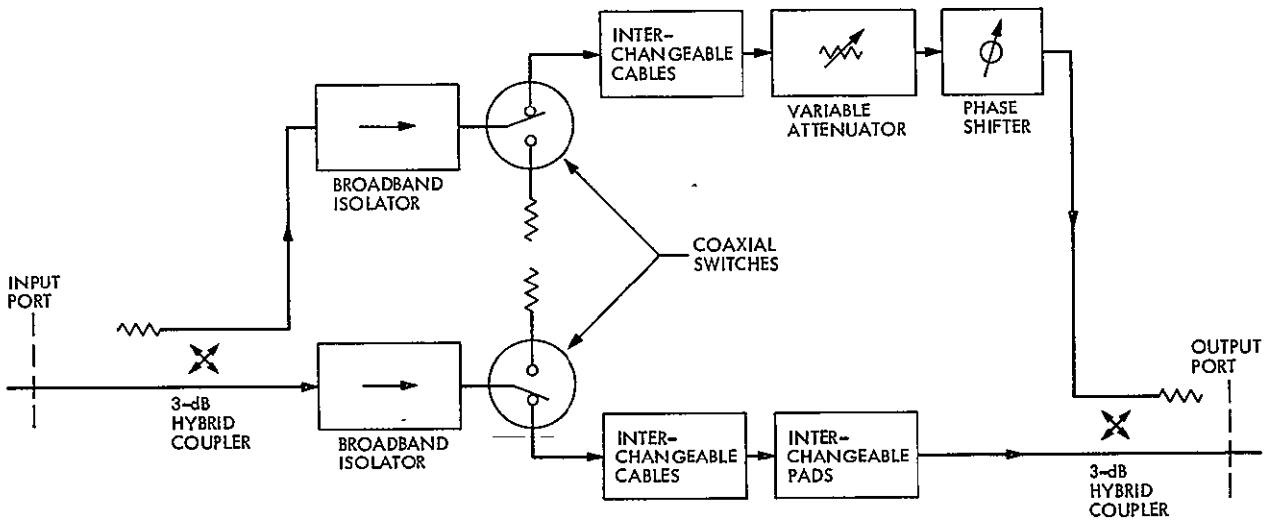

Fig 4 Multipath device block diagram

Appendix

Derivation of Equations for Phase and Group Delay Errors Caused by Multipath

Figure 1 shows the basic multipath configuration under study where two waves combine after traveling through two separate paths. This basic case can be generalized to include more waves and more paths, but it is sufficient to consider the basic case to show the effect of interference on group delay Let the wave at the input port be expressed as

$$E_{in} = |E_{in}| \exp(j\phi_0) \tag{A-1}$$

and the wave at the output port be the phasor sum of the primary path wave E_1 and the secondary path wave E_2 so that

$$\begin{aligned} E_{out} &= E_1 + E_2 \\ &= |E_1| \exp(j\phi_1) + |E_2| \exp(j\phi_2) \end{aligned} \tag{A-2}$$

Then from Eqs. (A-1) and (A-2)

$$\frac{E_{out}}{E_{in}} = \left|\frac{E_1}{E_{in}}\right| \exp j(\phi_1 - \phi_0) + \left|\frac{E_2}{E_{in}}\right| \exp[j(\phi_2 - \phi_0)] \tag{A-3}$$

Let

$$\phi_1 - \phi_0 = -\beta_1 \ell_1 \tag{A-4}$$

$$\phi_2 - \phi_0 = -\beta_2 \ell_2 \tag{A-5}$$

where

ℓ_1 = physical length of path 1, m

ℓ_2 = physical length of path 2, m

β_1, β_2 = phase constants, respectively, of paths 1 and 2, rad/m

Substitution of Eqs. (A-4) and (A-5) into Eq (A-3) gives

$$\frac{E_{out}}{E_{in}} = \left|\frac{E_1}{E_{in}}\right| \exp(-j\beta_1 \ell_1) \left[1 + \left|\frac{E_2}{E_1}\right| \exp[-j(\beta_2 \ell_2 - \beta_1 \ell_1)]\right] \tag{A-6}$$

The ratio $|E_2/E_1|$ is a parameter that is generally of interest so that it is convenient to let

$$A = \left|\frac{E_2}{E_1}\right| \tag{A-7}$$

Furthermore, let

$$\theta = -(\beta_2 \ell_2 - \beta_1 \ell_1) \tag{A-8}$$

and

$$F = 1 + A e^{j\theta} \tag{A-9}$$

so that substitution into Eq. (A-6) gives the output signal magnitude ratio of

$$\left|\frac{E_{out}}{E_{in}}\right| = \left|\frac{E_1}{E_{in}}\right| |1 + A e^{j\theta}| \tag{A-10}$$

and relative phase of

$$\arg\left(\frac{E_{out}}{E_{in}}\right) = -\beta_1 \ell_1 + \arg F \tag{A-11}$$

where

$$\arg F = \tan^{-1}\left[\frac{A \sin\theta}{1 + A\cos\theta}\right] \tag{A-12}$$

From substitution of Eq (A-11) into the definition of phase delay (Refs 9, 10) given as

$$t_p = \frac{-1}{\omega}\left[\arg\left(\frac{E_{out}}{E_{in}}\right)\right] \tag{A-13}$$

we obtain

$$t_p = t_{p1} + \epsilon_p \tag{A-14}$$

where

$$t_{p1} = \frac{\beta_1 \ell_1}{\omega} \tag{A-15}$$

$$\epsilon_p = -\frac{1}{\omega}\tan^{-1}\left[\frac{A \sin\theta}{1 + A\cos\theta}\right] \tag{A-16}$$

From setting the differential of ϵ_p with respect to ℓ_2 equal to zero, one finds that ϵ_p becomes maximum when $\theta = \pm\cos^{-1}(-A)$ so that the upper and lower bounds of phase delay error are

$$(\epsilon_p)_U = +\frac{1}{\omega}\tan^{-1}\left(\frac{A}{\sqrt{1 - A^2}}\right) \tag{A-17}$$

$$(\epsilon_p)_L = -\frac{1}{\omega}\tan^{-1}\left(\frac{A}{\sqrt{1-A^2}}\right) \qquad \text{(A-18)}$$

The worst possible case occurs when $A \to 1$ and the error bounds become $\pm 1/(4f)$. For example, at 2.0 GHz the worst-case phase delay error that can be caused by multipath is ± 0.125 ns.

The definition of group delay (Refs. 9, 10) is

$$t_g = -\frac{d}{d\omega}\left[\arg\left(\frac{E_{out}}{E_{in}}\right)\right] \qquad \text{(A-19)}$$

From substitution of Eq. (A-11) into Eq. (A-19), we obtain

$$t_g = t_{g1} + \epsilon_g \qquad \text{(A-20)}$$

where

$$t_{g1} = \frac{d\beta_1}{d\omega}\ell_1 \qquad \text{(A-21)}$$

$$\epsilon_g = -\frac{d}{d\omega}\arg F \qquad \text{(A-22)}$$

where arg F was given by Eq. (A-12). Note that t_{g1} is the group delay that would be obtained in the absence of multipath and ϵ_g is the group delay error or deviation from t_{g1}.

Performing the operation of Eq. (A-22) and assuming that over the frequency interval of interest

$$\frac{\partial A}{\partial \omega} = 0$$

we obtain

$$\epsilon_g = A(t_{g2} - t_{g1})\left(\frac{A + \cos\theta}{1 + 2A\cos\theta + A^2}\right) \qquad \text{(A-23)}$$

where

$$t_{g2} = \left(\frac{d\beta_2}{d\omega}\right)\ell_2$$

$$t_{g1} = \left(\frac{d\beta_1}{d\omega}\right)\ell_1$$

Note that t_{g1} is the delay through path 1 only in the absence of the multipath signal, while t_{g2} is the delay through path 2 only.

Performing a differentiation[1] of Eq. (A-23) with respect to ℓ_2 and setting the results equal to zero leads to the solutions of the values of θ which give upper and lower bounds of ϵ_g for two different cases. These are given as follows:

Case 1 Upper Bound

Assume $t_{g2} > t_{g1}$ and $\theta = -2\pi m$ where θ was given by Eq. (A-8) and m is a positive integer. In practice, m will usually be an integer greater than 10.

For these conditions, the leakage and primary waves are in phase and the group delay as given by Eq. (A-23) reaches an upper bound of

$$(\epsilon_g)_{U1} = (t_{g2} - t_{g1})\left(\frac{A}{1+A}\right) \qquad \text{(A-23a)}$$

At the same time, note from Eqs. (A-10) and (A-16) that the output signal magnitude ratio and phase delay error become

$$\left|\frac{E_{out}}{E_{in}}\right| = \left|\frac{E_1}{E_{in}}\right|(1 + A) \qquad \text{(A-10a)}$$

$$\epsilon_p = 0 \qquad \text{(A-16a)}$$

It is interesting to note that both the group delay and magnitude of the output signal reach an upper bound simultaneously while the phase delay error goes to zero.

Case 1 Lower Bound

Assume $t_{g2} > t_{g1}$ and $\theta = -(2n-1)\pi$ where θ is defined by Eq. (A-8) and n is a positive integer. In practice, n will usually be an integer greater than 10.

For these conditions, the leakage and primary waves are out of phase and the group delay error as given by Eq. (A-23) reaches a lower bound of

$$(\epsilon_g)_{L1} = -(t_{g2} - t_{g1})\left(\frac{A}{1-A}\right) \qquad \text{(A-23b)}$$

and the output signal magnitude ratio as given by Eq. (A-10) also reaches a lower bound of

$$\left|\frac{E_{out}}{E_{in}}\right| = \left|\frac{E_1}{E_{in}}\right|(1 - A) \qquad \text{(A-10b)}$$

[1] In the differentiation, it is assumed that the radian frequency ω is sufficiently large so that large changes of θ occur with small changes of ℓ_2. Then in the interval over which θ undergoes a 360-deg change, $\partial t_{g2}/\partial \ell_2 \simeq 0$. For those special cases where these assumptions are not valid or where more accuracy is required, one can obtain the exact bounds from incrementing ℓ_2 and performing numerical computations of Eq. (A-23).

while the phase delay error as given by Eq. (A-16) is zero.

Case 2 Upper Bound

Assume $t_{g1} > t_{g2}$ and $\theta = (2n-1)\pi$ where θ is defined by Eq. (A-8) and n is a positive integer. In practice, n will usually be an integer greater than 10.

Under these conditions, the leakage and primary waves are out of phase, but in contrast to Case 1, the group delay error reaches an upper bound of

$$(\epsilon_g)_{U2} = (t_{g1} - t_{g2})\left(\frac{A}{1-A}\right) \qquad \text{(A-23c)}$$

when the output signal magnitude ratio reaches a *lower* bound of

$$\left|\frac{E_{out}}{E_{in}}\right| = \left|\frac{E_1}{E_{in}}\right|(1-A) \qquad \text{(A-10c)}$$

and the phase delay error as calculated from Eq. (A-16) is zero.

Case 2 Lower Bound

Assume $t_{g1} > t_{g2}$ and $\theta = 2\pi m$ where θ is given by Eq. (A-8) and m is a positive integer. In practice, m will usually be an integer greater than 10.

Under these conditions the leakage and primary waves are in phase, but the group delay error goes to its lower bound of

$$(\epsilon_g)_{L2} = -(t_{g1} - t_{g2})\left(\frac{A}{1+A}\right) \qquad \text{(A-23d)}$$

Simultaneously, the output signal magnitude ratio reaches an upper bound of

$$\left|\frac{E_{out}}{E_{in}}\right| = \left|\frac{E_1}{E_{in}}\right|(1+A) \qquad \text{(A-10d)}$$

and the phase delay error goes to zero.

Differenced Range Versus Integrated Doppler

A parameter which is of primary importance to radio science experiments with a spacecraft is differenced range versus integrated doppler which can be expressed as (Ref. 8)

$$\text{DRVID} = t_g - t_p \qquad \text{(A-24)}$$

Then substitutions of Eqs. (A-14) to (A-16) and Eqs (A-20) to (A-23) give

$$\text{DRVID} = \left(\frac{d\beta_1}{d\omega} - \frac{\beta_1}{\omega}\right)\ell_1 + A(t_{g2} - t_{g1})\left(\frac{A + \cos\theta}{1 + 2A\cos\theta + A^2}\right) + \frac{1}{\omega}\tan^{-1}\left[\frac{A\sin\theta}{1 + A\cos\theta}\right] \qquad \text{(A-25)}$$

Note that in a dispersionless system

$$\frac{d\beta_1}{d\omega} = \frac{\beta_1}{\omega}$$

and in the absence of multipath, $A = 0$, so that

$$\text{DRVID} = 0$$

Reprinted from *The Deep Space Network Progress Report 42-25*, Feb. 15, 1975, pp 69–83

S/X Band Experiment: A Study of the Effects of Multipath on Two-Way Range

T. Y. Otoshi
Communications Elements Research Section

Equations are presented for determining two-way range errors caused by multipath The analysis of two-way range error is more complex than that for one-way range due to the fact that the uplink and downlink range errors oscillate at different rates when the leakage path length is varied. A limited amount of two-way range data was obtained with the Mu-I ranging machine, Mariner Venus/Mercury 1973 Radio Frequency Subsystem, and Block 3 receiver. The agreement between theoretical and experimental values was typically better than 2 ns.

I. Introduction

In this article, the term "one-way" range will be used to refer to either uplink or downlink range while the term "two-way" range will be used to refer to the sum of the uplink and downlink ranges. For the S/X band experiment the uplink frequency transmitted to the spacecraft transponder was 2113 MHz, while coherent S/X band downlink frequencies transmitted back to the ground station were 2295 and 8415 MHz In a dispersive media, the two-way range will not generally be equal to twice the one-way range.

The analysis of the effects of multipath on one-way range was presented previously by this author in Ref. 1 and by J. R Smith in Ref. 2 Theoretical equations for one-way range errors were verified experimentally by use of a multipath device, MVM'73 Radio Frequency Subsystem, Block 3 receiver/exciter subsystem (RCV) and the Mu-1 ranging machine.

This report presents theoretical equations which can be used to analyze the effects of multipath on two-way range. In addition, some experimental data, which show good agreement with the theory, will be presented.

II. Theoretical Equations

A. Exact Formulas

The geometry for two-way range error analysis may be seen in Fig 1. For this geometry the two-way range error is simply the algebraic sum of the one-way range error for the uplink signal and the one-way range error for the downlink signal.

The equation for two-way range can be expressed as

$$(t_g)_T = (t_{g1})_a + (t_{g1})_b + \epsilon_{ga} + \epsilon_{gb} \tag{1}$$

and the two-way range error as

$$(\epsilon_g)_T = \epsilon_{ga} + \epsilon_{gb} \tag{2}$$

where

$(t_{g1})_a$ = group delay of the uplink signal in the absence of multipath, s

$(t_{g1})_b$ = group delay of the downlink signal in the absence of multipath, s

ϵ_{ga} = error in the uplink delay due to multipath, s

ϵ_{gb} = error in the downlink delay due to multipath, s

For simplicity, assume that the primary and leakage paths are the same for the uplink and downlink signals (Fig 1) Then from the equations derived in Ref. 1, and assuming a free-space media for both leakage and primary paths

$$\epsilon_{ga} = \frac{(\ell_2 - \ell_1)}{c} A \left(\frac{A + \cos\theta_a}{1 + 2A\cos\theta_a + A^2} \right) \tag{3}$$

$$\epsilon_{gb} = \frac{(\ell_2 - \ell_1)}{c} A \left(\frac{A + \cos\theta_b}{1 + 2A\cos\theta_b + A^2} \right) \tag{4}$$

where

$$\theta_a = \frac{-2\pi f_a}{c} (\ell_2 - \ell_1) + \psi_a \tag{5}$$

$$\theta_b = \frac{-2\pi f_b}{c} (\ell_2 - \ell_1) + \psi_b \tag{6}$$

and

A = ratio of the magnitudes of the leakage and primary signals as measured at the input port to the transponder (Fig. 1)

ℓ_1, ℓ_2 = physical path lengths, respectively, of the primary and leakage paths going one-way, m

c = speed of light ($\cong 3 \times 10^8$ m/s)

f_a, f_b = uplink and downlink frequencies, respectively, in Hz

ψ_a, ψ_b = phase angles of reflection coefficients (if any) in the leakage path for uplink and downlink signals, respectively, in radians

The terms ψ_a and ψ_b in Eqs. (5) and (6) have been added for generality. It is assumed that the reflection coefficient phase angles do not change with frequency over the frequency interval of interest and, therefore, only affect the location of the upper and lower bounds of range error (see Appendix A).

It is also of interest to examine the effects of multipath on the AGC signal level as observed on the ground receiver. If the transponder is similar to that of the MVM'73 spacecraft where the downlink output signal of the transponder is kept constant even if the uplink signal is varying, then the AGC signal level error at the ground receiver will vary according to the relationship. (Ref. 1):

$$|F_b|_{dB} = 10 \log_{10} [1 + 2A\cos\theta_b + A^2] \tag{7}$$

If the transponder is a translator or a zero delay device, the AGC signal level error measured at the ground receiver will vary according to the relationship

$$|F_T|_{dB} = 10 \log_{10} [(1 + 2A\cos\theta_a + A^2)(1 + 2A\cos\theta_b + A^2)] \tag{8}$$

B. Approximate Formulas

The exact equations presented above are somewhat difficult to analyze because the uplink and downlink phases change at different rates In the cases of small leakage one can make approximations which show a type of modulation effect produced by the uplink and downlink error functions adding together. If x represents the terms having factors of A in the denominators of Eqs. (3) and (4) one can use the small x approximation that $(1 + x)^{-1} \approx 1 - x$ Then, from substitutions into Eq (2), omitting higher order terms of A after multiplication and the use of trigonometric identities, one obtains the approximate formula

$$\begin{aligned}(\epsilon_g)_T &\approx A \left(\frac{\ell_2 - \ell_1}{c} \right) \\ &\quad \times [\cos\theta_a + \cos\theta_b - A(\cos 2\theta_a + \cos 2\theta_b)] \\ &\approx 2A \left(\frac{\ell_2 - \ell_1}{c} \right) \left[\cos\frac{1}{2}(\theta_b - \theta_a) \cos\frac{1}{2}(\theta_b + \theta_a) \right. \\ &\quad \left. - A\cos(\theta_b - \theta_a)\cos(\theta_b + \theta_a) \right]\end{aligned} \tag{9}$$

The accuracy of the above approximate formula is better than 3% if $A \leq 0.1$. If the difference between the uplink

and downlink signals is small, then the error curves will be similar to an amplitude-modulated signal where the envelope of the modulation is proportional to cos $[(1/2)(\theta_b - \theta_a)]$ and the carrier signal is given by cos $[(1/2)(\theta_b + \theta_a)]$

Similarly, when the small leakage signal approximations are used in Eq (8), the following approximate formula is obtained

$$|F_T|_{dB} \simeq 10 \log_{10}\left[1 + 4A \cos\frac{1}{2}(\theta_b - \theta_a) \cos\frac{1}{2}(\theta_b + \theta_a)\right] \quad (10)$$

C. Sample Cases

Figures 2 through 13 are sample case plots of Eqs (2) and (8) for leakage signal levels of −30 dB, −20 dB, and −10 dB relative to the primary signal Figures 2 through 7 are plots applicable for 2113-MHz uplink and 2295-MHz downlink cases, while Figs 8 through 13 are applicable to 2113-MHz uplink and 8415-MHz downlink cases For these sample cases, the leakage path is initially assumed to be 3048 cm (100 ft) longer than the primary path Then the leakage path is increased and errors are plotted as a function of increasing differential path lengths Error curves for other differential path lengths will be similar in shape, but the amplitudes will differ by the ratio of the differential path lengths At some critical differential path length the errors become worst case, and the upper and lower bounds will be twice those for one-way range (See Appendix A)

In the sample case plots it is of interest to note the similarity of the periodicity and shapes of the range and signal level error curves This fact can be used to advantage, as will be described in the following suggested experiment

D. Application

Although the two-way theory is complex, the multipath effects can be separated out in practice Picture an experimental setup where the zero delay device horn is moved along the direction of the primary path Measurements of the signal level and range are simultaneously recorded as a function of the zero delay device horn position To obtain at least two cycles of change, the S-band zero delay horn should be moved a minimum of 27 2 cm (10 7 in) while at X-band, the ZDD horn should be moved at least 11 4 cm (4 5 in.). After the experimental data has been obtained, a curve fit can be made to the experimental AGC signal level data using Eq (8) Then determining the position at which the signal level amplitude error is zero, it can be assumed that at the same position the two-way range error is also zero (Figs 2 to 13) This procedure should produce an error of only a few nanoseconds if the peak-to-peak AGC signal level change is less than 2 dB For larger AGC ripples (indicating severe multipath conditions) a curve fit of experimental data should be made to both theoretical range and signal level equations given by Eqs (2) and (8)

III. Experimental Verification

Ranging tests were performed at the Telecommunications Development Laboratory (TDL) using the Block 3 RCV, MVM'73 Radio Frequency Subsystem, and the MU-1 ranging machine. The multipath device[1] described in Ref 1 was inserted into a cable path that simultaneously carried both the uplink 2113 MHz and downlink 2295 MHz range-coded signals A block diagram of the test setup at TDL may be seen in Fig 14 For the two-way range tests, the initial test parameters of the Block 3 RCV and MU-1 ranging machine were the same as previously reported in Ref 1

A cable of the appropriate length was inserted into the leakage path of the multipath device to make the one-way leakage path delay become 22 8 ns longer than the delay through the primary path The multipath device attenuator was adjusted so that the one-way leakage signal was −10 55 dB relative to the primary signal The leakage path length was then varied by means of a phase shifter (line stretcher) in the leakage path. Two-way range changes and received signal level were measured as functions of the phase shifter setting

Table 1 shows a comparison of experimental and theoretical values The theoretical two-way range values were computed from Eq (2) It can be seen that the agreement between theoretical and experimental range values were typically better than 2 ns From Table 1 it can also be seen that the theoretical values of signal level changes agreed with experimental values to within 0 5 dB Eq (7) was used for the theoretical values for signal level changes because the MVM'73 radio-frequency subsystem transponder was used for these tests rather than a zero delay device Although it is known that the group delay of the spacecraft receiver system changes as a function of received uplink signal level, no attempt was made to correct the experimental data for these changes

[1]The isolators in the multipath device were replaced by short lengths of Uniform Tubes UT141 semi-rigid cables

IV. Conclusion

Equations for two-way range error due to multipath have been presented Although only a limited amount of experimental data was obtained, reasonably good agreement was found between theory and experiment.

For a future experiment with a dish-mounted zero-delay device, one could mount a zero-delay horn on rails and then record two-way signal level and range changes as a function of horn position. With this data a correlation analysis can be made between experimental data and the theoretical equations. This should enable determination of the true range which would be obtained in the absence of multipath. It should be pointed out that this experimental procedure would be valid only if the multipath phenomenon is caused by one dominant leakage signal. If there are multiple leakage signals, the present analysis would have to be made more general.

Table 1. Results of two-way range test with the multipath device (Uplink frequency = 2.113 GHz, downlink frequency = 2 295 GHz)

Phase shifter setting	$\ell_2 - \ell_1$, cm	Range change			Downlink signal level change		
		Measured[a], ns	Theoretical[b], ns	Difference, ns	Measured, dB	Theoretical, dB	Difference, dB
0	684 00	0 00	0 00	0 00	—	+1 11	—
10	684 83	− 5 27	− 5 13	−0 14	0 00	0 0	0 00
20	685 67	−10 44	−10 81	0 37	—	−0 85	—
30	686 50	−14 75	−14 70	−0 05	−1 54	−1 03	−0 51
40	687 33	−15.75	−15 66	−0 09	−1 09	−0 45	−0 64
50	688 17	−15 09	−14 59	−0 50	−0 02	0 59	−0 61
60	689 00	−12 23	−11 38	−0 85	+1 19	1 71	−0 52
70	689 83	− 8 22	− 6 36	−1 86	—	2 68	—
80	690 67	− 4 32	− 1 31	−3 01	2 97	3 44	−0 47
90	691 50	0 16	2 57	−2 41	3 48	3 95	−0 47
100	692 33	2 34	5 15	−2 81	3 77	4 22	−0 45
110	693 17	4 21	6 63	−2 42	3 83	4 23	−0 40
120	694 00	5 45	7 20	−1.75	3 65	4 01	−0 36
130	694 83	5 10	6 93	−1 83	3 24	3 53	−0 29
140	695 67	4 29	5 76	−1 47	—	2 81	—
150	696 50	2 14	3 48	−1 34	1 54	1 86	−0 32
160	697 33	− 1 79	− 0 14	−1 65	0 37	0 76	−0 39
170	698 17	− 6 43	− 4 96	−1.47	—	−0 31	—
180	699 00	−10 74	− 9 42	−1 32	—	−0 99	—

[a]Calculated standard error on the measured relative range was typically ±0 5 ns

[b]Based on $A = 0\ 297$ ($-10\ 55$ dB)

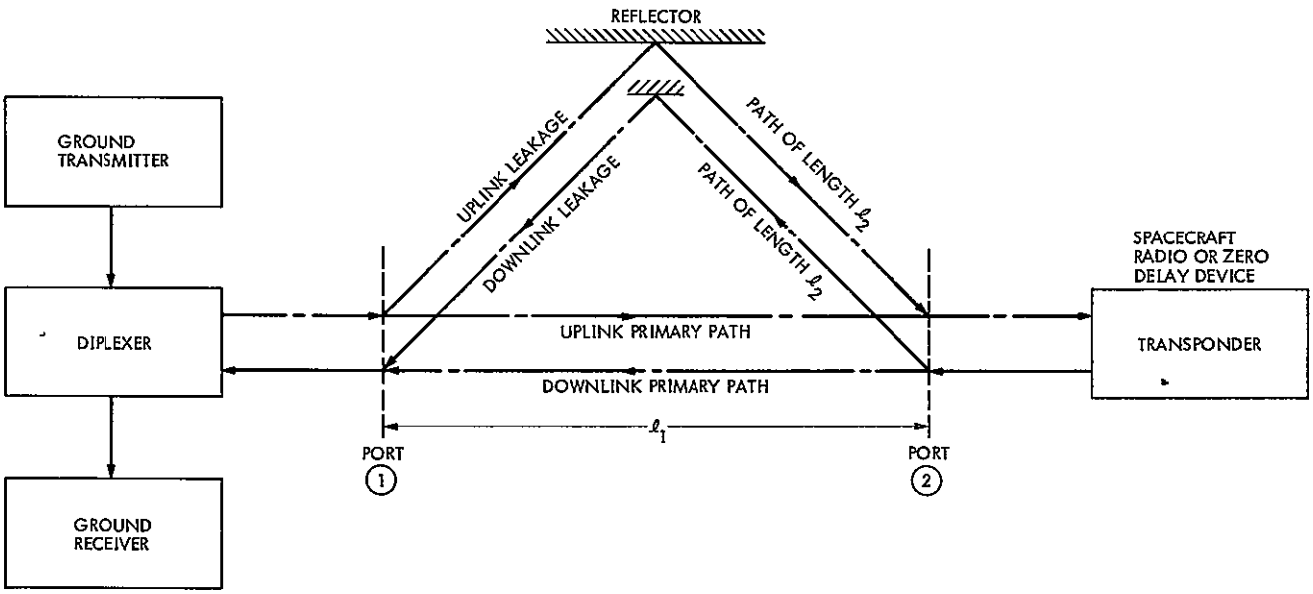

Fig 1. Geometry for analysis of the effect of multipath on two-way range

C.2

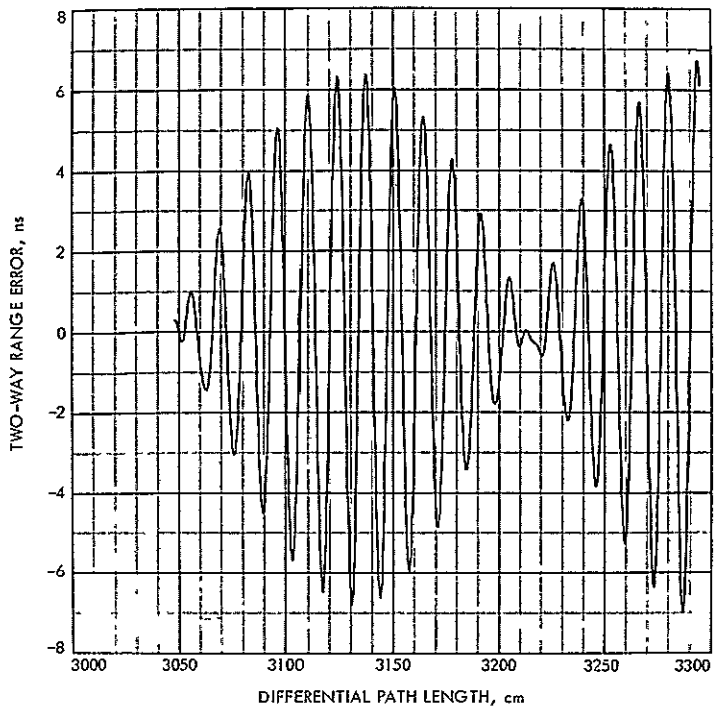

Fig 2 Two-way *range* error sample case $\ell_2 - \ell_1 = 3048$ cm (100 ft); one-way leakage signal is −30 dB relative to primary signal; uplink signal is 2113 MHz, and downlink signal is 2295 MHz; $\psi_a = \psi_b = 0$

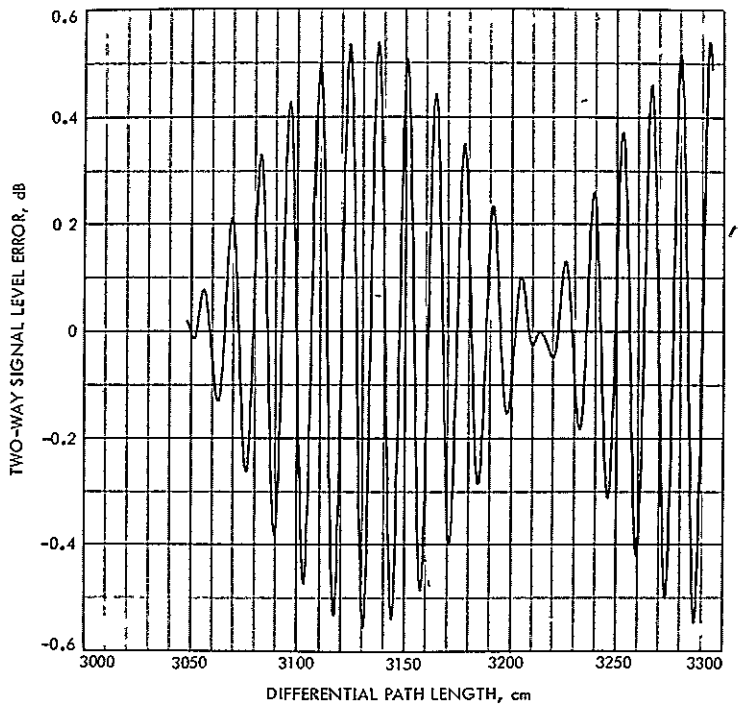

Fig. 3. Two-way *signal* level error sample case (same parameters as Fig. 2)

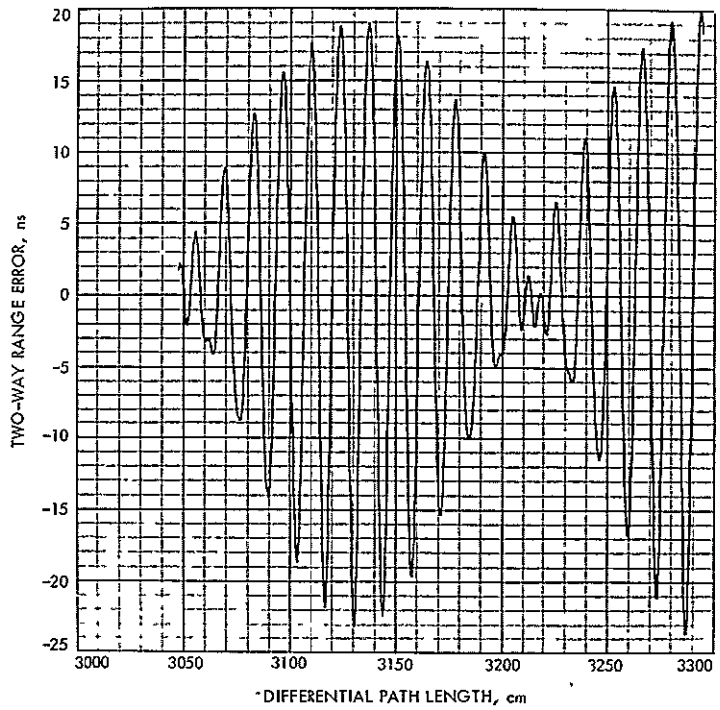

Fig 4 Two-way *range* error sample case: same parameters as Fig 2 except leakage signal is −20 dB relative to primary signal

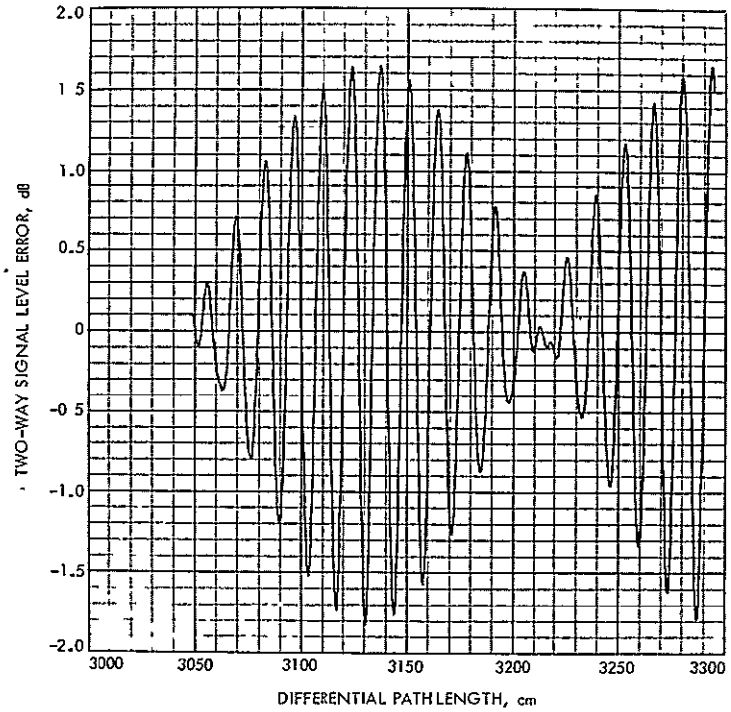

Fig. 5. Two-way *signal* level error sample case: same parameters as Fig. 2 except leakage signal is −20 dB relative to primary signal

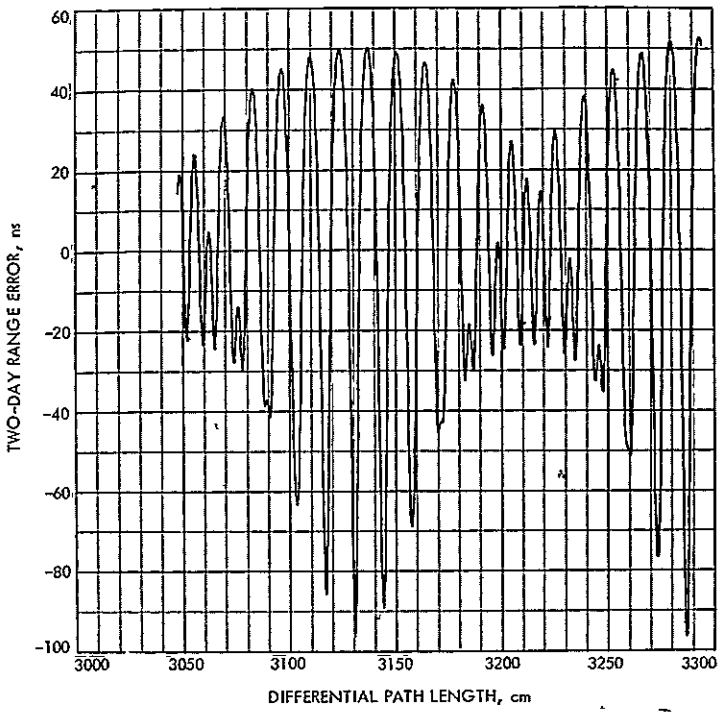

Fig. 6. Two-way *range* error sample case: same parameters as Fig. 2 except leakage signal is −10 dB relative to primary signal

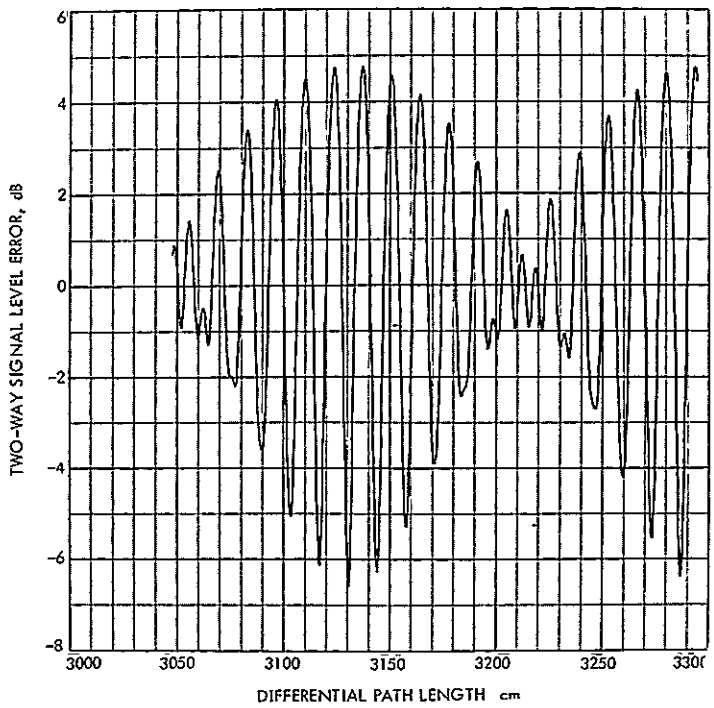

Fig 7. Two-way *signal* level error sample case: same parameters as Fig. 2 except leakage signal is −10 dB relative to primary signal

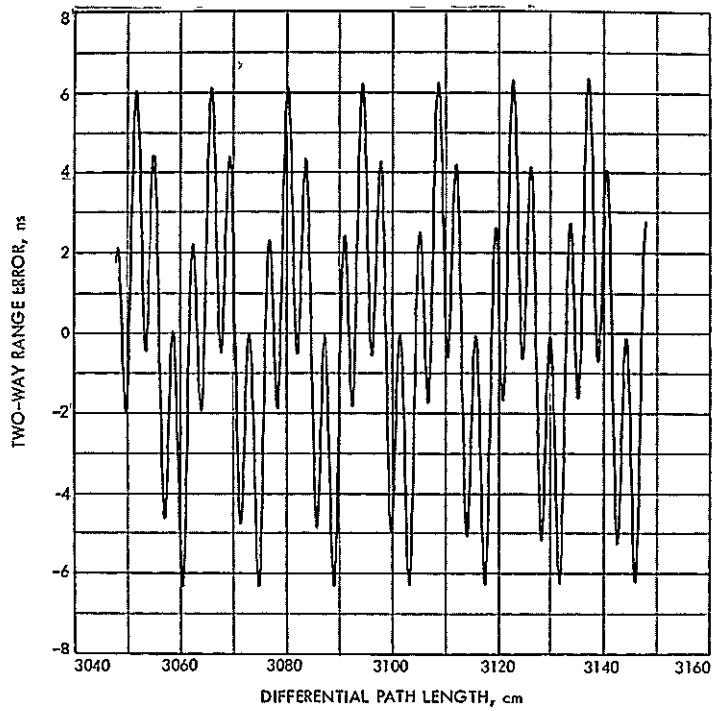

Fig 8. Two-way *range* error sample case· $\ell_2 - \ell_1 = 3048$ cm (100 ft); one-way leakage signal is −30 dB relative to primary signal; uplink signal is 2113 MHz, and downlink signal is 8415 MHz; $\zeta_a = \zeta_b = 0$

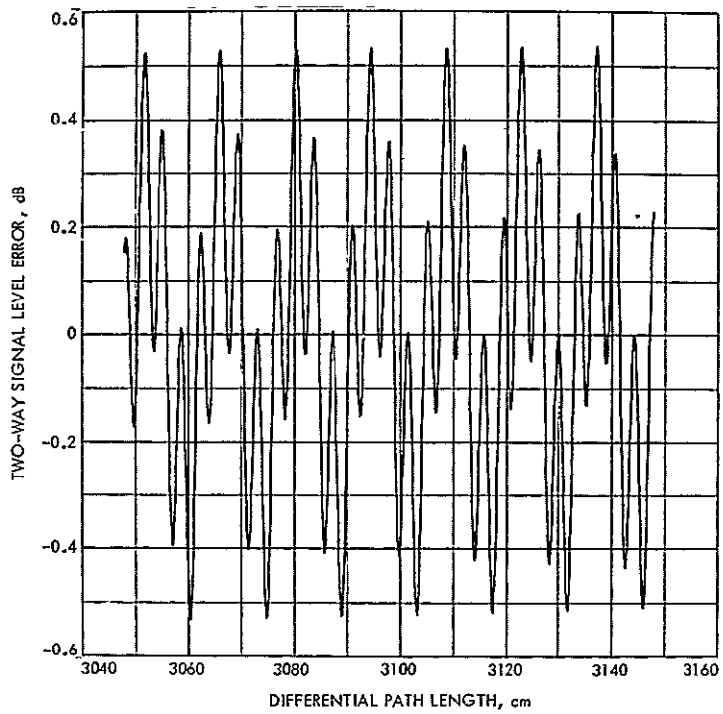

Fig. 9. Two-way *signal* level error sample case (same parameters as Fig. 8)

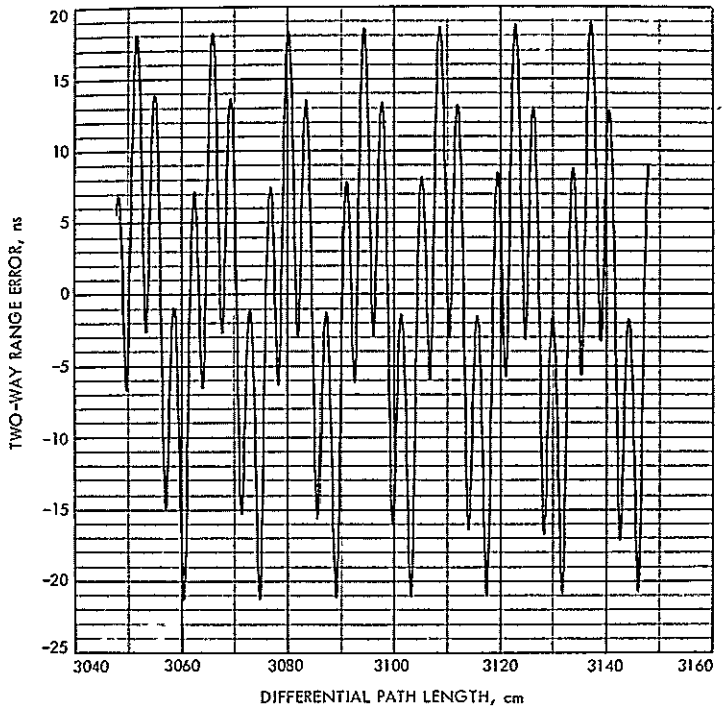

Fig 10. Two-way *range* error sample case same parameters as Fig 8 except leakage signal is −20 dB relative to primary signal

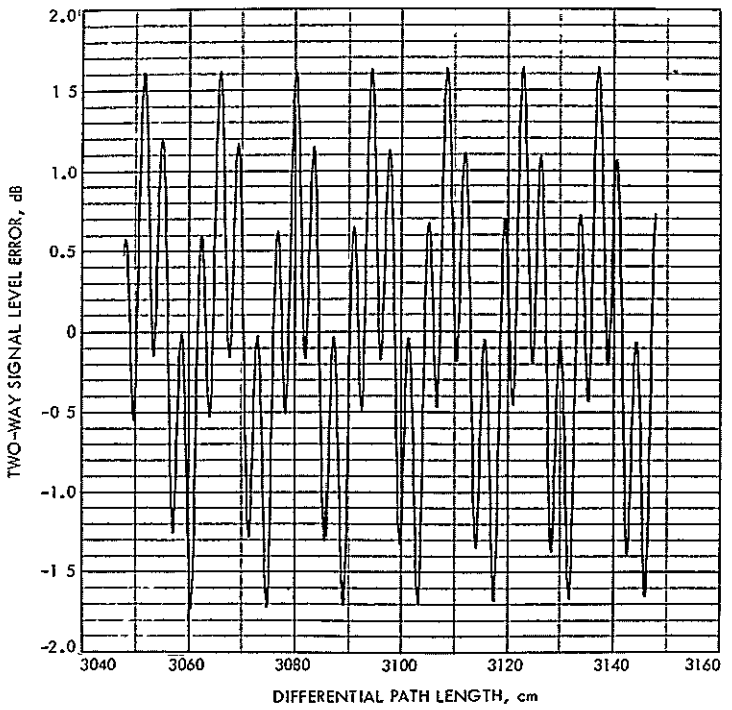

Fig. 11. Two-way *signal* level error sample case. same parameters as Fig. 8 except leakage signal is −20 dB relative to primary signal

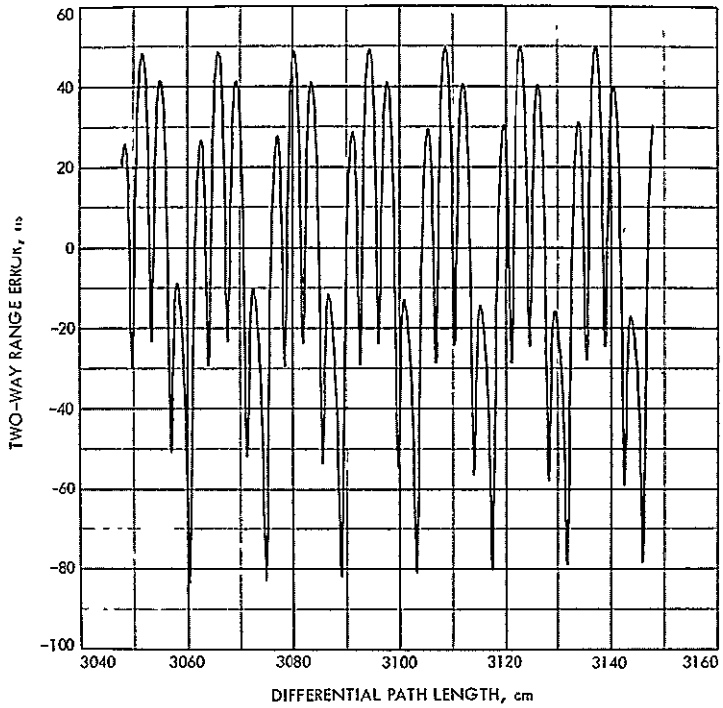

Fig 12 Two-way *range* error sample case same parameters as Fig. 8 except leakage signal is −10 dB relative to primary signal

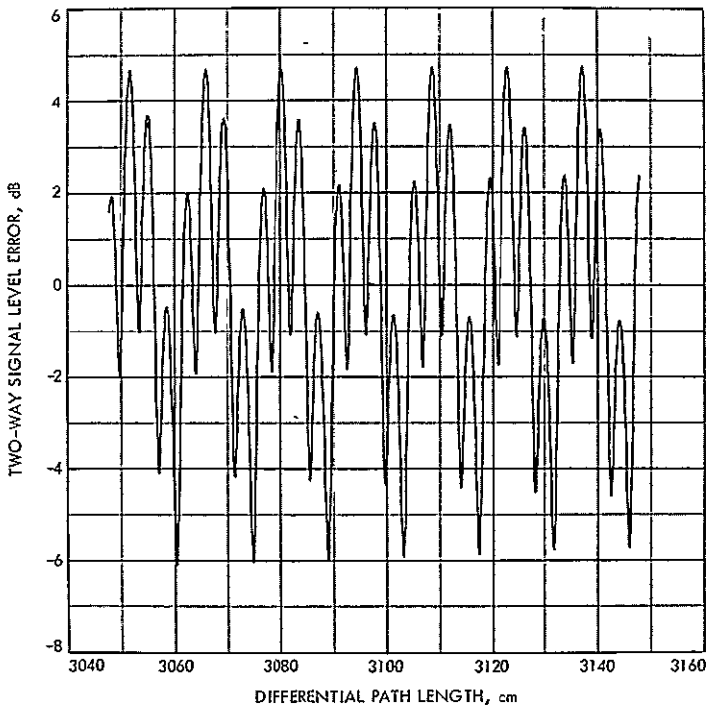

Fig. 13. Two-way *signal* level error sample case: same parameters as Fig. 8 except leakage signal is −10 dB relative to primary signal

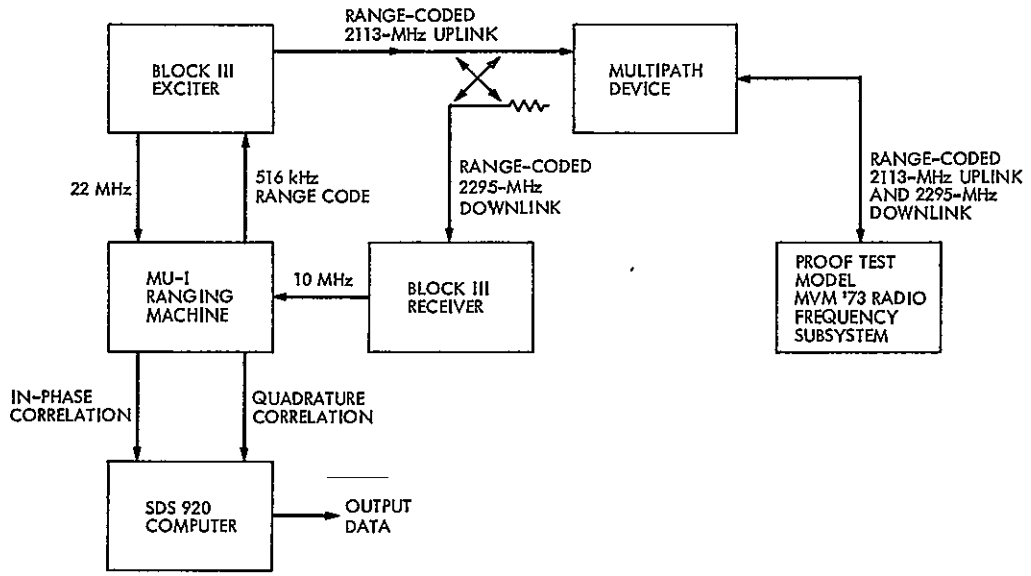

Fig. 14. Measurement setup for two-way range tests with the multipath device

Appendix A

Upper and Lower Bounds for Two-Way Range Error

As can be seen from the sample case plots (Figs. 2 to 13), the error for two-way range will be at a *local* upper or lower bound when the modulation envelope is at a maximum or minimum. At some critical differential path length, the two-way range error will be exactly two times the upper or lower bound of the one-way range error (Ref. 1). To find where this condition occurs, let θ_a and θ_b as given by Eqs (5) and (6) be related as follows

$$\theta_b = \theta_a - 2\pi k \tag{A-1}$$

where k is a positive integer. Then the two-way range error given by Eq. (2) becomes

$$(\epsilon_g)_T = 2A\left(\frac{\ell_2 - \ell_1}{c}\right)\left(\frac{A + \cos\theta_a}{1 + 2A\cos\theta_a + A^2}\right) \tag{A-2}$$

Also note that the two-way signal-level error as given by Eq (8) becomes

$$|F_T|_{dB} = 20\log_{10}[1 + 2A\cos\theta_a + A^2] \tag{A-3}$$

From Eq (A-3), it can be seen that the peak-to-peak change in signal level will be

$$\Delta_{dB} = 40\log_{10}\left[\frac{1 + A}{1 - A}\right] \tag{A-4}$$

which is exactly a factor of two greater than the dB signal level ripple for the one-way case (Ref. 1)

Upper Bound

Assuming that the conditions of Eq. (A-1) exist, then assume further that

$$\theta_a = -2\pi m \tag{A-5}$$

where m is a positive integer. Substitution of Eq (A-5) into Eqs (A-2) and (A-3) gives

$$(\epsilon_g)_T = \left(\frac{2A}{1 + A}\right)\left(\frac{\ell_2 - \ell_1}{c}\right) \tag{A-6}$$

$$|F_T|_{dB} = 40\log_{10}(1 + A) \tag{A-7}$$

These upper bounds of error for two-way range and signal level are exactly twice those of the corresponding one-way range case (Ref 1) To find the critical differential path length which produces these conditions, first substitute Eq (A-5) into (A-1) to obtain

$$\theta_b = -2\pi(m + k) \tag{A-8}$$

Then substitutions of Eqs. (5) and (6) into Eqs. (A-5) and (A-8), respectively, and solving for $\ell_2 - \ell_1$ results in

$$\ell_2 - \ell_1 = \left(\frac{c}{f_a}\right)\left[m + \frac{\psi_a}{2\pi}\right] \tag{A-9}$$

$$\ell_2 - \ell_1 = \left(\frac{c}{f_b}\right)\left[m + k + \frac{\psi_b}{2\pi}\right] \tag{A-10}$$

For simplicity assume that there is only one reflection coefficient in the leakage path and $\psi_a = \psi_b = \pi$. Then equating Eq. (A-9) to Eq (A-10) and manipulation results in

$$f_b = f_a\left[\frac{2(m + k) + 1}{2m + 1}\right] \tag{A-11}$$

The condition of Eq. (A-11) must be fulfilled if two-way range error is exactly twice the one-way range value. To show a practical application of Eq (A-11), one can find from trial and error that $m = 11$ and $k = 1$ are the minimum values of m and k which will give $f_b \simeq 2295$ MHz when $f_a = 2113$ MHz From substitution of these values in Eqs. (A-11) and (A-9)

$$f_b = 2296\,7 \text{ MHz}$$

$$\ell_2 - \ell_1 = 163\,3 \text{ cm } (5\,36 \text{ ft})$$

and from Eq (A-6)

$$(\epsilon_g)_T = 10\,89\left(\frac{A}{1 + A}\right)$$

where $(\epsilon_g)_T$ is given in nanoseconds.

Lower Bound

To find where the two-way lower bound is exactly twice the one-way lower bound, assume that the condition of Eq. (A-1) exists, and assume further that

$$\theta_a = -(2n-1)\pi \tag{A-12}$$

where n is a positive integer. Then Eqs (A-2) and (A-3) become

$$(\epsilon_g)_T = -\left(\frac{2A}{1-A}\right)\left(\frac{\ell_2-\ell_1}{c}\right) \tag{A-13}$$

$$|F_T|_{dB} = 40\log_{10}[1-A] \tag{A-14}$$

To find the differential path length which produces these lower bounds, substitute Eq (A-12) into Eq. (A-1) to obtain

$$\theta_b = -(2n-1)\pi - 2\pi k \tag{A-15}$$

Then substitutions of Eqs (5) and (6) into Eqs. (A-12) and (A-15), respectively, and then solving for $\ell_2 - \ell_1$ results in

$$\ell_2 - \ell_1 = \frac{c}{f_a}\left[\left(\frac{2n-1}{2}\right) + \frac{\psi_a}{2\pi}\right] \tag{A-16}$$

$$\ell_2 - \ell_1 = \frac{c}{f_b}\left[\left(\frac{2n-1+2k}{2}\right) + \frac{\psi_b}{2\pi}\right] \tag{A-17}$$

Assuming that $\psi_a = \psi_b = \pi$ and then from equating Eq. (A-16) to Eq (A-17), one obtains

$$f_b = f_a\left[\frac{n+k}{n}\right] \tag{A-18}$$

As an example of the use of Eq. (A-18) one can find from trial and error that values of $n = 23$ and $k = 2$ will give $f_b \simeq 2295$ MHz when $f_a = 2113$ MHz From substitutions of these values into Eqs (A-18) and (A-16), one obtains

$$f_b = 2296.7 \text{ MHz}$$

$$\ell_2 - \ell_1 = 326\,5 \text{ cm } (10\,71 \text{ ft})$$

and from Eq. (A-13)

$$(\epsilon_g)_T = -21.77\left(\frac{A}{1-A}\right)$$

where $(\epsilon_g)_T$ is given in nanoseconds.

Although in the examples given, the calculated downlink frequency of 2296 7 MHz is only approximately equal to 2295 MHz, one can expect to find local upper and lower bounds at differential path lengths close to 163 3 cm (5 36 ft) and 326 5 cm (10 71 ft) It is of interest to note that even for these small differential path length values, significant error in the S-band two-way range will occur if the multipath signal is strong. This type of strong multipath effect for small differential path lengths on the MVM'73 spacecraft was pointed out by J R. Smith (Ref. 3).

Acknowledgments

The experimental work at the Telecommunications Development Laboratory was supported by D. L. Brunn of the Spacecraft Radio Section The computer program for the sample case plots in this article was written by T Cullen of the Communications Elements Research Section.

References

1 Otoshi, T. Y., "S/X Band Experiment: A Study of the Effects of Multipath on Group Delay," in *The Deep Space Network Progress Report 42-24*, pp. 40–50, Pasadena, Calif , Dec. 15, 1974.

2 Smith, J. R , "Viking Ranging Investigation Team," IOM 3382-74-076, July 30, 1974 (JPL internal document)

3. Smith, J. R , "Viking Ranging Investigation Team," IOM 3382-74-102, Oct 15, 1974 (JPL internal document).

Reprinted from *The Deep Space Network Progress Report 42-27*, June 15, 1975, pp 87–96

S/X Band Experiment: Effect of Discontinuities on the Group Delay of a Microwave Transmission Line

R. W. Beatty[1]
Consultant

T. Y Otoshi
Communications Elements Research Section

The problem is considered of the effect of reflections from discontinuities at each end of a transmission line on the group delay at microwave frequencies. Previous work is briefly reviewed and a general analysis is made. Graphical data are presented based upon the formulas developed. Experimental results are given which confirm the theory.

I. Introduction

The effects of mismatch on the calculation and measurement of group delay or envelope delay have been investigated in the past because of the importance of delay distortion in transmission systems. In recent experiments with space probes, small variations in the delay of microwave signals have been measured in order to obtain data on planetary atmospheres and the distribution of gaseous matter in space. Small errors in the determination of group delay have significant effects in these applications, and a need has arisen for a more thorough analysis to be carried out.

II. Background

As Lewin et al. (Ref. 1) explained in 1950, the effect of reflections from discontinuities is similar to the multipath problem (Ref. 2). A small portion of the energy traveling down the transmission line is reflected back toward the source and re-reflected to add to the energy transmitted

[1]Dr. R W. Beatty was formerly with the National Bureau of Standards. He is presently a Consulting Electronics Engineer at 2110 Fourth Street, Boulder, Colo 80302.

to the load. In case of small reflections, one can neglect multiple reflections and consider only the dominant effect Since the reflected wave travels farther than the main wave, its phase varies faster with frequency variations. Consequently, the resultant phase shift ψ of the transmitted wave does not vary quite linearly with frequency, but has a cyclical variation superimposed on the linear variation. The group delay τ_g is related to the phase shift variation with frequency. At a frequency f_o, the group delay is defined as follows

$$\tau_g = -\frac{1}{2\pi} \cdot \frac{d\psi}{df}\bigg|_{f=f_o} \tag{1}$$

Hence, the group delay will also undergo cyclical variations due to reflections. Such an effect was observed by Lacy (Ref 3) in 1961.

Various analyses of this effect have appeared in the literature. In 1961 (Ref. 4), Lacy's analysis was limited to the case of reactive shunt discontinuities on lossless transmission lines and did not yield an explicit expression for group delay. In 1964 (Ref. 5), Cohn and Weinhouse gave a clear explanation of the effect and a simple analysis of the interaction phase error, stopping short of an explicit expression for group delay. In 1969 (Ref. 6), Drazy gave an expression for the error in group delay due to reflections from test port terminations. His expression was valid for small reflections and lossless components but was limited in application. There may be other treatments of this problem in the literature, but the authors are not aware of them.

III. Theory

The following analysis is intended to be more general than previous work and will serve to clarify the assumptions made in calculating and measuring group delay of transmission lines The analysis will be mainly useful for coaxial transmission line problems, but will be purposely kept general so as to include most uniconductor waveguide applications as well It is not assumed that the discontinuities must be shunt susceptances, or that the characteristic impedance of the transmission line is identical to the characteristic impedances of the systems on either side. It is not assumed that the reflections from the discontinuities are small or equal The discontinuities can be lossy or lossless and need not obey the reciprocity condition

Consider a *uniform* transmission line of length ℓ having discontinuities at each end. A network model is shown in Fig. 1, in which the discontinuities are represented by the 2-ports L and N and the energy is assumed to propagate in the *dominant mode* from port 1 towards port 2.

The group delay τ_g is given by Eq (1), where ψ is now ψ_{21}, the characteristic phase shift of the model, or the argument of S_{21}, its (transmission) scattering coefficient. If we employ conventional microwave network theory (Ref. 7), we can calculate S_{21} for the three cascaded 2-ports and obtain

$$S_{21} = \frac{\ell_{21}\, n_{21}\, e^{-\gamma\ell}}{1 - \ell_{22}\, n_{11}\, e^{-2\gamma\ell}} \tag{2}$$

where $[\gamma = \alpha + j\beta]$ is the propagation constant of the transmission line and ℓ_{21}, ℓ_{22}, n_{11} and n_{21} are scattering coefficients of the discontinuities. The attenuation and phase constants of the transmission lines are α and β, respectively. For a general transmission line such as a dominant mode uniconductor waveguide or coaxial line one can let

$$\beta = \frac{2\pi}{\lambda_g} = \frac{2\pi}{\lambda_0}\sqrt{\varepsilon' - \left(\frac{\lambda_0}{\lambda_c}\right)^2} \tag{3}$$

where λ_g is the waveguide wavelength of a dielectrically filled waveguide, λ_0 is the freespace wavelength, ε' is the relative permittivity of the dielectric material filling the waveguide, and λ_c is the cutoff wavelength. For transverse electric (TE) and transverse magnetic (TM) waves, λ_c is dependent on the physical dimensions of the waveguide opening, but for transverse electromagnetic (TEM) waves λ_c is equal to infinity

We can let

$$h = |\ell_{22}\, n_{11}|\, e^{-2\alpha\ell}$$

$$\theta = 2\beta\ell - \arg(\ell_{22}) - \arg(n_{11})$$

$$\phi = \beta\ell - \arg(\ell_{21}) - \arg(n_{21})$$

Then we can write

$$S_{21} = \frac{|\ell_{21}\, n_{21}|\, e^{-\alpha\ell} \cdot e^{-j\phi}}{1 - h\, e^{-j\theta}} \tag{4}$$

The characteristic phase shift ψ_{21} is then

$$\psi_{21} = \arg(S_{21}) = -[\phi + \arg(1 - h e^{-j\theta})] \tag{5}$$

The group delay is obtained by multiplying Eq (5) by -1 and differentiating the result with respect to angular frequency ($2\pi f$), and is

$$\tau_g = \tau_{g\ell} + \tau_{gn} + \tau_{go} + \Delta\tau \tag{6}$$

where

$$\tau_{g\ell} = -\frac{1}{2\pi}\frac{d}{df}\arg(\ell_{21})$$

$$\tau_{gn} = -\frac{1}{2\pi}\frac{d}{df}\arg(n_{21})$$

and if v_g is the group velocity in the dielectric filled transmission line having phase constant given by Eq (3) and c is the velocity of electromagnetic waves *in vacuo*,

$$\tau_{go} = \frac{1}{2\pi}\left(\frac{d\beta}{df}\right)\ell = \frac{\ell}{v_g} = \frac{\ell}{c}\left(\frac{\lambda_g}{\lambda_0}\right)\varepsilon' \tag{7}$$

Furthermore,

$$\Delta\tau = \frac{1}{2\pi}\frac{h(\cos\theta - h)\dfrac{d\theta}{df} + \left(\dfrac{dh}{df}\right)\sin\theta}{1 - 2h\cos\theta + h^2} \tag{8}$$

in which

$$\frac{1}{2\pi}\frac{d\theta}{df} = 2\tau_{go} - \frac{1}{2\pi}\frac{d}{df}[\arg(\ell_{22}) + \arg(n_{11})] \tag{9}$$

and

$$\frac{1}{2\pi}\frac{dh}{df} = \frac{|\ell_{22}\, n_{11}|}{2\pi}e^{-2\alpha\ell}$$

$$\times\left[\frac{1}{|\ell_{22}|}\frac{d|\ell_{22}|}{df} + \frac{1}{|n_{11}|}\frac{d|n_{11}|}{df} - 2\ell\frac{d\alpha}{df}\right] \tag{10}$$

We can see in Eqs. (6) to (10) how a change with frequency of the attenuation or phase shift of the line or the reflection coefficients of the discontinuities, for example, might affect the group delay In practical cases where the delays of the individual discontinuities are small, and we are interested in a relatively small bandwidth at microwave frequencies, we can neglect a number of terms that would contribute an insignificant amount to the final result. Then Eq. (6) reduces to

$$\tau_g = \tau_{go}\left[1 + \frac{2h(\cos\theta - h)}{1 - 2h\cos\theta + h^2}\right] = \tau_{go} + \Delta\tau \tag{11}$$

One can see that $\Delta\tau$ is a function of θ which varies with frequency, so that $\Delta\tau$ varies between the following limits

$$-\frac{2\tau_{go}h}{1+h} \leq \Delta\tau \leq \frac{2\tau_{go}h}{1-h} \tag{12}$$

or from substitutions

$$\frac{-2\left[\dfrac{\ell}{c}\left(\dfrac{\lambda_g}{\lambda_0}\right)\varepsilon'\right]\left[|\ell_{22}|\,|n_{11}|\mathcal{A}\right]}{1 + |\ell_{22}|\,|n_{11}|\mathcal{A}} \leq \Delta\tau$$

$$\leq \frac{2\left[\dfrac{\ell}{c}\left(\dfrac{\lambda_g}{\lambda_0}\right)\varepsilon'\right]\left[|\ell_{22}|\,|n_{11}|\mathcal{A}\right]}{1 - |\ell_{22}|\,|n_{11}|\mathcal{A}} \tag{13}$$

where $\mathcal{A} = e^{-2\alpha\ell}$ is the attenuation (power) ratio of the length of transmission line which has an attenuation $A = -10\log_{10}\mathcal{A}$. The reader is reminded that in the expression given above, λ_g is for a general case single-mode dielectric filled waveguide as may be seen from Eq (3). For an air-dielectric medium we may let $\varepsilon' = 1$, and for coaxial line TEM mode, we set $\lambda_c = \infty$.

IV. Graphical Data

A graph of the limits of $\Delta\tau$ is given in Fig 2 It is assumed for simplicity that $|\ell_{22}| = |n_{11}|$, and that $\tau_{go} = 100$ ns If $|\ell_{22}| \neq |n_{11}|$, one can assume that the line has equivalent identical discontinuities at each end where the equivalent discontinuity has a reflection coefficient magnitude equal to

$$\sqrt{|\ell_{22}|\,|n_{11}|}$$

For a transmission line having the same line attenuation but a τ_{go} different from 100 ns, one multiplies the result obtained from the graph by the ratio of the actual τ_{go} in nanoseconds to 100

As an example of the use of Fig. 2, assume that a transmission line has a delay of 20 ns and a line attenuation of 5 dB prior to adding discontinuities of $|\ell_{22}| = 0\,4$ and $|n_{11}| = 0.1$. Then an equivalent discontinuity placed at

each end of this line would have a reflection coefficient magnitude of $\sqrt{(0.4)\ (0.1)} = 0.2$. From Fig 2, one finds that if the reflection coefficient magnitude of each discontinuity is 0.2 and the line attenuation is 5 dB for a 100-ns line, the limits of cyclical variation are ±2.5 ns Then the limits of cyclical variation for the above 20-ns line example are ±(20/100) (2.5) ns

V. Experimental Results

Experimental results were obtained to confirm the theory for the case of fairly large reflections Metal disks having a diameter of 6.12 mm (0.241 in.) and a thickness of 0.152 mm (0.006 in.) were attached to the center conductors of short sections of 7-mm coaxial line to form the discontinuities L and N in Fig 1 The discontinuity assemblies may be seen in Fig 3. Over a frequency range of 8.365 to 8.465 GHz, a value of 0.42 for $|\ell_{22}|$ and $|n_{11}|$ of the disk assemblies was calculated using computer programs developed for 2-port standards (Ref. 8). Over the same frequency range a value of 0.43 was measured using an automatic network analyzer

The 30-ns coaxial line delay standard shown in Fig. 4 was connected between the discontinuities Measurements of τ_g and of $-20 \log_{10} |S_{21}|$ using an automatic network analyzer are shown in Figs 5 and 6, respectively. The group delay and the measured attenuation equal to $-10 \log_{10} e^{-2\alpha\ell}$ of the transmission line plus the short sections of 7-mm coaxial line with disks removed are also shown A comparison of calculated and measured results is shown in Table 1 The tabulated results show only limits near the center of the frequency range but are typical of the results over the frequency range of 8.365 to 8.465 GHz. The calculated limits do not include the additional effects of reflections from the coaxial line connectors. Closer agreement was obtained by measuring the $|\ell_{22}|$ and $|n_{11}|$ taking into account the coaxial connectors.

Good agreement between theory and experiment was also obtained when additional measurements were made with different disks, different transmission line lengths, and at an additional frequency range of 2.235 to 2.355 GHz. The details are not given here but will be included in a subsequent issue of this publication.

VI. Conclusions

No attempt was made to experimentally confirm all aspects of the general theory. However, for the special case considered [identical discontinuities at each end, and negligible frequency dependence of α, $|\ell_{22}|$, $|n_{11}|$, $\arg(\ell_{21})$, $\arg(n_{21})$, $\arg(\ell_{22})$, and $\arg(n_{11})$ over the bandwidth of interest], adequate confirmation of the theory was obtained.

The analysis presented applies both to transmission lines operating in the TEM mode or to single-mode propagation in waveguides in general The graphical data presented can be useful for: (1) estimating the limits on the variation of group delay with frequency or (2) determining how much reduction of discontinuities is necessary in order to achieve a given accuracy in predicting group delay.

Acknowledgment

The experimental work was expedited by the capable assistance of A. Rosenzweig and M. Culbertson of the Western Automatic Test Services at Sunnyvale, California.

References

1. Lewin, L., Muller, J J., and Basard, R , "Phase Distortion in Feeders," *Wireless Engineer*, pp 143-145, May 1950.

2. Otoshi, T Y., "S/X Band Experiment: A Study of the Effects of Multipath on Two-Way Range," *The Deep Space Network Progress Report 42-25*, pp. 69–83, Jet Propulsion Laboratory, Pasadena, California, Feb. 15, 1975.

3 Lacy, P , "Measuring Transmission Delay Distortion," *Microwaves*, Vol. 3, No 7, pp. 22–25, July 1964.

4. Lacy, P., "Analysis and Measurement of Phase Characteristics in Microwave Systems," 1961 WESCON Reprints, paper 23/3

5 Cohn, S B., and Weinhouse, N P., "An Automatic Microwave Phase-Measurement System," *Microwave J.*, Vol. 7, No. 2, pp. 49–56, February 1964.

6. Drazy, E J., "The Practical Use of Test Equipment for Microwave Filter Measurement," *1969 NEREM Record*, Technical Applications Sessions, pp. 1–5. Nov. 1969

7. Kerns, D. M., and Beatty, R. W., *Basic Theory of Waveguide Junctions and Introductory Microwave Network Analysis*, Pergamon Press, New York, New York, 1967.

8. Beatty, R W , "Calculated and Measured S_{11}, S_{21}, and Group Delay for Simple Types of Coaxial and Rectangular Waveguide 2-Port Standards," *NBS Tech. Note 657*, December 1974.

Table 1. Comparison of calculated and measured upper and lower limits of group delay and loss of a 30-ns line with a discontinuity assembly at each end

Parameter	Calculated value	Measured value[a]	Difference
Maximum delay	34 60 ns	34.38 ns at 8 407 GHz	0.22 ns
Mınımum delay	26 56 ns	26.70 ns at 8 415 GHz	−0.14 ns
Maxımum loss	6.51 dB	6.42 dB at 8.415 GHz	0.09 dB
Mınımum loss	5.36 dB	5 25 dB at 8 407 GHz	0 11 dB

[a]The frequency ınterval between successıve upper and lower lımıts ıs $1/(4\tau_{g0})$

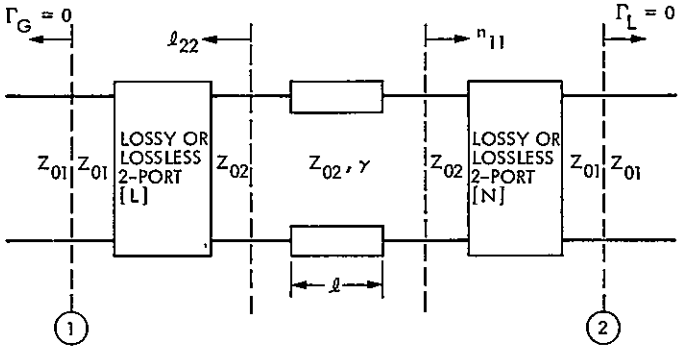

Γ_G = VOLTAGE REFLECTION COEFFICIENT OF GENERATOR AT PORT 1
Γ_L = VOLTAGE REFLECTION COEFFICIENT OF LOAD AT PORT 2

Fig. 1. Network model of transmission line and discontinuities

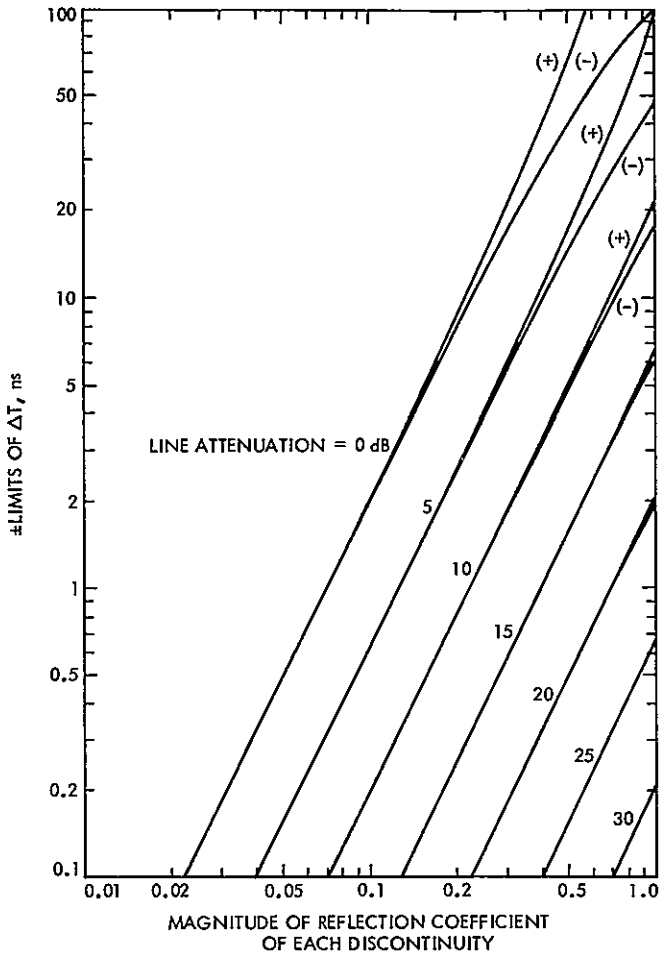

Fig. 2. Calculated limits of cyclical variation of group delay of a 100-ns transmission line with identical discontinuities at each end

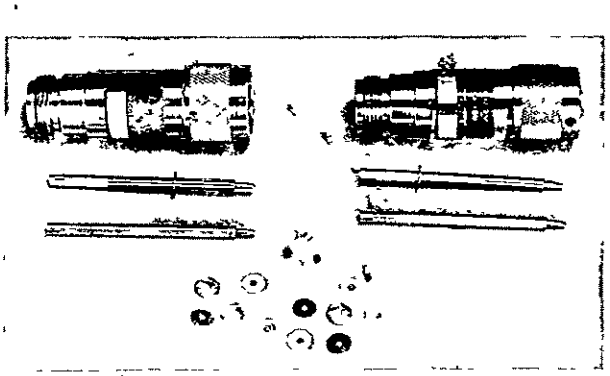

Fig. 3. 7-mm coaxial line discontinuity assemblies

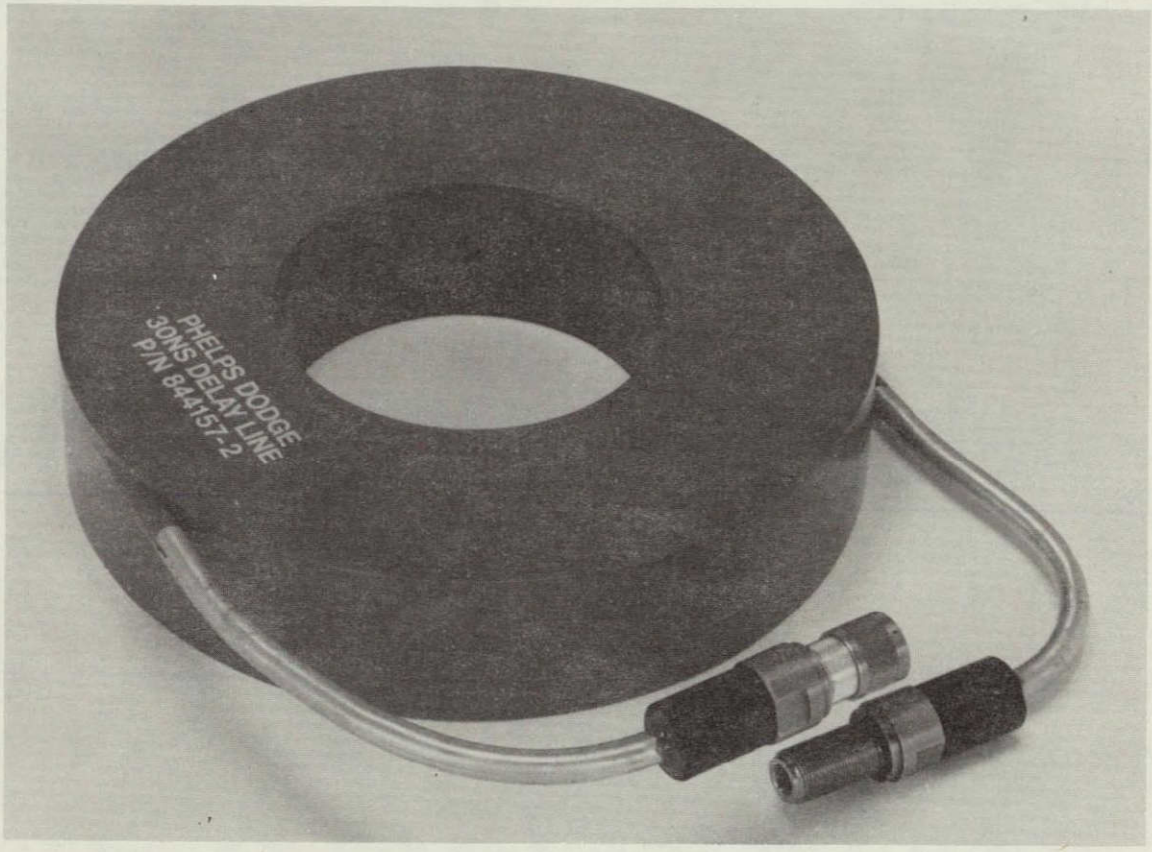

Fig. 4. Coaxial line delay standard of 30 ns

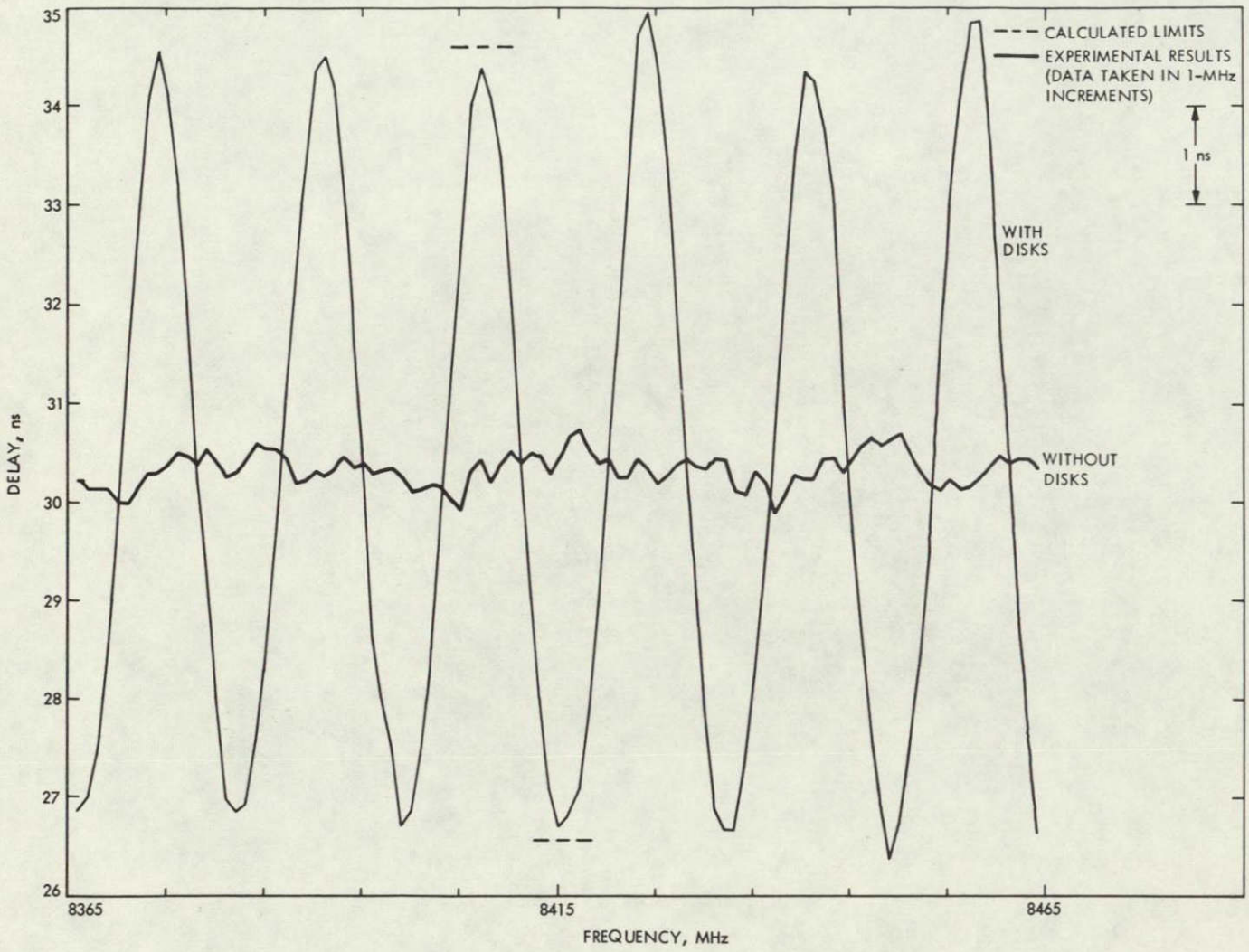

Fig. 5. Measured group delay of a 30-ns transmission line plus short end sections of 7-mm lines with and without 6.12-mm (0.241 in.) diam disks

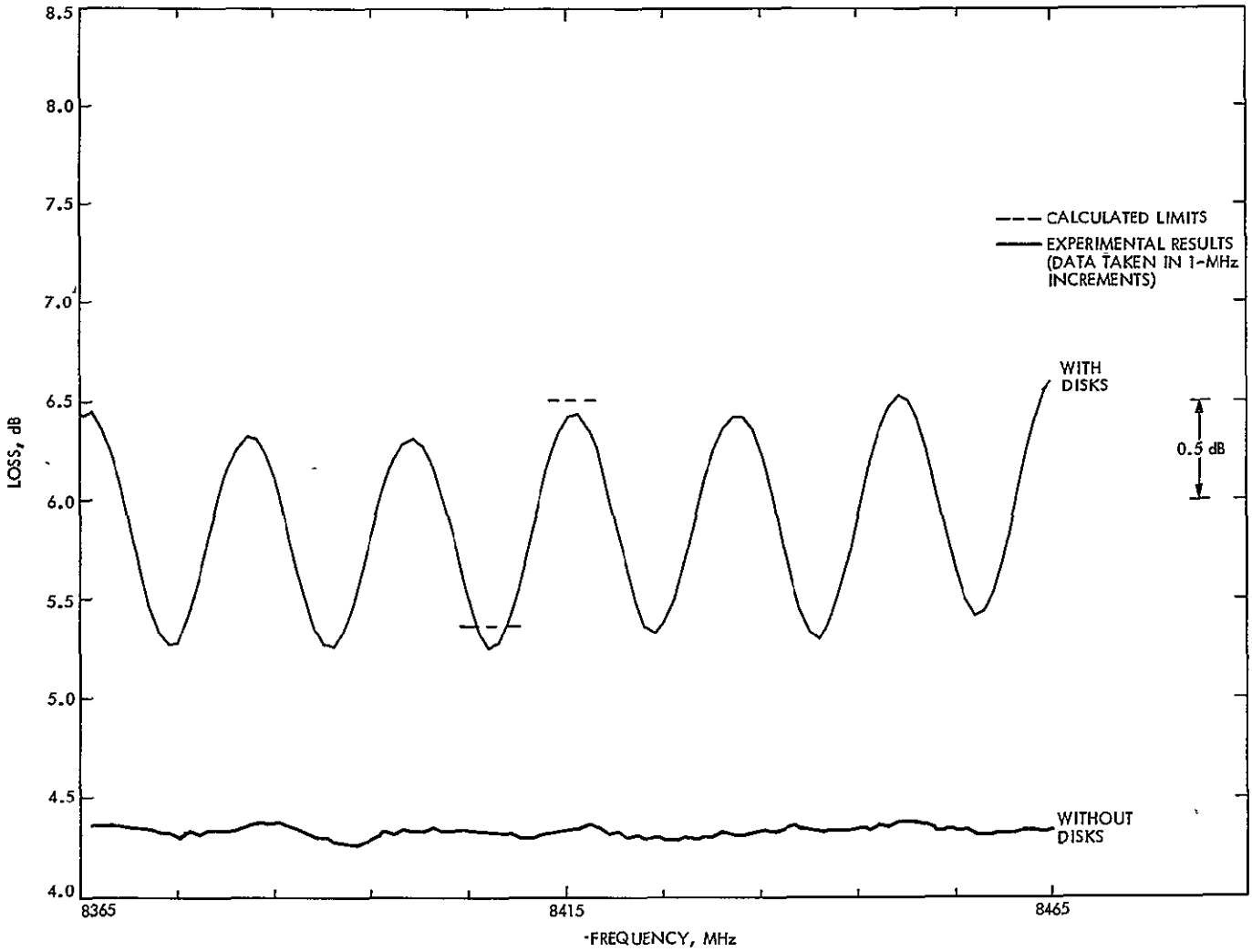

Fig. 6 Measured $-20 \log_{10} |S_{21}|$ of a 30-ns transmission line plus short end sections of 7-mm lines with and without 6 12-mm (0.241 in.) diam disks

Reprinted from *The Deep Space Network Progress Report 42-29*, Oct 15, 1975, pp 20–32

S-Band Zero-Delay Device Multipath Tests on the 64-Meter Antenna at DSS 43, DSS 63, and DSS 14

T. Y Otoshi
Communications Elements Research Section

This article presents the results of a study to correlate the results of zero-delay subreflector tests with the multipath theory. Good agreement between theory and experiment was obtained on both S-band range and signal level data at DSS 43, DSS 63, and DSS 14 It is shown that a movable subreflector technique can be used to isolate the principal multipath errors and enable a more accurate determination of the actual ground station delay.

I. Introduction

With the exception of DSS 14, at Goldstone, California, all stations of the Deep Space Network use the conventional zero-delay ranging configuration, in which the zero-delay device (ZDD) is mounted on the paraboloidal reflector (dish) surface. A zenith range measurement via the airpath to a dish-mounted ZDD and a Z-correction (Ref 1) provide needed ground station bias corrections for determining the true range to the spacecraft.

Results of airpath tests at DSS 14 showed that large changes in range occurred as a function of antenna elevation angle when a ZDD was mounted on the 64-m antenna dish surface (Ref 2). Other airpath tests made on the 64-m antenna S/X system at DSS 14 showed that large range changes also occurred when small changes were made in axial focusing of the hyperboloidal subreflector. Similar type phenomena were also observed on the 64-m antenna systems at DSS 43, Canberra, Australia, and DSS 63, Madrid, Spain (Ref. 3) Since the range dependence on elevation angle could be due to a multipath phenomenon, one cannot assume that a zenith measured value is the correct value. Because of the described airpath problems, the ZDD configuration at DSS 14 has been operated in a cable configuration (Ref 4) since January 12, 1974 However, DSS 43 and DSS 63 have continued to operate in the airpath configuration

Because of the current range residuals of 10 to 15 meters between DSS 63 and DSS 43 for Mariner 10 results (Ref 5), some attention has been devoted to the study of multipath as a possible cause of this discrepancy. A theory has recently been derived which results in good agreement between the multipath theory and experimental data. The purpose of this article is to present the results of some of this recent work. It will be shown that the multipath theory (with the aid of a com-

puter program) can be used to determine the true range delay of the station in the absence of multipath and thereby determine a correction to the observed station delay in the presence of multipath. Furthermore, the theory can be used to determine the physical location of the multipath source and its magnitude.

II. Theoretical Equations for Subreflector Tests

In the subreflector test, ranging measurements are performed via the airpath to a ZDD mounted on the dish surface. The test configuration may be seen in Fig. 1. The range-coded uplink signal, radiated out of the radio-frequency (RF) feed horn, is reflected off the hyperboloidal subreflector toward the dish surface. The dish-mounted ZDD horn receives a portion of this energy, and after mixing with a coherent local oscillator frequency, a coherent downlink signal is radiated back toward the hyperboloidal subreflector and reflected back toward the RF feed. The range-coded downlink signal received by the RF feed travels to the receiver system and subsequently arrives at the ranging machine.

In the ranging test, the total system round trip delay time is measured as a function of subreflector position. If the major part of the multipath signal is interacting in the region between the feed horn and the feed cone or its support structure, the subreflector movement will cause the multipath signal to go in and out of phase with the primary signal. Since the only required modification to previous theoretical work published by this author (Ref. 6) is to express the differential path length in terms of indicated subreflector position, only the equations will be presented. The derivations can be found in Ref. 6.

For the configuration of Fig. 1 the equation for two-way range can be expressed as

$$(t_g)_\eta = K_1 + \varepsilon_{ga} + \varepsilon_{gb} \tag{1}$$

where

K_1 = total system group delay (uplink and downlink) in the absence of multipath, s

ε_{ga} = error in the uplink delay due to multipath, s

ε_{gb} = error in the downlink delay due to multipath, s

For simplicity, assume that the primary and leakage paths are the same for the uplink and downlink signals (see Fig. 1). Then from the equations derived in Ref. 6, and assuming a free space media for both leakage and primary paths,

$$\varepsilon_{ga} = \left(\frac{(\ell_2 - \ell_1)}{c}\right) A \left(\frac{A + \cos\theta_a}{1 + 2A\cos\theta_a + A^2}\right) \tag{2}$$

$$\varepsilon_{gb} = \left(\frac{(\ell_2 - \ell_1)}{c}\right) A \left(\frac{A + \cos\theta_b}{1 + 2A\cos\theta_b + A^2}\right) \tag{3}$$

where

$$\theta_a = \frac{-2\pi f_a}{c}(\ell_2 - \ell_1) + \psi_a \tag{4}$$

$$\theta_b = \frac{-2\pi f_b}{c}(\ell_2 - \ell_1) + \psi_b \tag{5}$$

and

A = ratio of the magnitudes of the leakage and primary signals as measured at the output port of the ZDD horn (see Fig. 1)

ℓ_1, ℓ_2 = physical path lengths, respectively, of the primary and leakage paths going one-way, cm

c = speed of light ($\approx 3 \times 10^{10}$ cm/s)

f_a, f_b = uplink and downlink frequencies, respectively, Hz

ψ_a, ψ_b = phase angles of reflection coefficients (if any) in the leakage path for uplink and downlink signals, respectively, rad

The exact relationship of $(\ell_2 - \ell_1)$ to subreflector movement is difficult to derive due to defocusing effects and the changes in incidence angles that differ for the primary wave and the multipath wave. As a first-order approximation,

$$\ell_2 - \ell_1 \approx (\Delta\ell_0 + 2S_1)\,2.54 \tag{6}$$

where

$\Delta\ell_0$ = differential path length when the indicated subreflector position is zero, in

S_i = indicated subreflector position, in.[1]

[1]The subreflector position on the equipment is indicated in inches rather than in centimeters. To be meaningful this indicated position should not be converted to the metric system.

The automatic gain control (AGC) downlink signal level change observed by the ground receiver will vary according to the relationship

$$|F_T|_{dB} = 10 \log_{10} [(1 + 2A \cos \theta_a + A^2)(1 + 2A \cos \theta_b + A^2)] \quad (7)$$

and the AGC signal level (in dBm) observed at the ground receiver is

$$AGC = K_2 + |F_T|_{dB} \quad (8)$$

where K_2 = the AGC signal level which would be observed in the absence of multipath (in dBm)

III. Theoretical and Experimental Data

A. Subreflector Tests

Figures 2 through 7 are computer printouts and plots showing a comparison of theoretical and experimental data obtained from subreflector tests at DSS 43, 63, and 14 The uplink and downlink test frequencies were approximately the Helios spacecraft frequencies of 2115 and 2297 MHz, respectively

The printouts and plots were generated by a computer program to perform a least squares fit of theoretical values to experimental data. The theoretical data are based upon Eqs. (1) through (8), and a best fit is made first to the experimental ranging data to determine the best fit value of (1) true station delay K_1 in the absence of multipath, (2) the differential length $\Delta\ell_0$ as defined by Eq. (6), and (3) the relative strength of the leakage signal A expressed in decibels The program then uses these best fit values of $\Delta\ell_0$ and A to calculate the theoretical AGC signal levels as a function of subreflector settings

This sequence for best fit was chosen because the range data are a result of long term averaging, while the AGC data are either typically noisier or generally lag behind real-time changes The AGC data are also dependent upon the accuracy of the calibration curves and operation only at the signal levels where the calibration curves apply

Note from the computer printouts on Figs. 2, 4, and 6 that the best fit values of $\Delta\ell_0$ are typically about 3327.4 cm (1310 in). This value compares favorably with values of approximately 3332.5 cm (1312 in.) obtained from measuring physical path lengths on scaled drawings (see table in Fig. 1) From Fig. 1, it can be seen that this value is associated with a multipath wave reflected off the cone platform. The values of approximately −15 to −20 dB for A_{dB} agree with those calculated independently by Ludwig (Ref. 7) These values are also consistent with beam efficiency values published in Ref 8 for the portion of the beam illuminating the cone platform An attempt to explain the higher value of about −10 dB for A_{dB} at DSS 63 will be made later after discussion of the plotted curves.

Examination of the plotted curves shows that reasonably good agreement was obtained between theory and experiment for DSS 43 and DSS 14. The typical deviations in range are about 3 ns, and typical deviations in AGC are about 0 3 dB. These deviations might be due to another smaller multipath effect caused by a wave bouncing off the cone roof and not accounted for by the theory

The larger discrepancy for DSS 63 was previously attributed to a cone missing from the cone platform. However, it was recently learned that a cone was also missing from the cone platform on the DSS 43 antenna during 1974 and during the subreflector test Therefore, the stronger multipath effect and larger discrepancy at DSS 63 might be due to the location of the missing cone with respect to the location of the ZDD The ZDD locations and tricone configurations at DSS 43, DSS 63, and DSS 14 for the subreflector tests are shown in Fig. 8 Note that at DSS 63 the missing cone is at Bay 1, while at DSS 43, the missing cone is at Bay 3. Because of the different locations of the missing cone with respect to the ZDD, a stronger multipath signal could exist at DSS 63 than at DSS 43.

The large disagreement of calculated and experimental AGC values at DSS 63 can be explained as follows. The AGC calibrations at DSS 63 were performed in the region of −140 to −170 dBm while actual multipath tests were performed at −120 dBm The measured signal levels for the tests were outside the calibrated region, and therefore the measured AGC variations were much smaller than the actual variations. G. Pasero at DSS 63 stated that when the test was repeated for AGC data only at a later date in the calibrated range of the receiver, the peak-to-peak AGC variation observed was about 10 dB This peak-to-peak variation agrees favorably with the calculated values shown on the plots

All of the subreflector test results presented apply only to the antenna pointed at zenith and at the S-band test frequencies involved. Results of subreflector tests at 45 and 20 deg elevation angles have been reported in Ref 3, but as yet no curve fit has been made to these data.

B. Antenna Tipping Test

Another airpath test that is often performed is the antenna tipping test. In this test the total system range delay is continuously measured while the antenna is slowly tipped from the zenith position to the horizon. Figures 9 and 10 show the results of the tipping test for DSS 43 and DSS 63, respectively. No current tipping test data were obtained at DSS 14. The tipping tests were performed on a different day from the subreflector tests, and the measured zenith range delays differed by about 10 to 20 ns. To avoid confusion, the tipping test data were converted to show changes relative to the zenith position. A polynomial curve fit was made to the data to show trends only. The polynomial curve fit is not based on the multipath equations. However, it is interesting to note that when the antenna is tipped from the zenith position to the horizon, the subreflector moves from the normal operating point outward about 0.5 to 0.7 in. (Ref. 9). If one examines the subreflector data for DSS 43 and DSS 63, (see Figs. 3a and 5a) and moves from the operating point to a point about 0.5 in. in the positive direction, the magnitude and phase (sign) of the range change generally agree with the antenna tipping data. Therefore one can assume that the phenomena associated with the antenna tipping tests are correlated to the same multipath phenomenon observed on the subreflector test.

IV. Corrections to Measured Station Range Delay

In the preceding section it was shown that the true station delay could be determined with the aid of a computer program. The definition of true range is that which would have been measured in the absence of multipath. Since the subreflector position during pre- and post-track zero-delay calibration is known and since the true range is given by the computer program, one can calculate a correction for the measured station delay. In addition, one can predict what the observed range residuals would be between stations. For example, let

$BIAS'_{DSV}$ = measured DSS round trip delay in the *presence* of multipath

$BIAS_{DSV}$ = true DSS round trip delay in the *absence* of multipath

Using the equation in Ref. 1 the measured round-trip light time (RTLT) will be

$$RTLT' = R_{total} - BIAS_{S/C} - BIAS'_{DSV} + Z \qquad (9)$$

but the true RTLT is

$$RTLT = R_{total} - BIAS_{S/C} - BIAS_{DSV} + Z \qquad (10)$$

where R_{total} is the total measured range and Z is the Z-correction.

If $BIAS'_{DSV}$, $BIAS_{DSV}$ are given in nanoseconds the range residual in meters is computed from

$$\underset{(\text{meter})}{\text{Range Residual}} = [\underset{(\text{ns})}{RTLT'} - \underset{(\text{ns})}{RTLT}]\,[0.15] \qquad (11)$$

Substitutions of Eqs. (9) and (10) into Eq. (11) gives

$$\underset{(\text{meter})}{\text{Range Residual}} = [\underset{(\text{ns})}{BIAS_{DSV}} - \underset{(\text{ns})}{BIAS'_{DSV}}]\,[0.15] \qquad (12)$$

For DSS 43, the 1974 pre- and post-track ZDD calibrations were done with the subreflector at 0 in. Then from the data on Fig. 2

$$BIAS_{DSV} - BIAS'_{DSV} = 3198.4 - 3227.2$$
$$= -28.8\,\text{ns}$$

$$\text{Range Residual} = -4.3\,\text{meters}$$

For DSS 63, the 1974 pre- and post-track ZDD calibrations were done with the subreflector at −0.5 in. From the data on Fig. 4,

$$BIAS_{DSV} - BIAS'_{DSV} = 4210.8 - 4155.9$$
$$= 54.9\,\text{ns}$$

and

$$\text{Range Residual} = 8.2\,\text{meters}$$

Since DSS 14 does not operate in the airpath configuration, there is no need to compute residuals for DSS 14.

It is interesting to note that the above residuals are in excellent agreement with the residuals published by Christensen for Mariner 10 at Mercury Encounter I on March 29, 1974 (Ref. 5). Unfortunately, the results presented here cannot be used conclusively to explain the residuals. The main reason is that during Mariner 10 Mercury Encounter I on March 29, 1974, the ZDD horn at DSS 43 was located at the outer edge of the 64-m dish surface. The ZDD horn was moved to a new location closer to the center of the antenna on August 1, 1974 (see Fig. 8). The DSS 43 test results reported in this article were obtained at the new location.

Another reason why the results may not apply to the Mariner 10 residuals is the slight differences in test frequencies If one were to assume that the same multipath conditions existed at DSS 63 as during the Mariner 10 Mercury Encounter I period, calculations show that for the Mariner 10 uplink/downlink frequencies of 2 11352 GHz/2.29523 GHz, the range residual would have been +5 0 meters. It can generally be expected that the multipath-caused residuals will change significantly with uplink/downlink frequency changes as small as 1 or 2 MHz.

Since the multipath error can change in magnitude and phase with (1) frequency, (2) ZDD horn location, or (3) the RF feed configuration, it is important to document these parameters for future reference. The test configurations for the tests done at DSS 43, DSS 63, and DSS 14 are shown in Fig. 8 Table 1 shows the critical parameters of interest which if altered would invalidate the range correction data obtained

V. Summary and Recommendations for Future Work

It has been shown that even though multipath effects are present on the antenna, the effect can be separated out by the movable subreflector technique. This method assumes that the dominant interaction is occurring between the subreflector and the cone or its support structure. If there are multipath effects outside this region, one must use a movable ZDD horn on the dish surface such as that described in Ref. 6. Range measurements made over a band of frequencies might also reveal multipath effects and enable identification of multipath sources

If the station periodically (every 3 months) obtains data from the subreflector test, then through the use of the computer program, one could determine the station delay more accurately Since the computer program also assists in locating the multipath source, a simple antenna redesign might be done to eliminate the problem entirely. One solution may be to restore the hyperboloid vertex plate which is not present on 64-m antennas

Although good agreement was obtained between theory and experiment for the tests described in this article, it is still desirable to confirm the location of multipath source. Plans are being made to perform an experiment placing absorbers on the cone platform of the DSS 14 64-m antenna and seeing if the dominant multipath effect disappears for both S- and X-band. The results of this test will be reported in a future issue of this publication

References

1. *TRK-2-8 Module of DSN System Requirements Detailed Interface Design Document 820-13, Rev. A*, Jet Propulsion Laboratory, Pasadena, Calif., July 1, 1973 (an internal document)

2 Stelzried, C. T., Otoshi, T. Y, and Batelaan, P. D, "S/X Band Experiment Zero Delay Device Antenna Location," in *The Deep Space Network Progress Report 42-20*, pp. 64–68, Jet Propulsion Laboratory, Pasadena, Calif., Apr. 15, 1974

3. Otoshi, T. Y., and LuValle, J., "Zero Delay Device Airpath Tests at DSS 43 and 63," IOM 3333-75-048, Jet Propulsion Laboratory, Pasadena, Calif, Apr. 1, 1975 (an internal document).

4 Otoshi, T. Y, and Stelzried, C T., "S/X Experiment A New Configuration for Ground System Range Calibrations With the Zero Delay Device," in *The Deep Space Network Progress Report 42-20*, pp. 57–63, Jet Propulsion Laboratory, Pasadena, Calif., Apr 15, 1974

References (contd)

5 Christensen, C., "Corrected Mariner 10 Range Residuals," IOM 391.8-268, Jet Propulsion Laboratory, Pasadena, Calif., Apr. 24, 1975 (an internal document).

6 Otoshi, T. Y., "S/X Band Experiment. A Study of the Effects of Multipath on Two-Way Range," in *The Deep Space Network Progress Report 42-25*, pp. 69–83, Jet Propulsion Laboratory, Pasadena, Calif., Feb. 15, 1975.

7 Ludwig, A. C., "Multipath Calculations for Range Error Calibration Probe," IOM 3333-75-161, Jet Propulsion Laboratory, Pasadena, Calif., Aug. 22, 1975 (an internal document).

8 Bathker, D. B., *Predicted and Measured Power Density Description of a Large Ground Microwave System*, Technical Memorandum 33-433, Jet Propulsion Laboratory, Pasadena, Calif., Apr. 15, 1971. See Eta S Column in Table II, p. 31.

9 Katow, M. S., "64-m Subreflector–Gravity Deflections," IOM 3324-75-136, Jet Propulsion Laboratory, Pasadena, Calif., Sept. 2, 1975 (an internal document).

Acknowledgments

The author would like to acknowledge the assistance of J. LuValle of Network Operations in writing the test procedure for overseas station tests. Splendid cooperation was obtained from G. Pasero of DSS 63 and R. Denize of DSS 43, who took the data and furnished additional details about the test configurations. H. Marks of Informatics wrote the Engineering Calibration Program used in the tests and has made the program tapes and documentation available to all stations in the Network. T. Cullen of the Communications Elements Research Section wrote the sophisticated computer program that enabled the theoretical portion of this work to be successful. The subreflector technique was originally suggested by Dr. R. W. Beatty, Consulting Electronics Engineer, for purposes of checking ranging system measurement accuracy. His suggested subreflector tests subsequently led to the discovery of the multipath phenomenon.

Table 1. Multipath test configuration and tabulation of critical multipath-dependent parameters

DSS	Test frequencies, GHz		Normal subreflector operating position, in	ZDD horn location	S-band cone	S/X dichroic plate installed	Approximate period for which test results are valid
	Uplink	Downlink					
43	2 115770	2 297670	0	Dish surface as indicated on Fig 8	SPD	No	August 1, 1974 (new horn location) to February 13, 1975 (when XRO[a] cone and S/X feed installed)
63	2 115700	2 297593	−0 5 (0 5 in IN)	Dish surface as indicated on Fig 8	SPD	No	Throughout 1974 to February 1975 (when S/X feed installed)
14	2 115650	2 297540	−0 5 (0 5 in. IN)	Box on side of Mod III section on same level as cone platform (Fig 8)	SPD	Yes	March 19, 1975 when SPD[b] cone/ XRO cone installed) to present

[a]X-band receive only
[b]S-band polarization diversity

APPROXIMATE PATH LENGTHS FOR PRIMARY AND MULTIPATH (LEAKAGE) WAVES			
ZDD HORN LOCATION	DISTANCE FROM RF FEED PHASE CENTER TO ZDD HORN PHASE CENTER		
	LEAKAGE WAVE PATH LENGTH, cm (in.)	PRIMARY WAVE PATH LENGTH, cm (in.)	DIFFERENTIAL PATH LENGTH, cm (in.)
"A"	6941.82 (2733)	3609.34 (1421)	3332.48 (1312)
"B"	7569.20 (2980)	4231.64 (1666)	3337.56 (1314)

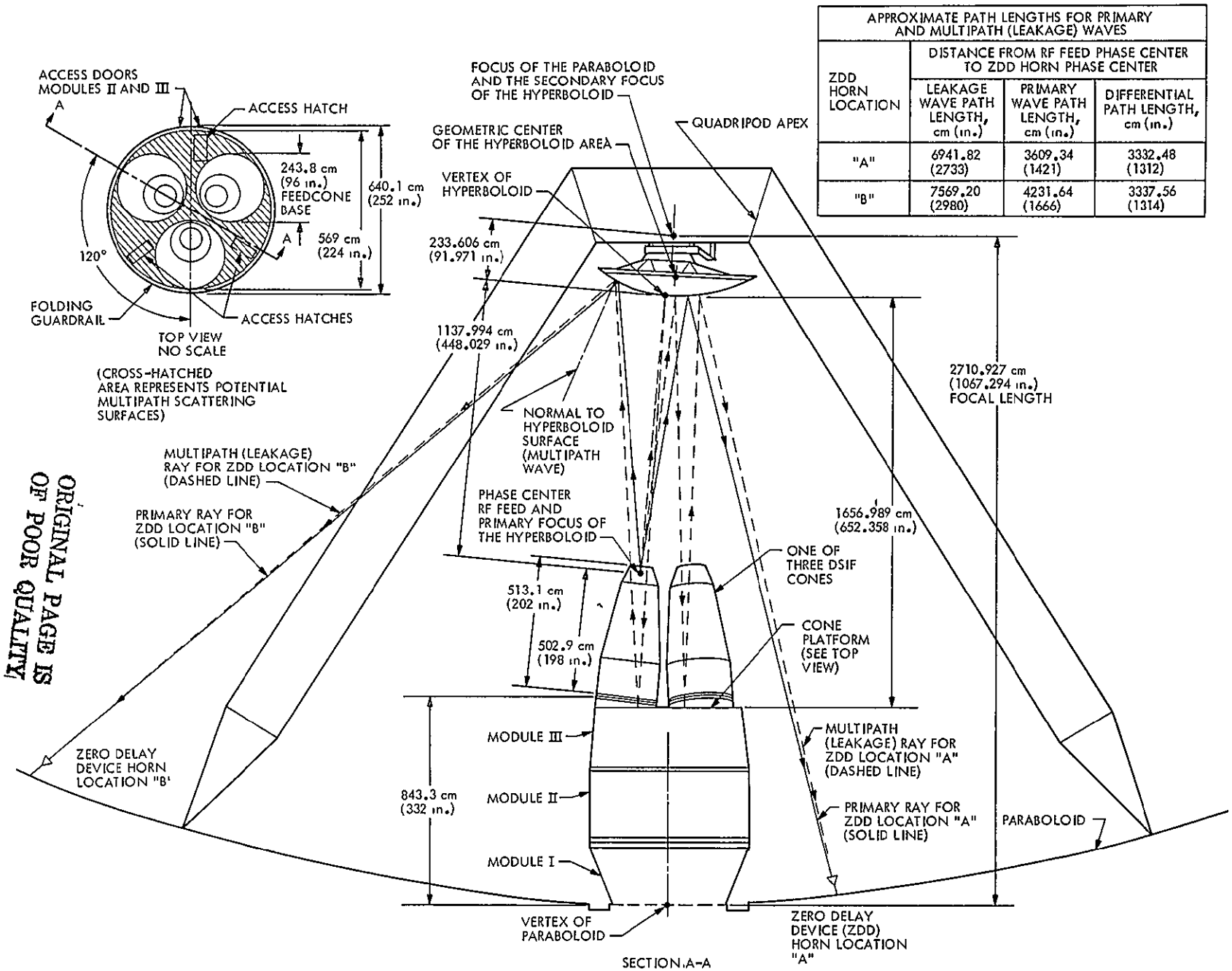

ORIGINAL PAGE IS OF POOR QUALITY

Fig 1. 64-m antenna geometry for multipath tests

DSS 43 SUBREFL TESTS AT ZENITH, 1974 GMT DAY 362

FA= 2.115770 GHZ FB= 2.297670 GHZ

ADBL=-24.0000 DB ADBU=-15.0000 DB

DLZL= 1295.000 INCH DLZU= 1325.000 INCH

SUBREF POSITION (INCH)	FXPER. RANGE DELAY (NS)	CALC. RANGE DELAY (NS)	RANGE DIFF. (NS)	FXP AGC (DBM)	CALC AGC (DBM)	AGC DIFF. (DB)
-3.000	3226.80	3223.15	3.646	-121.14	-120.72	-.421
-2.500	3227.90	3227.77	.126	-120.00	-120.25	.252
-2.000	3202.20	3203.23	-1.028	-122.34	-122.47	.135
-1.500	3162.60	3164.89	-2.286	-125.59	-125.20	-.385
-1.000	3171.20	3174.40	-3.203	-125.22	-124.55	-.668
-.500	3210.80	3211.96	-1.164	-121.98	-121.70	-.272
.000	3227.20	3226.98	.220	-119.87	-120.35	.481
.500	3210.40	3212.25	-1.845	-121.07	-121.66	.586
1.000	3181.40	3178.36	3.040	-124.05	-124.21	.165
1.500	3178.60	3172.65	5.954	-124.55	-124.70	.154
2.000	3195.50	3196.94	-1.440	-122.81	-122.79	-.026

BEST FIT VALUES FOR OPTION 1

	K1 (NS)	ADB (DB)	DLZ (INCH)	K2 (DBM)
FIRST ESTIMATE	3198.51	-15.45	1311.500	
FINAL ESTIMATE	3198.41	-15.38	1311.286	-122.6793

Fig. 2 Sample printout of computer program for DSS 43 subreflector tests

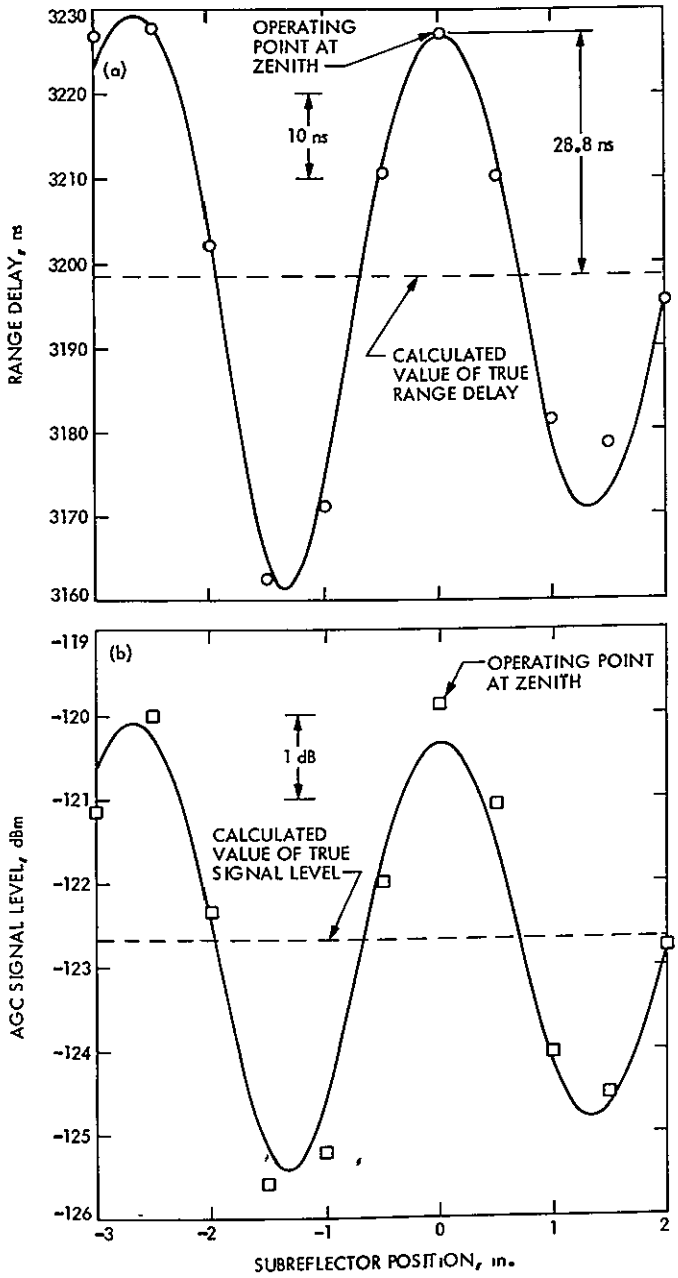

Fig 3. Comparison of theoretical and experimental results for subreflector tests at DSS 43 on 1974 GMT Day 362 (zenith measurement): (a) Range delay, (b) Downlink received signal level

DSS 63 SUBREFL TESTS AT ZENITH, 1975 GMT DAY 29

FA= 2.115700 GHZ FB= 2.297593 GHZ

ADBL=-24.0000 DB ADBU=-12.0000 DB

DLZL= 1295.000 INCH DLZU= 1325.000 INCH

SUBREF POSITION (INCH)	EXPER. RANGE DELAY (NS)	CALC. RANGE DELAY (NS)	RANGE DIFF. (NS)	EXP AGC (DBM)	CALC AGC (DBM)	AGC DIFF. (DB)
-3.000	4217.20	4198.45	18.746	-127.47	-129.64	2.173
-2.500	4258.40	4255.99	2.415	-127.27	-124.21	-3.057
-2.000	4253.10	4263.42	-10.317	-127.27	-123.17	-4.105
-1.500	4213.30	4235.41	-22.106	-127.30	-126.62	-.677
-1.000	4122.60	4134.17	-11.572	-128.25	-133.43	5.186
-.500	4155.90	4159.18	-3.278	-128.16	-132.18	4.020
.000	4253.30	4245.23	8.070	-127.33	-125.58	-1.748
.500	4276.90	4264.77	12.128	-127.27	-122.99	-4.275
1.000	4256.10	4250.93	5.169	-127.27	-124.90	-2.373
1.500	4201.10	4178.04	23.064	-127.67	-131.02	3.352
2.000	4122.40	4121.87	.534	-128.69	-133.94	5.247
2.500	4201.70	4223.11	-21.406	-127.71	-127.68	-.026
3.000	4259.60	4261.05	-1.446	-127.28	-123.56	-3.718

BEST FIT VALUES FOR OPTION 1

	K1 (NS)	ADB (DB)	DLZ (INCH)	K2 (DBM)
FIRST ESTIMATE	4215.10	-12.00	1299.500	
FINAL ESTIMATE	4210.83	-9.74	1299.573	-127.8646

Fig. 4 Sample printout of computer program for DSS 63 subreflector tests

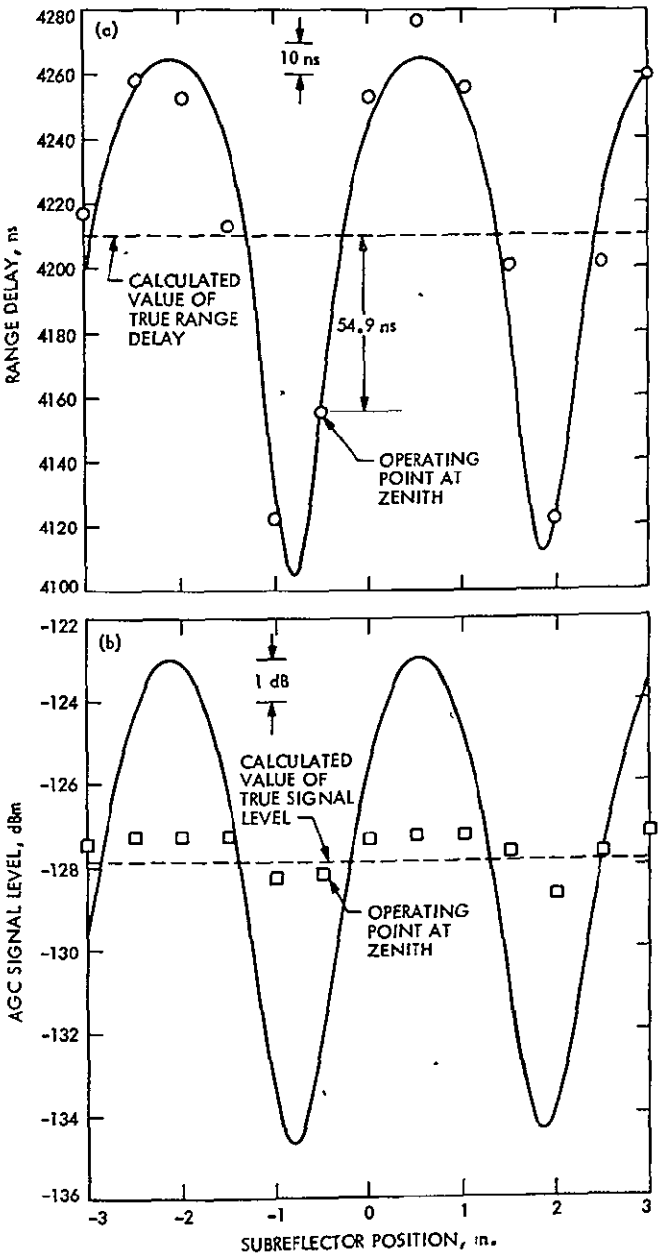

Fig 5. Comparison of theoretical and experimental results for subreflector tests at DSS 63 on 1975 GMT Day 29 (zenith measurement): (a) Range delay, (b) Downlink received signal level

HELIOS PASS 215 POST CAL DSS 14, 1975 GMT DAY 193

FA= 2.115650 GHZ FB= 2.297540 GHZ

ADBL=-24.0000 DB ADBU=-15.0000 DB

DLZL= 1295.000 INCH DLZU= 1325.000 INCH

SUBREF POSITION (INCH)	FXPER. RANGE DELAY (NS)	CALC. RANGE DELAY (NS)	RANGE DIFF. (NS)	FXP AGC (DBM)	CALC AGC (DBM)	AGC DIFF. (DB)
-3.000	3276.20	3272.74	3.465	-135.64	-135.57	-.070
-2.500	3255.90	3261.34	-5.442	-136.50	-136.34	-.163
-2.000	3286.10	3285.53	.574	-134.68	-134.61	-.066
-1.500	3304.30	3305.28	-.983	-132.40	-132.93	.532
-1.000	3305.30	3304.02	1.275	-132.73	-133.05	.318
-.500	3279.60	3282.72	-3.118	-134.88	-134.81	-.071
.000	3266.50	3263.51	2.995	-136.14	-136.19	.051
.500	3276.60	3275.99	.605	-135.32	-135.29	-.026
1.000	3295.00	3298.83	-3.834	-133.22	-133.50	.277
1.500	3306.70	3305.02	1.685	-132.75	-132.97	.217
2.000	3289.00	3290.37	-1.370	-134.72	-134.17	-.548
2.500	3266.60	3270.71	-4.107	-136.36	-135.67	-.687
3.000	3278.70	3271.84	6.856	-135.35	-135.59	.236

BEST FIT VALUES FOR OPTION 1

	K1 (NS)	ADB (DB)	DLZ (INCH)	K2 (DBM)
FIRST ESTIMATE	3286.38	-19.05	1308.500	
FINAL ESTIMATE	3286.46	-19.15	1308.580	-134.4510

Fig. 6. Sample printout of computer program for DSS 14 subreflector tests

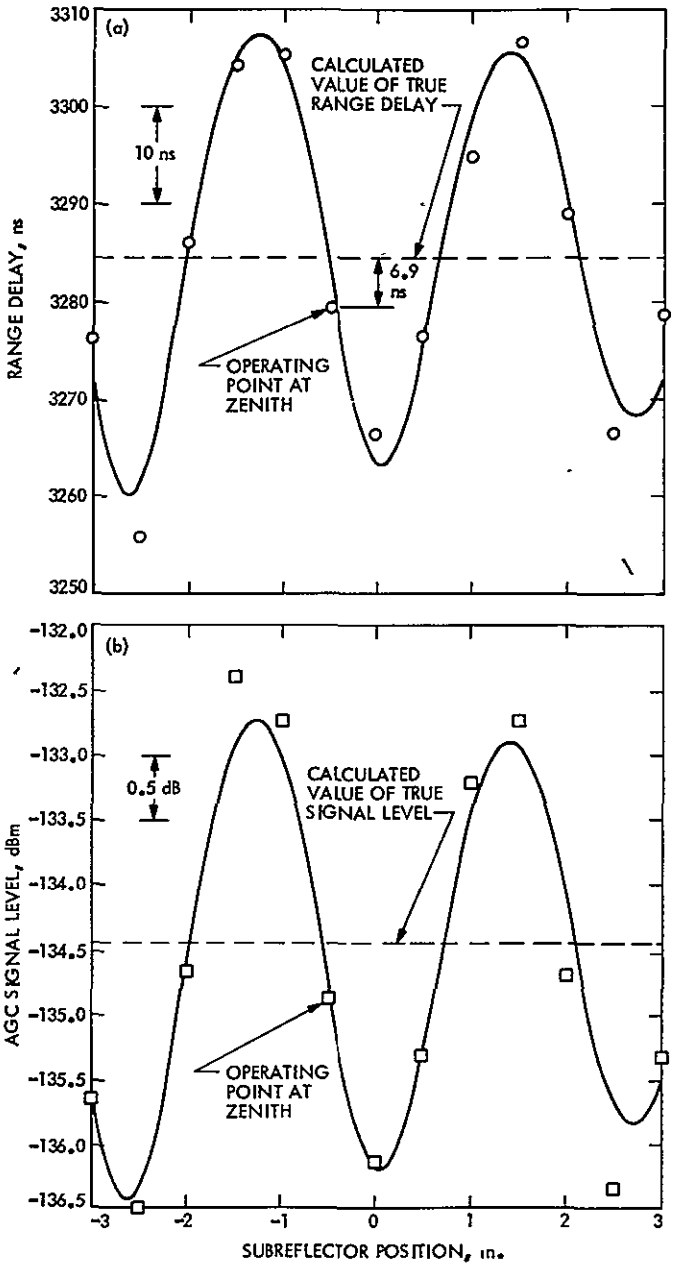

Fig 7. Comparison of theoretical and experimental results for subreflector tests at DSS 14 on 1975 GMT Day 193 (zenith measurement): (a) Range delay, (b) Downlink received signal level

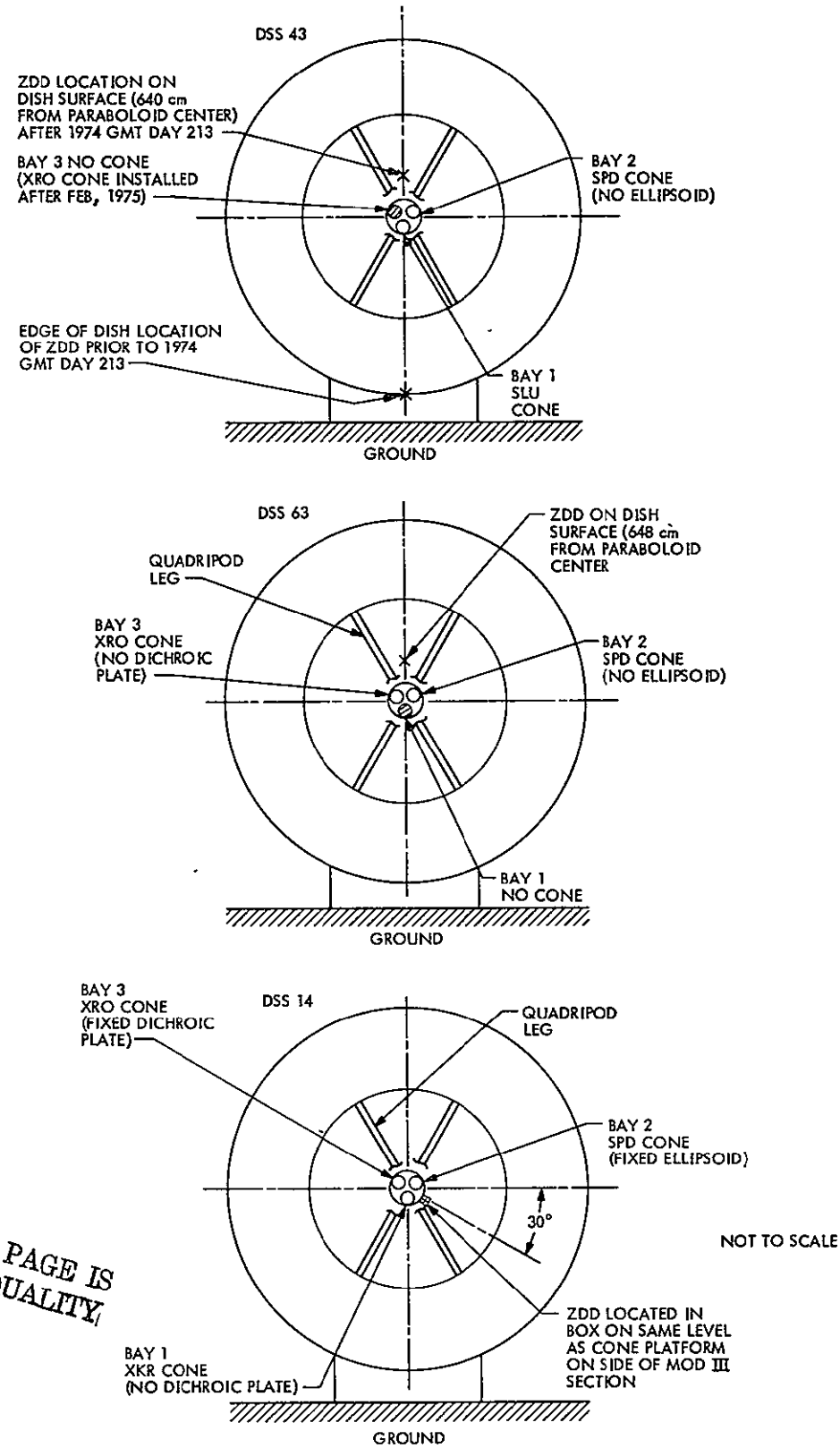

Fig. 8 DSS 43, DSS 63, and DSS 14 zero-delay device locations and tricone configuration for subreflector tests

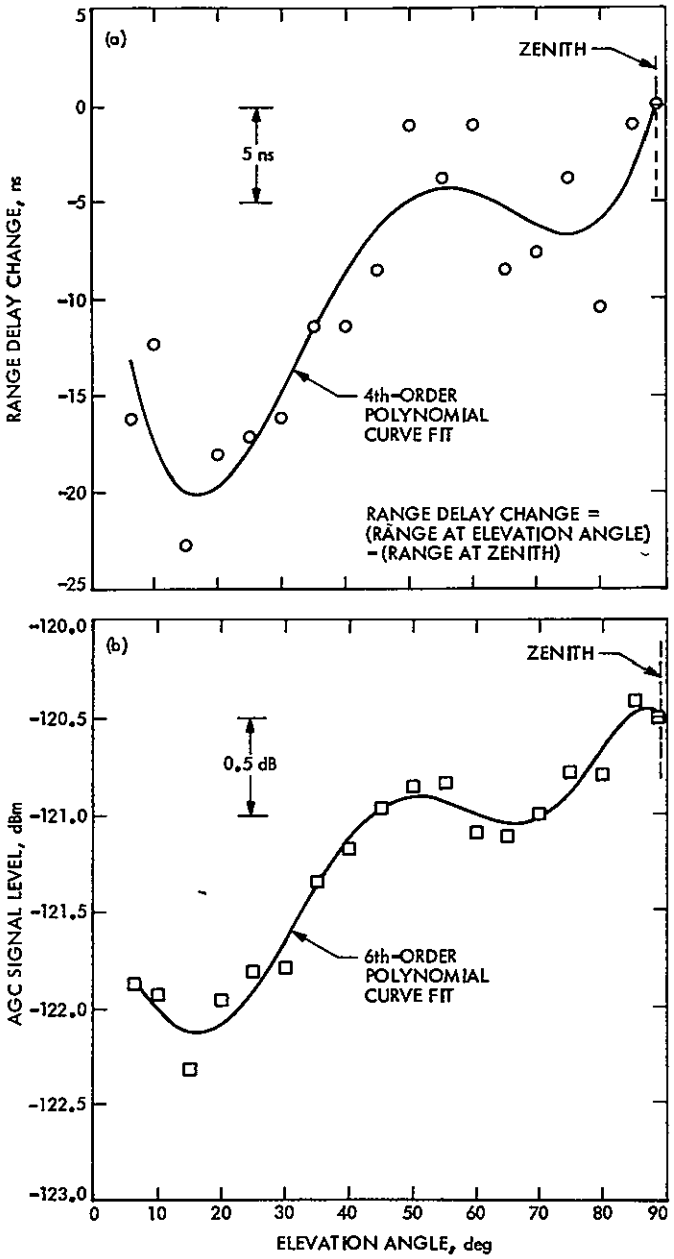

Fig. 9. DSS 43 antenna tipping tests at S-band, 1974 GMT Day 359: (a) Range delay change, (b) Downlink received signal level

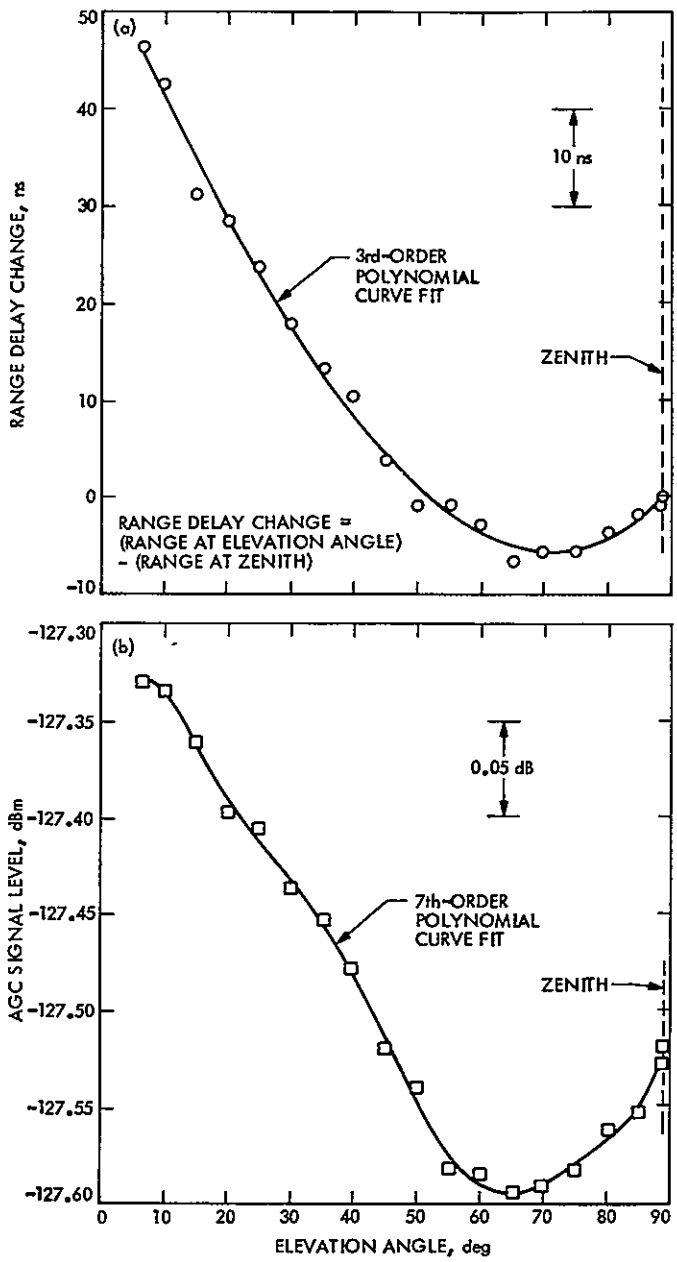

Fig. 10. DSS 63 antenna tipping tests at S-band, 1975 GMT Day 27: (a) Range delay change, (b) Downlink received signal level

NASA—JPL—Coml, L.A. Calif